IMMISCIBLE LIQUID SEPARATION

IN A HYDROCYCLONE

THE EFFECT OF DROP SIZE DISTRIBUTION, FEED CONCENTRATION, AND VOLUME SPLIT ON THE SEPARATION OF TWO IMMISCIBLE LIQUIDS IN A HYDROCYCLONE

By

KENNETH ANTON BURRILL

B.Eng.Sc. (U.W.O.)

A Thesis

Submitted to the Faculty of Graduate Studies

in Partial Fulfilment of the Requirements

for the Degree

Master of Engineering

McMaster University

May, 1967

ACKNOWLEDGEMENTS

I would like to express my sincere thanks to Dr. D. R. Woods for his encouragement and helpful discussions throughout the course of this work.

Thanks are due to Mr. J. Whorwood of the McMaster Photography Department for his advice on photographic problems encountered in this work.

The flash unit used is the design of Mr. K. Pollock and was constructed by Mr. J. Meinen. Their efforts are particularly appreciated.

The assistance of all the technical staff is gratefully acknowledged, especially the help of Mr. L. Suggett.

Financial assistance through an N.R.C. bursary and an N.R.C. research grant is also gratefully acknowledged.

Finally, the patience and efforts of my wife, Gayle, are sincerely appreciated.

K.A. Burrill

K. A. Burrill

Hamilton, February 1967.

MASTER OF ENGINEERING (1967)
(Chemical Engineering)

McMaster University
Hamilton, Ontario

TITLE: The Effect of Drop Size Distribution, Feed Concentration, and Volume Split on the Separation of Two Immiscible Liquids in a Hydrocyclone.

AUTHOR: Kenneth A. Burrill

SUPERVISOR: Professor D. R. Woods

NUMBER OF PAGES: xiii, 172

SCOPE AND CONTENTS: The separation of a mixture of carbon tetrachloride in water was studied in a 2 inch diameter glass hydrocyclone. First, the effect of a mixing valve and of oil/water ratio on the volume/surface diameter of the dispersion in the feed to the hydrocyclone was studied using a statistical experiment design. Secondly, the effect of feed drop size distribution, oil/water ratio, and overflow/underflow split on the separation in the hydrocyclone was determined, again using a statistical experiment design. In both designs, five levels of each variable were studied. Flow rate, design shape, and temperature were kept constant. The range of variables was:

1. Mixing Valve Pressure Drop — 17.95 to 88.25 mm. Hg
2. Oil/Water Ratio — 0.132 to 0.211
3. Overflow/Underflow Split — 4/1 to 8/1

From the first part of the work it was found that oil/water ratio had no significant effect on the volume/surface diameter, and that there was a linear relationship between the volume/surface diameter and mixing valve pressure drop.

From the second part of the work it was found that volume split had the most significant effect on hydrocyclone separation for the range of variables studied. The oil/water ratio had the next most significant effect on separation, and finally, drop size distribution was also found to be significant, but was the least important of the three variables. The interactions of the variables were not significant. The hydrocyclone separation could be predicted. The prediction of the overflow drop-size distribution agreed very well with the distribution observed photographically. Both predictions required assumptions that short-circuit flow and drop-drop coalescence were negligible.

TABLE OF CONTENTS

Page

Page

LIST OF TABLES

LIST OF FIGURES

I INTRODUCTION

I INTRODUCTION

I·a State of the Art

A cyclone uses centrifugal force to bring about the physical separation of its feed components. The centrifugal force is generated by injecting the feed at a high velocity, tangentially to the wall of the cyclone. To evaluate the design and operating variables solely on the basis of a theoretical model is presently impossible. The complexity of the flow patterns in the cyclone, and the large number of variables dictate that a cyclone design be based partially on empirical findings.

To further elucidate the state of the art, cyclones will be divided into two categories: those that use a liquid/liquid feed, and those that do not.

I·a·1 Non Liquid/liquid Cyclones

Most investigations on cyclone behaviour have been with solid/liquid and solid/gas feeds. Cyclones with gas feeds are generally greater than three feet in diameter. Cyclones with liquid feeds (hydrocyclones) range from about 0.5 inches up to 20 inches in diameter.

To predict the separation for a given design, information is needed on the velocity profiles. These profiles have been measured by ter Linden (T-3) using a Pitot probe for gas cyclones, and by Kelsall (K-1) using an ultra microscope technique for liquid cyclones, each on a given design of cyclone. Rietema (R-2) has used the Navier-Stokes equations to determine tangential velocities in a liquid cyclone, making several justifiable assumptions concerning the coupling of the three velocity components (axial, radial, and tangential). The resulting velocity profiles are qualitatively similar to those of Kelsall.

A particle size classification curve (Y-3) has been found experimentally; this may be used with the feed particle size distribution and the known velocity profiles to predict cyclone separation. Many correlations exist to select the cyclone diameter for a given pressure drop and feed flow rate (Y-3)(B-4)(R-2)(M-5). Mitzmager and Mizrahi (M-5) have given the most complete correlation, using dimensionless groups. This correlation does not allow for valves on the cyclone outlets, and appears to be only applicable to cyclone operation with an air core.

Once the cyclone diameter is found, the sizes of the other cyclone variables can be calculated from the "optimum" ratios suggested by Rietema (R-2), and Simkin and Olney (S-3).

I·a·2 Liquid/liquid Cyclones

Mass transfer in hydrocyclones used to contact and separate two (or more) immiscible liquids has been studied by about a dozen workers. Few studied the effect of design and operating variables on physical separation. Simkin and Olney (S-3) found optimum design values for hydrocyclones, and also studied the effect of inlet velocity, feed drop size distribution, oil/water feed ratio, and volume split (overflow rate/underflow split) on the cyclone separation. They did not determine the effect of oil/water feed ratio on feed drop size, and the effect of increased feed rate on feed drop size distribution and on cyclone separation made interpretation of results difficult. For their work, coarse drops were used (0.5 to 1.0 mm. diameter) whereas on an industrial scale the drops are likely to be small (.01 to 0.5 mm.) (0-1).

I·b Object and Scope of the Work

Their small size and large throughput make hydrocyclones attractive. Aside from the mass transfer, if liquid/liquid cyclones could be used to separate the oil/water mixtures that abound in oil refineries, their use would prove valuable. Unfortunately, little work has been done on those aspects of a liquid/liquid feed that make it different from a solid/liquid feed. Those aspects of liquid/liquid feeds are:

(1) the change in feed drop size distribution with flow rate,

(2) the possibility of getting coalescence of the droplets in the cyclone,

(3) the possibility of getting drop break-up in the cyclone because of shearing.

For a hydrocyclone, suggestions have been given for the optimum design dimensions and shape (S-3). However, the effect of operating variables is not well understood. Therefore, values of design variables may be selected on the basis of Simkin and Olney's work, but information on the following operating variables would be needed to predict separation:

(1) physical properties of the liquid/liquid feed

(2) feed drop size distribution

(3) volume fraction dispersed phase in the feed

(4) the volume split (overflow rate/underflow split)

The above operating variables were selected for the study of a carbon tetrachloride/water system. The information obtained was compared with that predicted, and differences were explained.

The work was divided into two parts. First, a study of the drop size distributions in the feed was made. This entailed photographing the feed dispersion and determining the resulting volume/surface diameter $\langle D_p \rangle_{32}$ of the distributions. This mean diameter was then correlated with the oil/water ratio and the mixing valve pressure drop. Secondly, a study of the effect of the operating variables on cyclone separation was performed. The variables studied in this phase of the work were drop size distribution, oil/water ratio and volume split.

Ranges of the variables studied are given in Table I-1, along with reasons for the limits. All other independent variables (such as temperature and total flow rate) were kept constant.

TABLE I-1 RANGES OF INVESTIGATED VARIABLES

VARIABLE	RANGE	REASON FOR LIMITS
Feed Drop Size $\langle D_p \rangle_{32}$	160 microns to 300 microns	Poor photographic contrast
		Mixing valve fully open
Oil/Water Ratio	11.8 volume % oil to 17.4 volume % oil	Lower limit of rotameter
		Poor photographic contrast
Volume Split	4/1 to 8/1	Arbitrary
		Arbitrary

II LITERATURE REVIEW

II LITERATURE REVIEW

II·a Introduction

This work entailed using a liquid/liquid system as feed to a hydrocyclone. Consequently, the literature review consists of, first, a consideration of emulsions, and secondly, a consideration of the cyclone literature.

II·b Emulsions

The subject of emulsions covers an enormous amount of material. Therefore, only those aspects of emulsions that are directly concerned with this work will be considered briefly. This review considers some of the properties of emulsions and the methods of characterization of emulsion droplets and distributions.

II·b·1 Emulsion Properties

An emulsion is defined as a mixture of two at least partially immiscible liquids, with one liquid dispersed as droplets in the other liquid. The emulsion can be unstable or stable. An unstable emulsion is one where the droplets settle out and coalesce shortly after the emulsion is formed. A stable emulsion is one where the droplets do not settle out and do not coalesce.

Droplet size, in most cases, ranges from 0.01 μ to 500 μ. Emulsions are coarse if the droplet sizes are $> 20\,\mu$ and fine if the droplet sizes are $< 20\,\mu$ (C-2). In this work, rather than use the term "unstable emulsion", the term "dispersion" is used to imply an unstable emulsion of relatively coarse droplets.

Emulsions may contain surface active agents whose purpose is to stabilize the emulsion. These agents prevent drop-drop coalescence when the concentration of dispersed phase is about 15% by volume (M-1). One very important property of emulsions is viscosity. Generally, the viscosity of an emulsion increases as all drops are made smaller in size, and as the drop size distribution is made more uniform (O-2).

The next section considers some means of describing the drop size distribution present in an emulsion.

II·b·2 <u>Characterization of Emulsion Drop Size Distributions</u>

The Gaussian Distribution Law has been applied to the description of particle size distributions. Distributions that appear to follow this law give straight lines when plotted as particle diameter versus percent of total drops smaller than this diameter (on a probability scale). Many distributions generated by crushing, grinding, or shearing forces are log-normal distributions. A straight line will result if these distributions are plotted as logarithm of particle diameter versus percent of total drops smaller than this diameter.

The diameter at the 50% probability point is the geometric mean diameter $\langle D_p \rangle_g$. If the diameter at the 15.87% point is divided into $\langle D_p \rangle_g$, a measure of the scatter or range of the dispersion results, called the geometric standard deviation σ_g. Together $\langle D_p \rangle_g$ and σ_g completely specify a drop size distribution, if it is log-normal.

Both $\langle D_p \rangle_g$ and σ_g may be used to specify other mean diameters. Dallavalle (D-3) presents the Hatch-Choate equations which may be used to predict a mean surface diameter, and a mean volume diameter, if $\langle D_p \rangle_g$ and σ_g are known.

Mugele and Evans (M-8) discuss the different methods of characterizing drop size distributions, and conclude that the log-probability procedure is fundamentally correct. These authors also consider the case where a maximum drop size can exist in an emulsion, due to the mechanism by which the drops are formed, and due to the flow conditions of the emulsion (S-5). A special "upper-limit function" is defined so that the presence of a maximum drop size does not cause deviation from a straight line on log-probability paper.

Several recent papers have appeared in the literature which deal with the proper method of calculating cumulative volume percents from measured particle diameters. Wise (W-2) gives a procedure for calculating true volume or surface distributions from measured drop size distributions. This method is not necessary when the drop size distribution follows the log-normal law.

A very important procedure to apply to log-normal distributions is given by Gwyn et al (G-1). This paper corrects for the drop size distribution sample not containing an elusive "larger drop" than the largest drop observed in the sample.

The definition of mean diameters is given in appendix 5, along with an example of the Gwyn et al procedure.

II.c Cyclones

The literature on cyclones will now be considered, but only the literature on liquid/liquid cyclones will be considered in detail. In the "Cyclone Theory" section and the "Operation and Design" section, important papers from the entire cyclone literature will be referred to, but not considered in depth.

TABLE II-1 AVAILABLE LITERATURE ON LIQUID/LIQUID CYCLONES

EMPHASIS OF WORK	L/L SYSTEM	CYCLONE DIA. (inches)	REFERENCE	COMMENTS
Exploratory	Carbon tetrachloride plus benzene/water	3, 8	Klein (K-3) Ellefson (E-1)	No information on drop size distribution
Study effect of continuous phase viscocity on separation	Water in oil of 3, 11, 30 centistokes	5	Van Rossum (V-1)	
Study of dual cyclone	Hexone/water	.25 - .40	Bresee (B-6)	Excellent separations
Study of variables and mass transfer	Kerosene/water White oil/water	4	Simkin and Olney (S-3)	Provides optimum cyclone dimensions
Exploratory	Carbon tetrachloride/ water	.40 - .60	Bradley (B-3)	
Contacting and separation for extraction	Isobutanol/water		Tepe and Woods (T-2)	Separation poor
Mass transfer	(Hexone + acetic acid)/ water		Rekemeyer (R-1)	
Mass transfer	TBP in Amsco/.08N. HNO_3		Cerny (C-1)	
Mass transfer	-same as Cerny	.40	Hitchon (H-2)	
Mass transfer	Benzoic acid in Kerosene/.08N. HNO_3		Simms (S-4)	
Mass transfer	Carbon tetrachloride/ water, benzene/water chloroform/water and solutes	1.5	Molyneux (M-7)	
Mass transfer	Several systems used	.75	Whatley (W-1)	

Throughout this thesis, the terms "cyclone" and "hydrocyclone" will be used interchangeably, with the understanding that the cyclone feed has liquid as the continuous phase.

II·c·1 Liquid/liquid Cyclones

The details of the literature in this area can best be given by Table II-1. It may be seen that the investigations carried out were with vastly different liquid/liquid systems, and for many sizes of cyclones. Emphasis has been more on the mass transfer ability of the cyclone, rather than a consideration of the cyclone variables themselves.

II·c·2 Cyclone Theory

In the cyclone field, there are two main theories to explain the observed cyclone behaviour. These theories will be considered in detail in appendix 4, but will be briefly mentioned here.

The first theory is the work of Kelsall (K-1), Bradley (B-2) (B-4) and Lilge (L-1), and has been used by many other workers. To introduce this theory, first consider the flow patterns in a cyclone, as given in Figure II-1. Flow is seen to be down at the walls and up at the centre. Therefore, it may be seen that at some radius in the cyclone there is zero vertical velocity. The locus of zero vertical velocity is indicated by the dotted line in Figure II-1. The radial liquid velocity is high near the cyclone wall (directed inwards) and decreases toward the centre of the cyclone. Since cyclone centrifugal force throws a particle toward the wall, the particle's motion toward the wall will be retarded by the inward liquid flow. There will be a particular radius in the cyclone at which the centrifugal force on a

FIGURE II-1 VERTICAL AND RADIAL FLOWS IN A CYCLONE

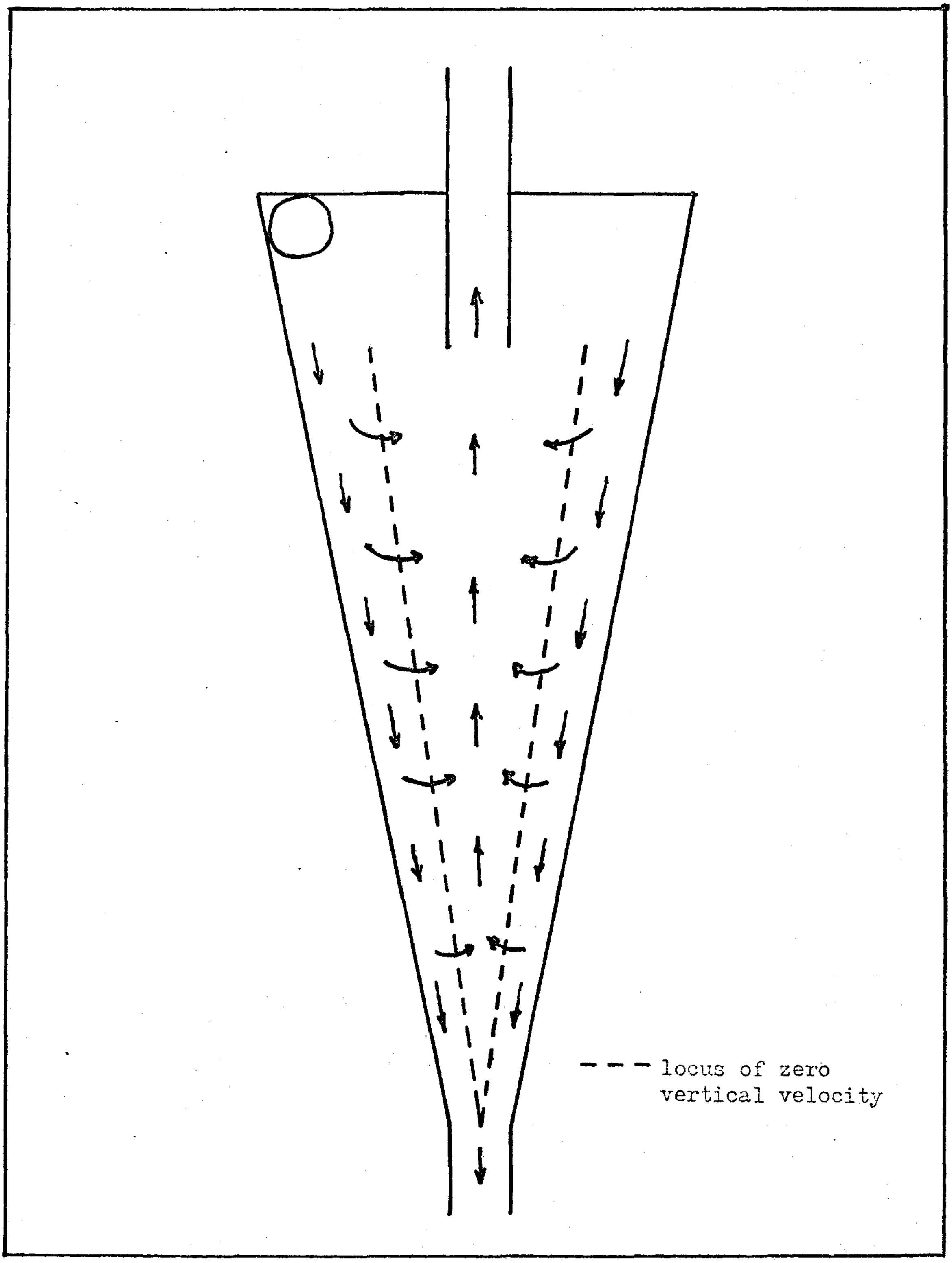

particle of a given size is equal to the drag force on the particle. Large particles will be in equilibrium near the wall, and small particles will be in equilibrium near the cyclone centre. Particles which are in equilibrium between the locus of zero vertical velocity and the cyclone centre will be carried by the upward axial flow to the overflow, and vice versa for the particles on the other side of the zero vertical velocity locus. A very sharp classification of particles is then expected. Normally, however, the particle classification is not sharp, presumably due to turbulence in the cyclone. A particle which is in equilibrium on the locus of zero vertical velocity will have a 50% chance of going to the overflow and a 50% chance of going to the underflow, and so it is termed the $(D_p)_{50}$ size particle. Normalizing the observed classification curve results in Figure II-2. The observed curve's shape is supposedly entirely general (Y-3). Therefore if the $(D_p)_{50}$ size can be predicted (see appendix 4), the expected cyclone performance can be evaluated from a knowledge of Figure II-2 if the feed particle size distribution is known.

Criticism of this model is wide-spread and is well summarized by Mizrahi (M-6).

The second model is the work of Rietema (R-2). This model assumes the cyclone is operating with an air core as shown in Figure II-3. A particle which goes 50% to the underflow, if injected at the centre of the feed inlet, will just reach the apex of the cyclone. Rietema derived an expression containing $(D_p)_{50}$ which was a function of cyclone dimensions and velocity ratios.

The assumption of turbulence causing the observed particle

FIGURE II-2 EXPECTED AND OBSERVED PARTICLE SIZE CLASSIFICATION

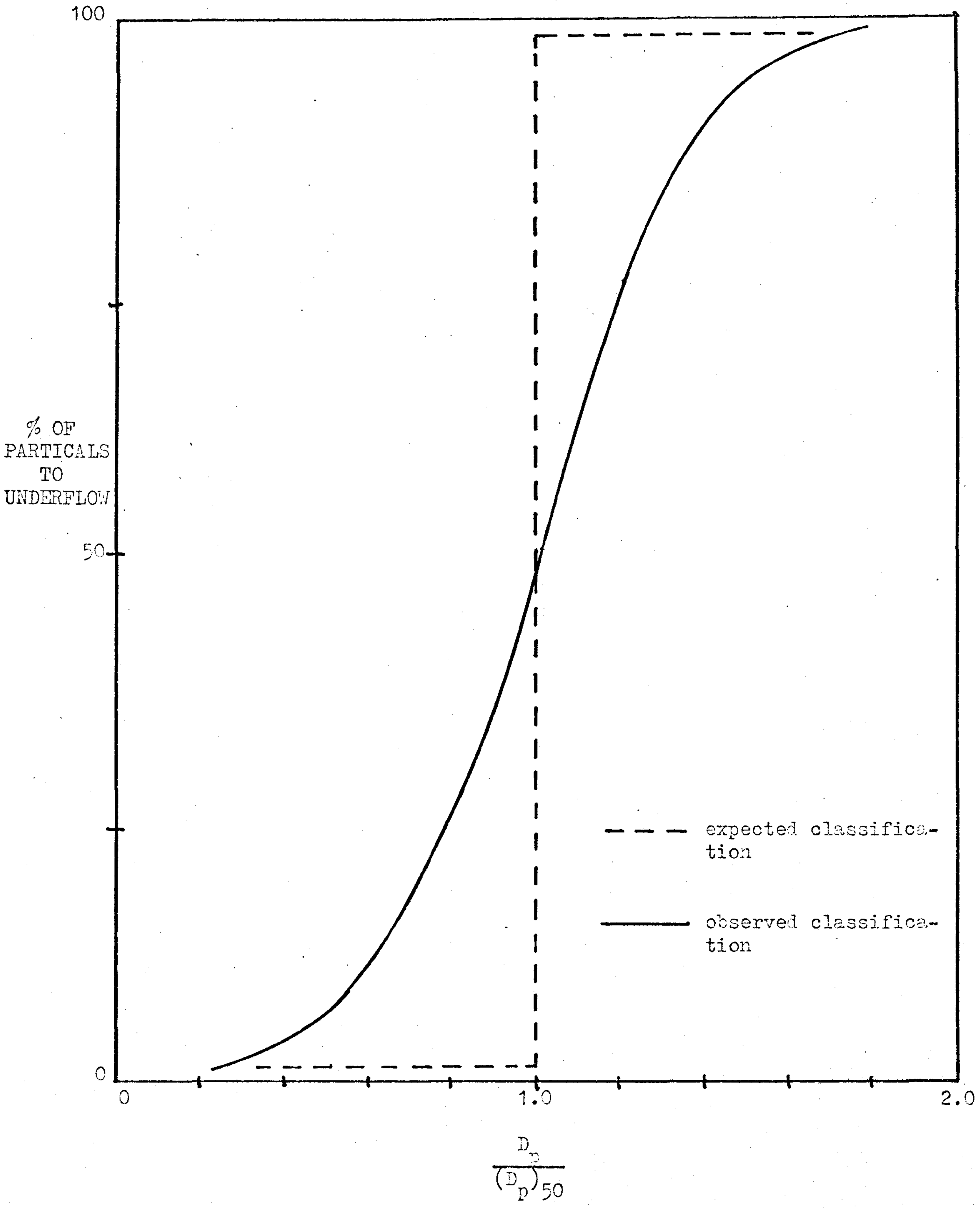

FIGURE II-3 ILLUSTRATION OF RIETEMA'S CYCLONE MODEL

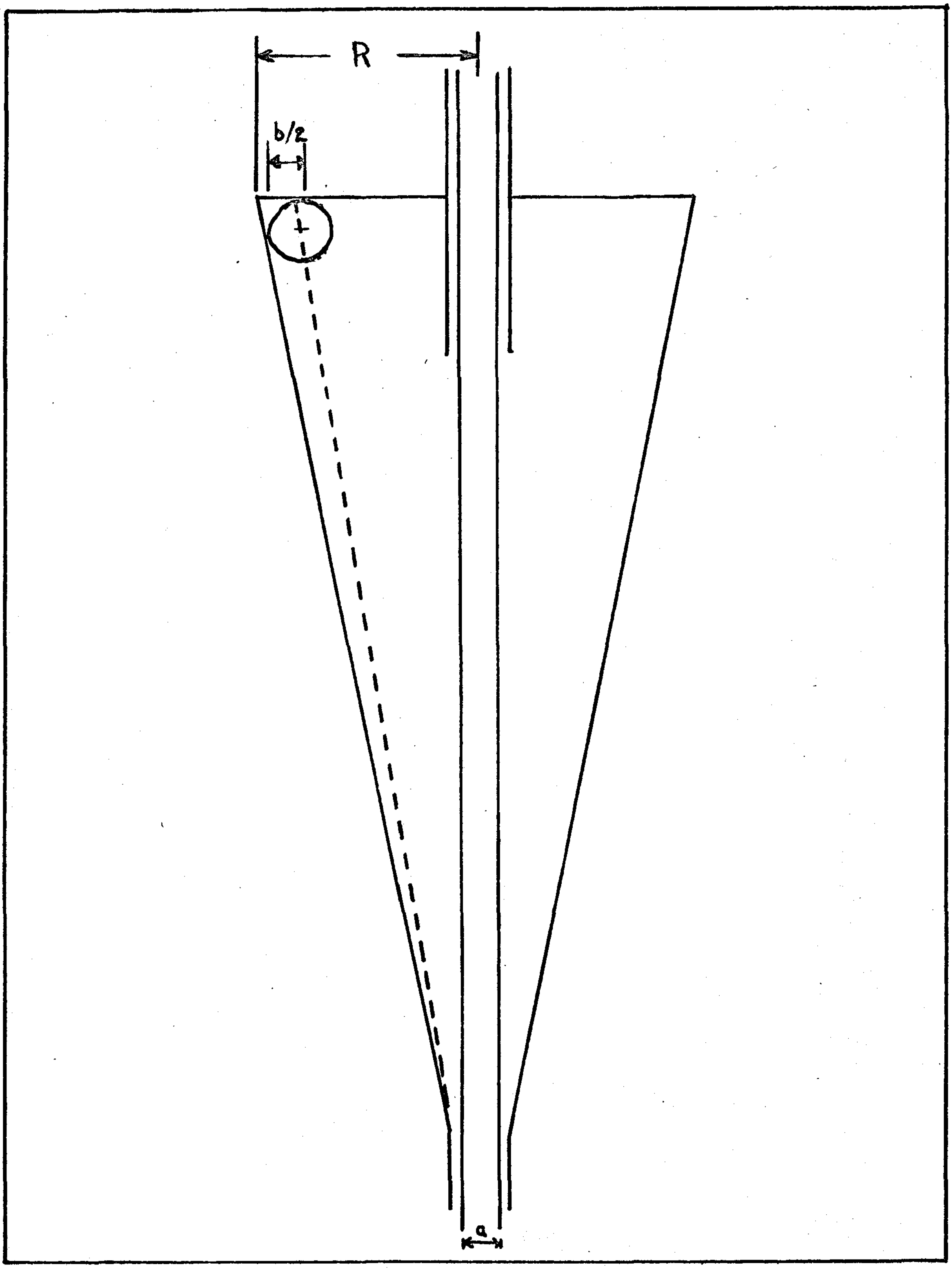

classification was rejected by Rietema who assumed no turbulence in his derivation and justified it. Mizrahi (M-6) has extended Rietema's analysis to show how such an observed classification curve can arise without turbulence.

Rietema's model appears to be realistic, although it makes no allowance for the several separation mechanisms that Mizrahi mentions as being operable in a cyclone.

II·c·3 Cyclone Operation and Design

As discussed in the above section, it is apparent that the cyclone acts as a classifier. However, it is also possible to operate the cyclone as a thickner. The criterion for this latter operation is to concentrate the feed particles and remove clear liquid. There are many papers with illustrations of the cyclone acting as a classifier (K-4)(M-3) and as a thickner (B-1)(V-2)(Y-1).

One aspect of cyclone operation repeatedly appearing in the cyclone literature is called short circuiting. This is feed which passes directly from the feed inlet, across the cyclone roof, and down the outside of the overflow pipe to the overflow. The existence of short circuit flow has been shown quite drammatically by Lindner (L-2) using paint to make boundary layer flows visible. Bradley (B-5) has also done similar work using dyes. Kelsall (K-1) estimates short circuit flow at 15% for his particular design and operating variables.

To design a cyclone requires a knowledge of $(D_p)_{50}$. It also requires an estimate of the cyclone pressure loss to be expected. A general correlation has recently been given by Mitzmager and Mizrahi (M-5), but it makes no allowance for valves on the cyclone overflow and underflow. Several papers (L-1)(R-2)(M-7) give examples of cyclone design for solid/liquid feeds.

To conclude this section, some mention should be made of the criterion of cyclone separtion. This criterion can be an efficiency such as the one defined by Simkin and Olney (S-3) which is easily derivable from a cyclone material balance. Tengbergen and Rietema (T-1) considered the question of efficiency and decided that

$$E = \left[\frac{Q_{2\ \text{oil}}}{Q_{1\ \text{oil}}} - \frac{Q_{2\ \text{water}}}{Q_{1\ \text{water}}} \right]$$

adequately represents cyclone performance. Simkin and Olney's and Tengbergen and Rietema's definitions are equivalent. For this work Simkin and Olney's definition was used. It is

$$E_s = \frac{Q_2}{Q_1} \left[\frac{Y_2 - Y_1}{1 - Y_1} \right] + \frac{Q_3}{Q_1} \left[\frac{Y_1 - Y_3}{Y_1} \right]$$

Note that these definitions do not define efficiency uniquely because they are a function of both flow rates and compositions. For this work, Q_1 was held constant, making efficiency unique for varying operating conditions.

III EXPERIMENTAL APPROACH

III EXPERIMENTAL APPROACH

III·a Introduction

The objectives of this work dictated that the experimental work be divided into two parts. First, the incoming feed drop size distribution had to be controlled and measured. Secondly, the effect of the three variables, feed drop size distribution, oil/water ratio, and volume split on hydrocyclone separation efficiency had to be determined.

This chapter considers the variables in the work, the equipment that was used to measure and control the variables, and then outlines the procedure used in both parts of the experimental work.

III·b Variables in the Design and Operation of a Hydrocyclone

The two sets of variables are:

1.) the hydrocyclone design variables

2.) the operating variables

The hydrocyclone design variables determine its shape and dimensions. They are:

Cyclone diameter	D_C
Inlet diameter	D_1
Overflow diameter	D_2
Underflow diameter	D_3
Included cone angle	θ
Overall vertical length of cone	L
Vortex finder length	L_2
Height of cylinder	H
Presence of valves on outlets	yes or no
Round feed cross section	yes or no

The cyclone dimensions are shown in Figure III-1. For this work, no cylindrical section at the inlet was used since the literature is conflicting as to whether a cylindrical section is necessary. The common ground seems to be that a cylindrical section provides lower cyclone pressure drop, and ease of fabrication when the feed inlet is attached. Both these criteria were not important in this work. A round feed cross section was used.

The cyclone diameter D_C was arbitrarily chosen as 2 inches I.D. Using references (R-2) and (S-3) which give "optimum" cyclone dimensions, the remaining design variables could be found. They were:

$D_1 = D_2 = D_3 =$ 0.475 inches I.D.

$\theta = 10^{\circ}$

$L =$ 8.5 inches

$L_2 =$ 2.0 inches

The presence of valves was desirable since the cyclone was to be used for different operating conditions. Ordinarily, $D_3 < D_2$ and the cyclone discharges directly into the atmosphere allowing an air core to develop.

The operating variables determine the efficiency with which a given cyclone will operate. For a liquid/liquid feed, the variables are:

1.) Feed Condition

   a.) immiscible liquid/liquid system physical properties

   b.) oil/water ratio

   c.) drop size distribution

   d.) concentration of surface active agents

FIGURE III-1 HYDROCYCLONE DIMENSIONS NEEDED FOR DESIGN

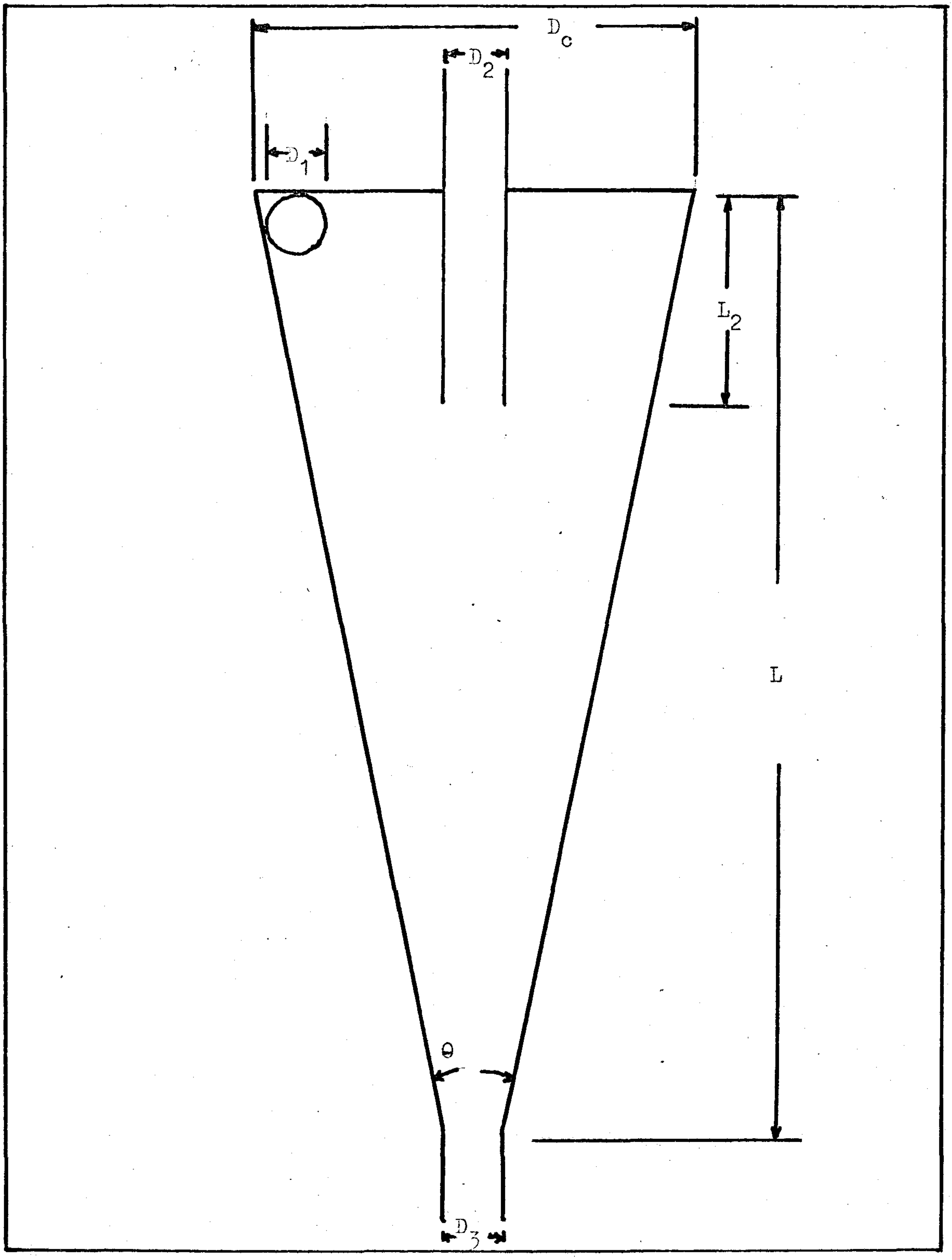

2.) Inlet velocity

3.) Volume split (overflow rate/underflow split)

4.) Pressure drop ($P_1 - P_2$, for example)

5.) Air core

The immiscible liquid/liquid system carbon tetrachloride/water was chosen. The oil (carbon tetrachloride) was dispersed in the water. The limitations of the photographic technique determined the upper limit for the oil/water ratio and the fineness of the feed drop size distribution. The concentration of surface active agents was not controlled, but was measured indirectly (see Appendix 1). The feed was at room temperature. Inlet velocity was kept constant because it represented another variable in both the feed drop size distribution and cyclone separation studies. Volume split was considered to be an important variable. The installation of valves on the outlet lines of the cylone permitted the volume split to be varied easily.

Since the cyclone volume split could be changed, the cyclone pressure drop also became a variable, although not easily controlled. In this work, the pressures P_1, P_2, and P_3 did change and no attempt was made to control them.

Using a valve on the underflow opening restricted the formation of an air core in the cyclone. In this work all efficiency data were taken with no air core present.

Therefore, the variables that were chosen for study were:

1.) feed drop size distribution

2.) oil/water ratio

3.) volume split

III·c Equipment

The equipment may be divided into two functional sections; feed preparation, and the test section. A photograph of the entire equipment is given in Figure III-2.

III·c·1 Feed Preparation Section

The carbon tetrachloride and water were taken separately from the reservoir (1) and pumped by two feed pumps (2) to their respective rotameters (3). After the oil was dispersed in the water at a mixing tee, the dispersion passed through a mixing valve (4) where the drop size distribution was changed. A mercury manometer measured the pressure drop across the mixing valve, and a Bourdon pressure gage (5) measured the feed pressure P_1. Just before entering the test section, the drop size distribution was photographed at the optical cell (6) using an electronic flash and 35 mm. camera.

To summarize, as the feed enters the test section, it consists of a predetermined amount of oil in water, and of a predetermined drop size distribution at a certain flow rate and pressure. Feed temperature was room temperature (25° $\pm$ 2°C).

III·c·2 Test Section

The test section consisted of the hydrocyclone (7) and the overflow and underflow tanks (8) and (9) which were used to measure overflow and underflow rates, respectively. Manometers measured the overflow and underflow pressures P_2 and P_3.

Samples of the overflow and underflow streams were taken directly by placing flasks under both streams, simultaneously.

FIGURE III-2 PHOTOGRAPH OF EXPERIMENTAL APPARATUS

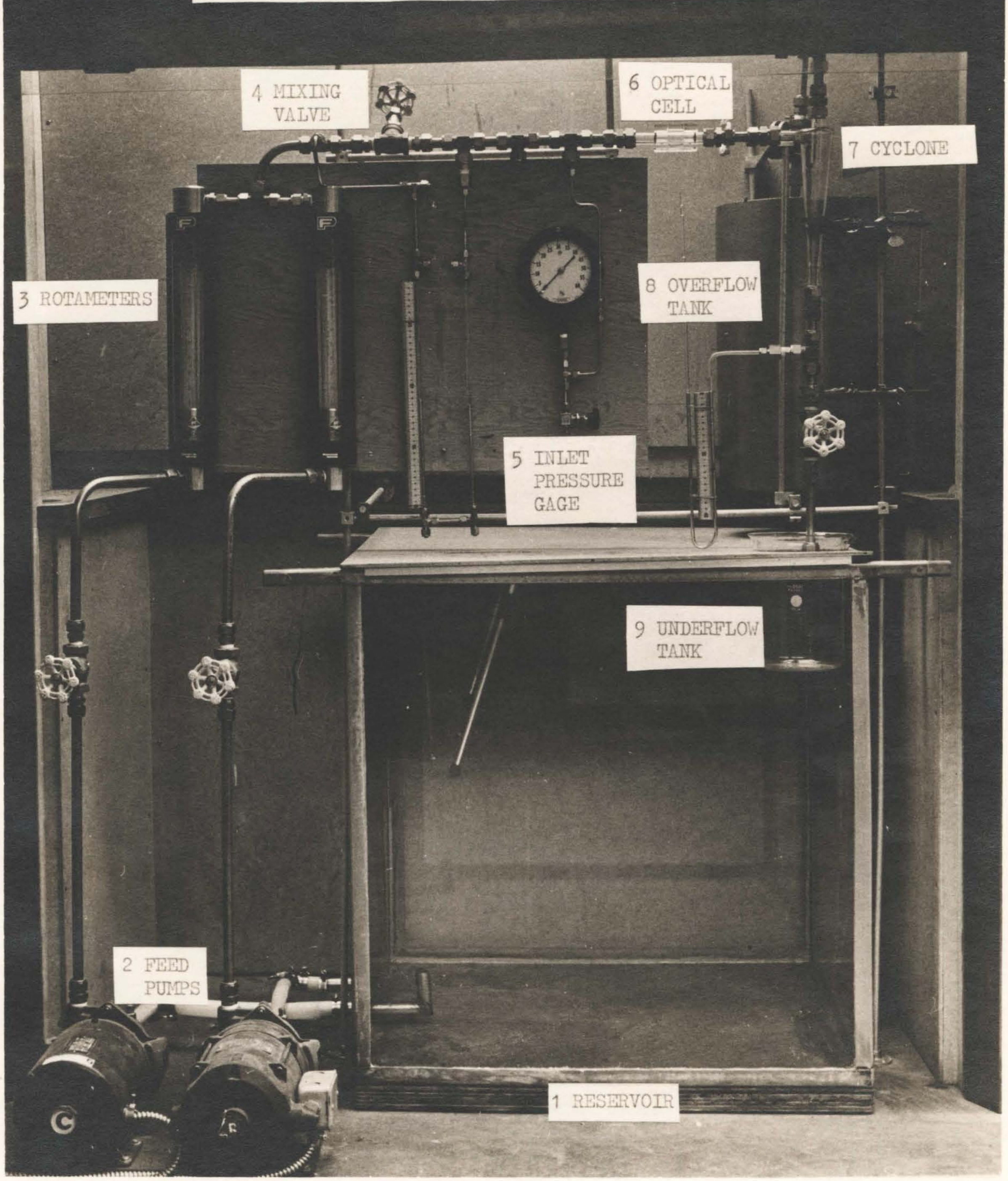

III·d Procedures

The procedure used to determine the feed drop size distribution is considered first, and then the cyclone separation procedure is outlined.

III·d·1 Determining the Feed Drop Size Distribution

The effect of oil/water ratio and mixing valve pressure drop on the volume/surface diameter of the feed drop size distribution was determined first. A composite statistical experiment design for the two variables at five levels was used (a total of 12 runs).

Several photographs of the feed dispersion were taken for each run, and about 500 to 2000 drops were sized and counted for each run, using a Zeiss particle size analyzer. From the size distribution given by the analyzer, a volume/surface diameter could be calculated. This photographic method of sampling the feed dispersion did not disturb the dispersion in any way. Details of this method are given in Appendices 2 and 5.

III·d·2 Effects of the Variables on Cyclone Separation

Once the feed drop size distribution was known as a function of the oil/water ratio and mixing valve pressure drop, the effect of feed drop size distribution, oil/water ratio, and volume split on the cyclone separation could be determined. The experimental work was planned on the basis of a composite statistical experiment design for the three variables at five levels (20 trials).

Since the feed drop size distribution could be controlled by the mixing valve, it was not measured during the separation study. By adjusting the valve on the cyclone underflow, the volume split was set by trial and error, three trials usually being sufficient. The cyclone overflow valve was fully open. Then, for a particular oil/water ratio and feed drop size distribution, the outlet streams were sampled twice within about 30 seconds. Runs lasted about 2 to 3 minutes, since the overflow stream contained very small oil drops and was retained in the overflow tank, rather than being discharged immediately back into the reservoir.

The overflow sample contained 0-5 volume percent carbon tetrachloride in water, and was analyzed by extraction of the oil with hexane and measurement of the refractive index of the extract. The underflow sample was 75-90 volume percent carbon tetrachloride and was analyzed by turbidimetric titration. Details are given in Appendix 2. Both analyses were accurate to within 5%. The mutual solubility of carbon tetrachloride and water was too small to be measured by the above techniques.

Steady state was reached very rapidly within the cyclone, since residence time in the cyclone was about 0.5 seconds, and since the two samples of each stream showed no time trend.

IV RESULTS AND DISCUSSION

IV RESULTS AND DISCUSSION

IV·a Introduction

This chapter considers the results of the drop size distribution work and the cyclone separation work. Since theory in both areas is meagre, explanations of results are qualitative for most of the discussion.

IV·b Effect of the Variables on the Feed Dispersion

Details of the experimental procedure and data obtained are in the appendices. First consider the statistical results.

IV·b·1 Statistical Results

The data on Sauter mean diameter $\langle D_p \rangle_{32}$ versus mixing valve pressure drop (x_1) were correlated by the following equation (using least squares)

$$\langle D_p \rangle_{32} = 324.64 - 1.69\, x_1$$

where

$\langle D_p \rangle_{32}$ = Sauter mean diameter (microns)

x_1 = mixing valve pressure drop (mm.Hg)

The effect of oil/water ratio was not significant and so is not included in this equation. The multiple correlation coefficient for this equation is

$$r_{y/x} = 0.743$$

which is significant at the 95% confidence level. When a second order polynomial was fitted to the data, all partial regression coefficients but that coefficient for x_1 were found not to be significantly different from zero.

A plot of equation (1) with the data is given in Figure IV-1.

IV·b·2 Discussion of the Effect of the Variables on Drop Size Distribution

First consider oil/water ratio. To explain why this variable had no effect on the drop size distribution for the range that was studied, two explanations may be advanced. The reproducibility of $\langle D_p \rangle_{32}$ shows a fair degree of scatter, the standard deviation of observations at the centre point being 13μ. This scatter may be masking the oil/water ratio effect, inferring that the oil/water ratio effect is small. Neglecting it will have little effect on $\langle D_p \rangle_{32}$.

To confirm the above reasoning the work of McDonough et al (M-4) is cited. It gives the following empirical relationship for immiscible liquids flowing through an orifice

$$\text{interfacial area } A \propto (\text{volume fraction dispersed phase } \phi)^{0.9}$$

or $$A \propto \phi^{0.9}$$

In other words,

$$\langle D_p \rangle_{32} = \frac{6\phi}{A} = (\text{constant})\,(\phi)^{0.1}$$

Therefore increasing the volume fraction of dispersed phase gives a small increase in $\langle D_p \rangle_{32}$ for the same pressure drop across the orifice. No explanation was offered for this behaviour. If the oil/water ratio did have an effect on $\langle D_p \rangle_{32}$ for this work, it was too small to be noticeable compared to the experimental error.

FIGURE IV-1 EFFECT OF MIXING VALVE PRESSURE DROP ON VOLUME/SURFACE DIAMETER $\langle D_p \rangle_{32}$

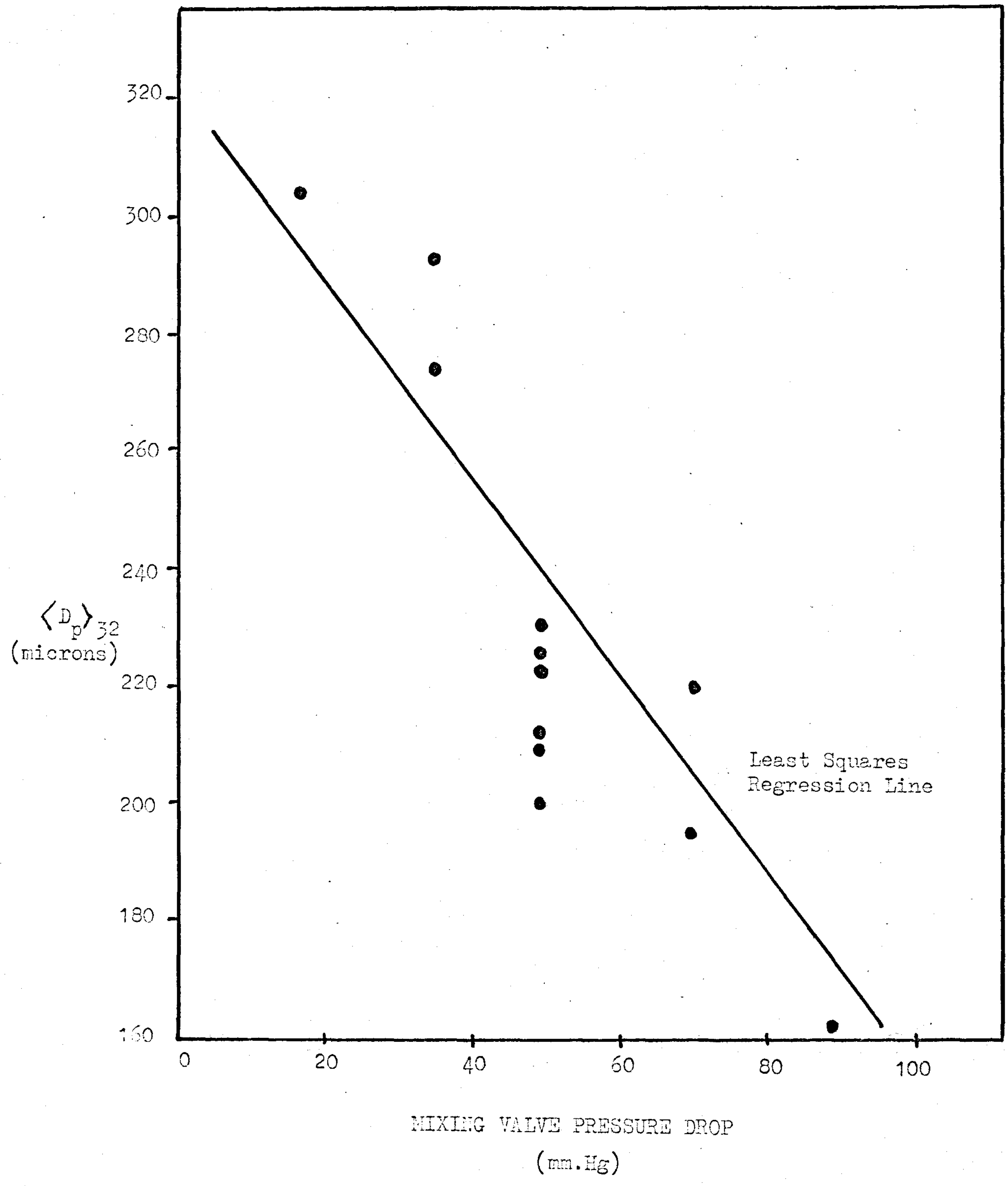

The second explanation is based on the mechanism by which the drops are formed. For this work, drops of oil are formed in the water at a mixing tee, and these drops are then broken up at the mixing valve. The mechanism by which drops of one phase form when injected into another phase, and the mechanism by which drops are broken up at an orifice is not well understood. Intuitively, the relative volumes of one phase to the other would not seem to have an effect on $\langle D_p \rangle_{32}$ unless drop-drop coalescence occurred. For the experimental apparatus, the estimated time for the dispersion to travel from the mixing tee to the optical cell was 0.3 seconds. There, coalescence would have to be occurring very rapidly for the drop size distribution to be changed considerably before it was photographed and entered the hydrocyclone. It may be concluded, then, that the oil/water ratio does not seem to have an effect on drop size distribution and that this can be attributed either to no drop-drop coalescence, or to a large scatter in the data masking any small effect of the oil/water ratio on $\langle D_p \rangle_{32}$.

Consider the mixing valve pressure drop. With the mixing valve fully open, the drop size distribution is given by run 10. When the valve is closed the drop size distribution is given by runs 8 and 9 for P_1 = 52.95 and P_2 = 88.25 mm.Hg pressure drop, respectively. Figure IV-2 shows qualitatively what is occurring.

The three distributions show that large drops ($>100\,\mu$) are being broken up at the valve. The number of small drops ($<100\,\mu$) is therefore increased. This accounts for the increased percentage of small drops in the distribution as the mixing valve is closed.

The greater the pressure drop across the mixing valve, the more

FIGURE IV-2 EFFECT OF MIXING VALVE PRESSURE DROP ON FEED DROP SIZE DISTRIBUTION (OIL/WATER RATIO CONSTANT)

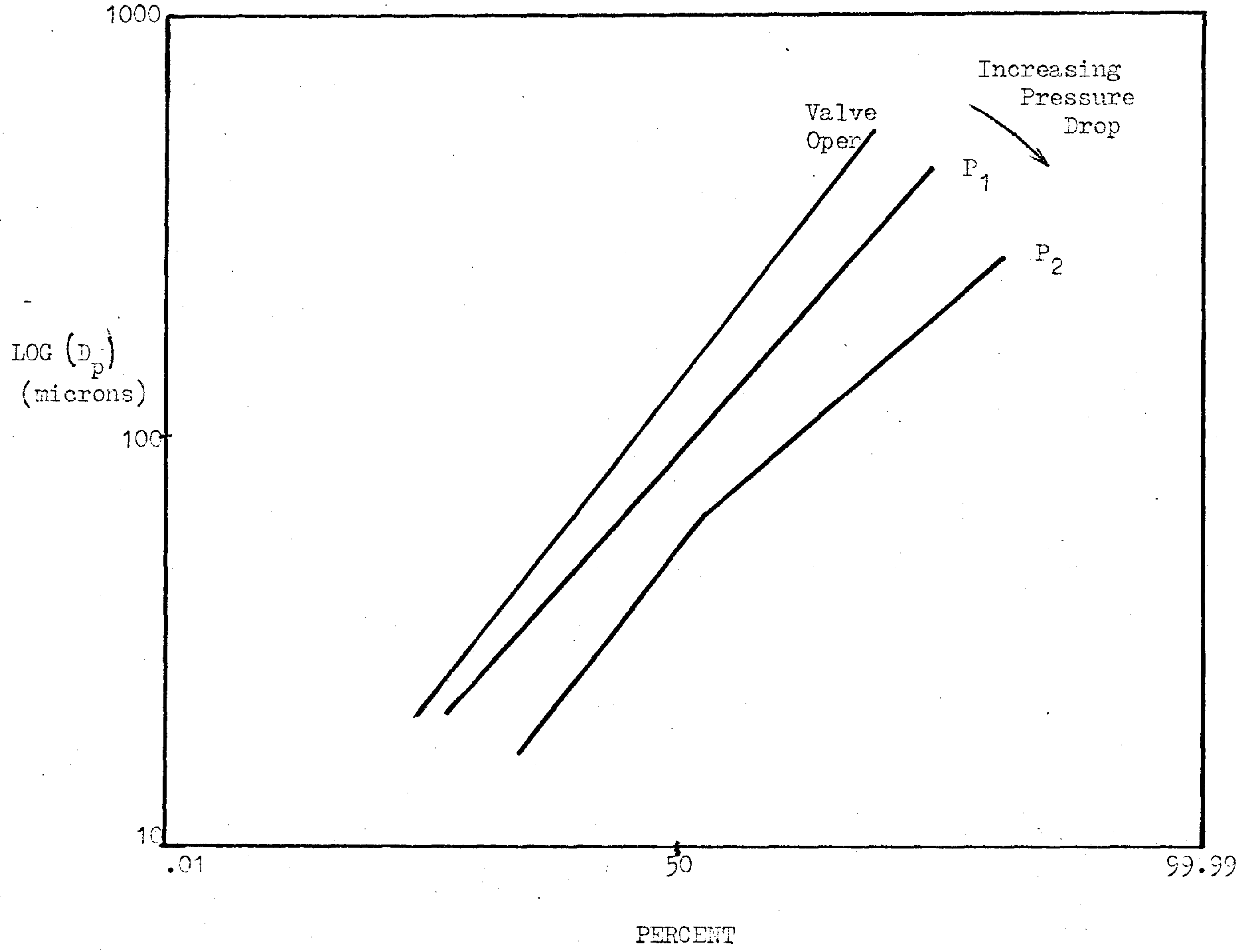

interfacial area produced (see (M-4)). Therefore the number of large drops in the distribution decreases with increasing pressure drop. In effect, two distinct drop size distributions are being created. This is quite evident from Figure IV-2. The experimental cumulative number distributions given in Appendix 3 show that the large drops deviate markedly from the log-normal distribution as defined by the small drops, when mixing valve pressure drop increases. Table IV-1 shows the changing number of drops observed in the photographic samples as pressure drop increases.

In connection with the work of Mugele and Evans (M-8), it is seen that the mixing valve serves to limit the maximum drop size. The fact that the cumulative number distributions given in Appendix 3 seem to asymptote maximum values of drop diameter indicates that there are "upper-limit" sizes in the drop size distributions. An example is shown in Figure IV-3. The distributions in this work are the type considered by Mugele and Evans for the "upper-limit" function that they propose. Their analysis was not used, however, since the Gwyn *et al* corrections were applied directly to the drop size distributions.

IV·c Effect of the Variables on Cyclone Efficiency

Details may be found in Appendix 3. Here a summary of the results are presented and an attempt is made to explain their significance.

IV·c·1 Statistical Results

The cyclone efficiency E_s (defined in Chapter 2) was experimentally determined as a function of the oil/water ratio (x_1), the volume split (x_2) and the feed drop size distribution (x_3). Regression of the data with a second order polynomial showed that the second order regression

TABLE IV-1 NUMBER OF DROPS OBSERVED AT VARIOUS SIZE INTERVALS FOR INCREASING MIXING VALVE PRESSURE DROP

	NUMBER OF DROPS COUNTED IN SIZE INTERVAL PER TOTAL OF 1000 DROPS OBSERVED		
SIZE INTERVAL (μ)	P = 17.65 mm.Hg	P = 52.95 mm.Hg	P = 88.25 mm.Hg
50 - 65	86	109	118
70 - 90	140	146	149
110 - 125	67	72	81
152 - 173	65	45	33
185 - 210	69	37	21

FIGURE IV-3 EXAMPLE OF DEVIATION OF LARGE DROPS FROM THE LOG-NORMAL DISTRIBUTION

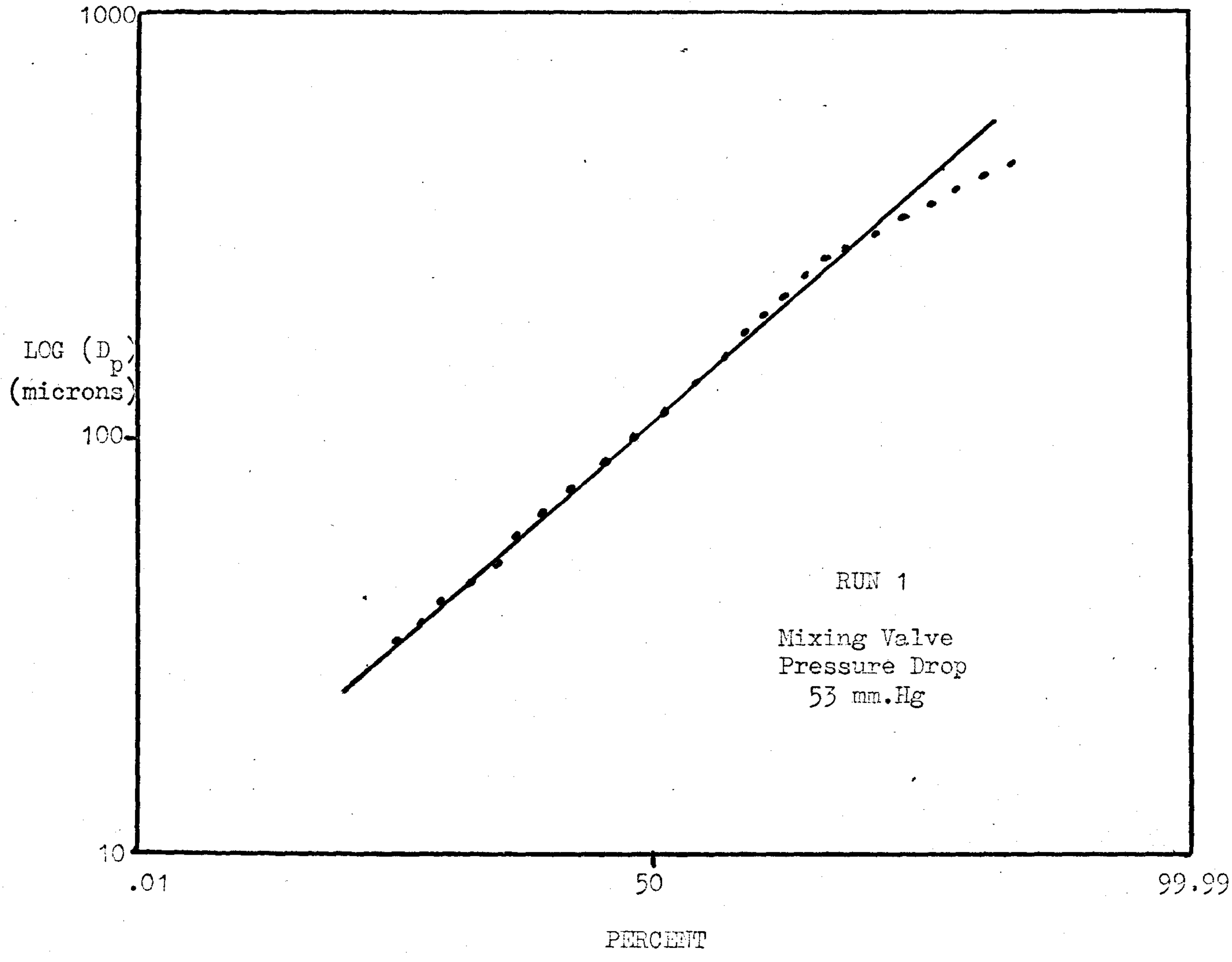

coefficients were not significantly different from zero at the 95% confidence level. A linear relation was subsequently fitted and this resulted in the following equation

$$E_s = 79.45 - 4.419x_1 - 8.837x_2 - 2.939x_3$$

where the values of the independent variables are coded from -2 to +2 as given in Table A3-6, and the cyclone efficiency is in percent. The multiple correlation coefficient for this equation is 0.959 which is significant at the 95% level.

Since the standard errors of the partial regression coefficients are equal here, the magnitude of the coefficients themselves gives an indication of the importance of the variables. Therefore, from the above expression, the variables can be listed in decreasing order of importance as:

Volume split (x_2)
Oil water ratio (x_1)
Drop size distribution (x_3)

This list of the variables is applicable only for the ranges of the variables studied in this work.

IV·c·2 Discussion of the Effect of Cyclone Variables on Efficiency

Since this work has been divided into two sections (1) determination of feed drop size distributions, and (2) measurement of hydrocyclone efficiencies, mention is made of whether $\langle D_p \rangle_{32}$ (Sauter mean diameter) changed with time. Each variable is considered in turn.

(i) Effect of Drop Size Distribution on Cyclone Efficiency

Drop size distribution was seen to be the least important of the three variables studied. Its effect on efficiency may be seen in Figure IV-4. These results do not contradict what would be expected, since the more small drops there are in the feed, the more small drops there are that go to the overflow.

The drop size distribution work was done over a period of three weeks. This was then immediately followed by efficiency measurements which took two weeks. Since $\langle D_p \rangle_{32}$ was determined four times for all variables constant, at the centre point of the experiment design, then any time trend in $\langle D_p \rangle_{32}$ should be apparent. Table IV-2 shows the runs done at the centre point in the order that they were carried out, and the resulting $\langle D_p \rangle_{32}$. Any time trend in $\langle D_p \rangle_{32}$ may be completely overshadowed by experimental error, and Table IV-2 indicates that this may be the case. Therefore it is reasonable to assume that $\langle D_p \rangle_{32}$ would remain close to the predicted values during the cyclone efficiency work.

The Sauter mean diameter $\langle D_p \rangle_{32}$ was chosen to represent the drop size distributions because it is directly related to the forces influencing separation in the cyclone. The concept of a particle being in equilibrium because the centrifugal force on it equals the drag force due to radial flow of liquid was presented in Chapter 2. The centrifugal force on a particle is a function of its mass, and therefore its volume. The drag force is directly proportional to the particle area normal to the direction of flow, and therefore the particle surface area. Since $\langle D_p \rangle_{32}$ is defined as:

$$\langle D_p \rangle_{32} = \frac{(6)(\text{sum of particle volumes})}{(\text{sum of particle surface areas})}$$

FIGURE IV-4 EFFECT OF FEED DROP SIZE DISTRIBUTION ON CYCLONE EFFICIENCY

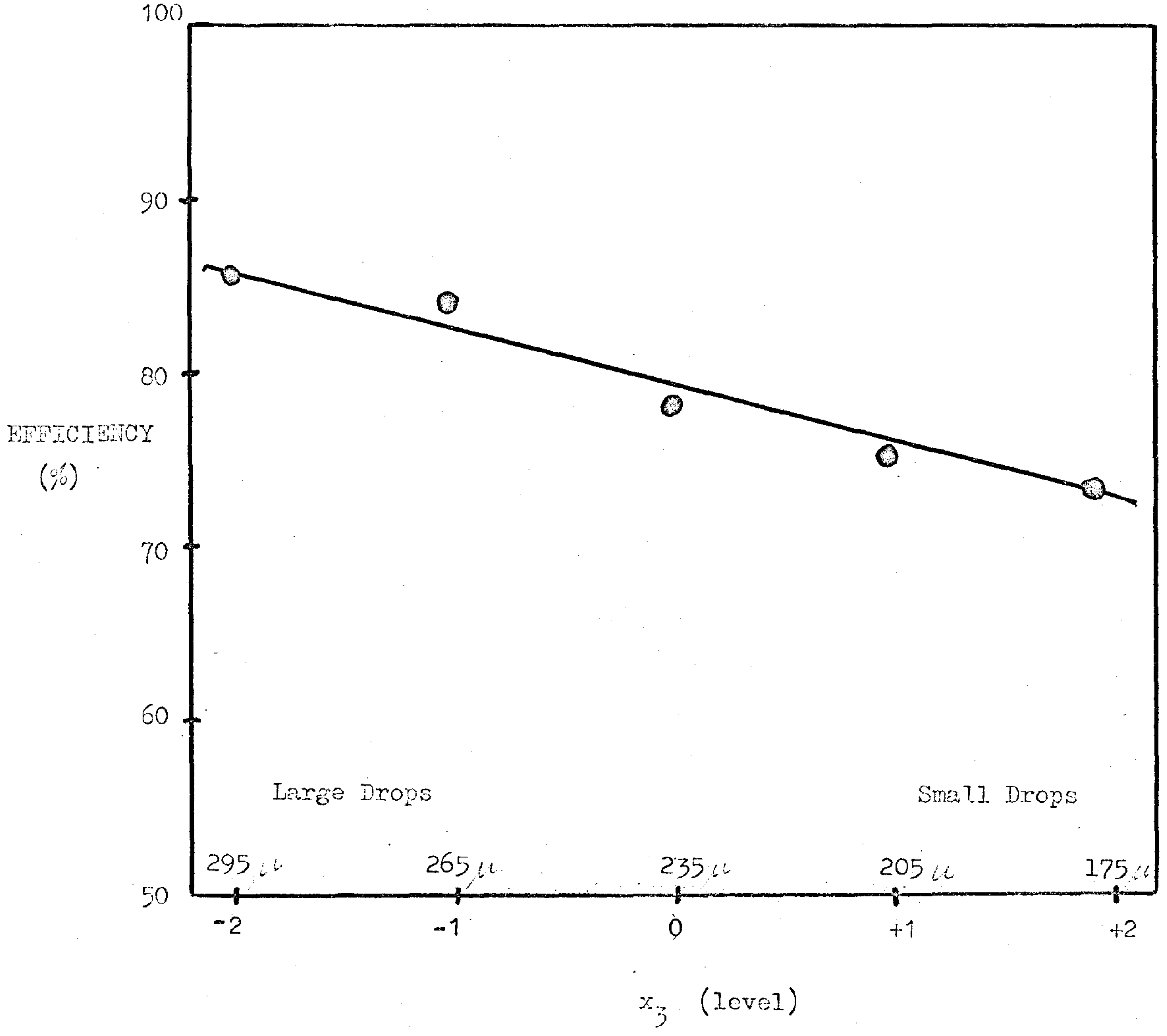

Data at zero levels for x_1 and x_2

Efficiencies for x_3 at -1 and +1 levels were determined by averaging efficiencies to give zero levels for x_1 and x_2.

TABLE IV-2 POSSIBILITY OF A TIME TREND IN THE VOLUME/SURFACE DIAMETER $\langle D_p \rangle_{32}$

RUN (in order done)	$\langle D_p \rangle_{32}$ (μ)
1	212.1
2	223.2
7	230.5
8	199.6

Standard deviation at centre point is 13.5 μ .

it is a direct measure of the forces acting on a drop. A small $\langle D_p \rangle_{32}$ indicates small drops, high drag, and hence many small drops in the cyclone overflow. A high $\langle D_p \rangle_{32}$ indicates large drops, predominance of centrifugal force, and few drops in the overflow.

Consideration will now be given to a calculation of the immiscible oil concentration in the overflow to see whether this concentration increases as the Sauter mean diameter decreases. First consider the observation that the underflow is never completely oil, but is always a mixture of oil in water, even though the underflow rate is less than the oil being separated. This infers that there is little or no drop-drop coalescence. Now consider a sample calculation of the overflow oil concentration.

Data

All variables at the zero level.

Q_1 = 4.042 IGPM

Q_2 = 3.465 IGPM

Q_3 = 0.577 IGPM

Q_{oil} = 0.594 IGPM

Q_{water} = 3.448 IGPM

Assuming $(D_p)_{50}$ = 40μ, it is found by using the particle size classification curve that 0.003 IGPM of oil pass to the cyclone overflow because of drops too small to be separated by the cyclone.

Assuming that the underflow will never have less than 15% void space between the oil drops, then:

water in underflow = .15x.577 = .086 IGPM

oil to underflow = .577 - .086 = .490 IGPM

Therefore oil to overflow is

$$.594 - .490 = 0.104 \text{ IGPM}$$

Therefore, calculated overflow oil concentration becomes

$$\frac{0.104}{3.465} \times 100 = 3.0\% \text{ oil}$$

Similarly, the overflow oil concentration for other levels of the drop size distribution can be found, assuming constant 15% water in the underflow when the underflow rate is less than the oil being separated. The results of these calculations are given in Table IV-3.

Since a constant underflow water percentage was assumed, all calculated overflow oil concentrations are equal. This is because the underflow void fraction has been assumed independent of drop size distribution (which it is not), and because the 0.003 IGPM of oil going to the overflow is not sensitive to changes in feed drop size distribution.

The explanation of the differences between the observed and calculated overflow oil concentrations is as follows. Uniform spheres, hexagonally packed, will have a void space of 26% (C-2). If there is a size distribution of spheres, small spheres may fit in the void spaces left by the packing of larger spheres. The greater the variation in the sphere sizes, the smaller the void space will become.

The drop size distribution becomes more uniform as the level of x_3 increases (-2 level to the +2 level). Therefore, the water in the voids is less than 15% for the drop size distribution at the -2 level, and greater than 15% at the +2 level. Hence, at the -2 level, more oil will go out the underflow than was assumed, and so less oil will go to the overflow. At the +2 level, less oil goes out the underflow

TABLE IV-3 OIL CONCENTRATION IN CYCLONE OVERFLOW AS A FUNCTION OF DROP SIZE DISTRIBUTION, ASSUMING 15% WATER IN UNDERFLOW

LEVEL OF x_3	OBSERVED % OVERFLOW OIL CONCENTRATION	CALCULATED % OVERFLOW OIL CONCENTRATION
-2	2.32	3.00
-1	2.38	3.00
0	3.25	3.00
+1	3.42	3.00
+2	3.83	3.00

x_1 and x_2 at zero level

than was assumed, and so more oil will go to the overflow.

This explanation of the observed results is dependent on no drop-drop coalescence. First, measurements made on drop drag showed that surface active agents were present in the carbon tetrachloride/water system used. This is sufficient to prevent drop-drop coalescence. It should also be pointed out that carbon tetrachloride drops did not wet the walls of the glass cyclone. Therefore no layer of oil would be present at the cyclone wall, even if drops did coalesce. Finally, the overflow drop size distribution was photographed, and is given in Figure IV-5. To explain this observed distribution, consider Figure IV-6. Small feed droplets fed at the cyclone wall may not reach their equilibrium envelopes and therefore may exit at the cyclone underflow. Thus the rising mixture of droplets at A contains both small drops and large drops which are unable to pass out the underflow. Assuming no drop-drop coalescence, the dispersion at A is similar to the feed dispersion. Since it is known that 17% of the feed oil is unable to go out the underflow when all variables are at the zero level, the overflow drop size distribution may be calculated if a $(D_p)_{50}$ value is known. Figure IV-5 shows that for a $(D_p)_{50}$ of 25μ and for a percent feed oil to overflow of 15%, the best fit is obtained. Table IV-4 gives a summary of the curve fits obtained for various conditions.

The prediction of the overflow drop size distribution is further evidence for no drop-drop coalescence. It is also further evidence that $(D_p)_{50}$ is about 25μ.

FIGURE IV-5 OBSERVED AND PREDICTED OVERFLOW DROP SIZE DISTRIBUTION

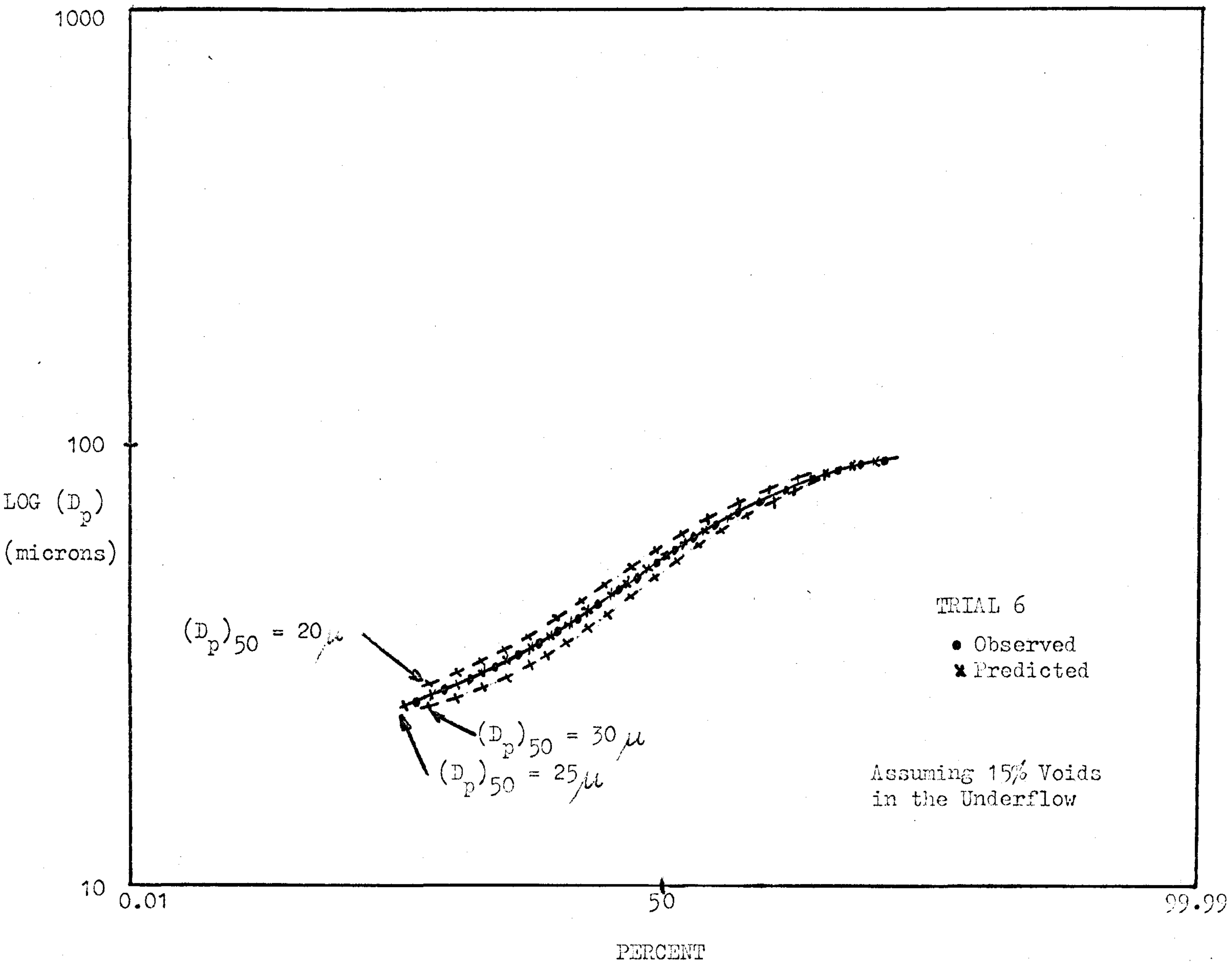

FIGURE IV-6 SCHEMATIC REPRESENTATION OF OIL DROPS AT THE CYCLONE UNDERFLOW

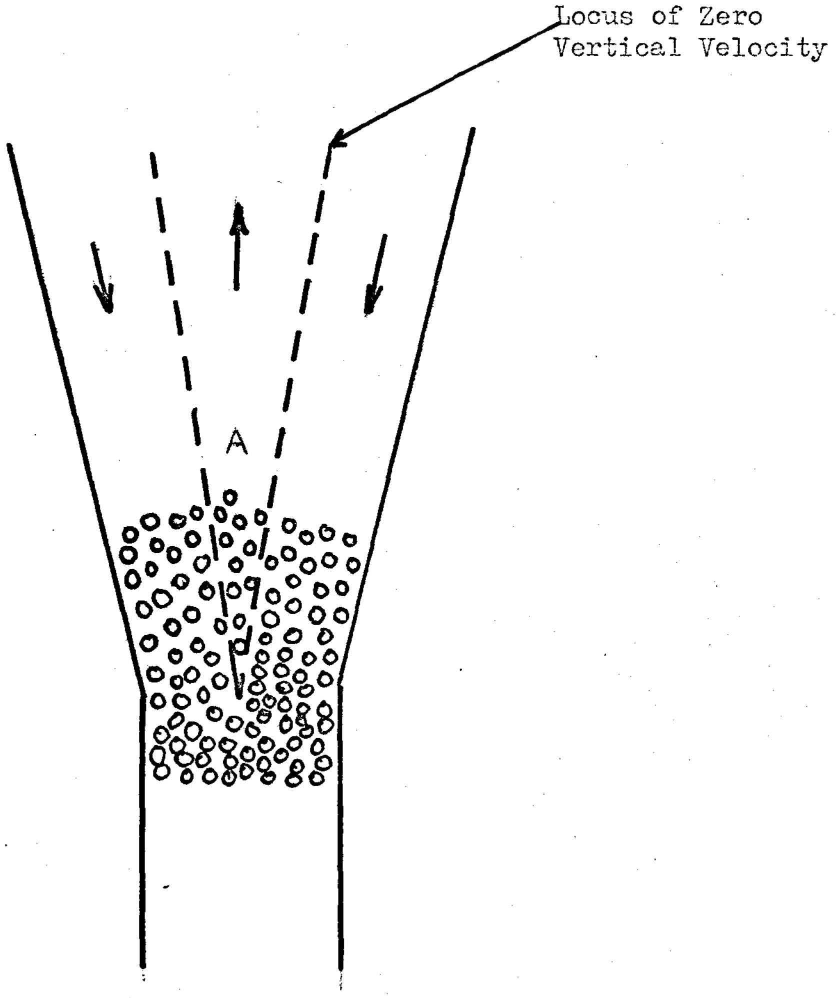

TABLE IV-4 SUMMARY OF CURVE FITS FOR VARIOUS VALUES OF $(D_p)_{50}$ AND OF PERCENT FEED OIL TO OVERFLOW

$(D_p)_{50}$ used	Effect of $(D_p)_{50}$ and % Oil to Overflow on fit		
	10%	15%	20%
20 μ	4	3	4
25 μ	2	1	2
30 μ	4	3	4

1 Excellent fit

2 Good

3 Fair

4 Poor

(ii) Effect of Oil/Water Ratio on Cyclone Efficiency

The feed oil/water ratio was seen to be the second most important variable. Its effect on hydrocyclone efficiency may be seen in Figure IV-7. Intuitively, if the fraction of oil in the feed rises, then the greater the amount of oil in the overflow will be, for the same volume split.

The overflow oil concentration may be calculated in the same manner as before. The calculated values along with observed overflow oil concentrations are given in Table IV-5. Considering the possible errors in determining flow rates and sample compositions, the calculated and observed overflow oil concentrations are in reasonable agreement.

(iii) Effect of Volume Split on Cyclone Efficiency

The volume split was seen to be the most important variable of the three variables studied. Its effect on hydrocyclone efficiency is shown in Figure IV-8.

The overflow oil concentration may be calculated as before, assuming a constant 15% water in the underflow. The results are given in Table IV-6. Once again the agreement between observed and calculated overflow oil concentrations is reasonable, considering the possible measurement errors.

Cyclone efficiency is seen to be highest for a volume split of 4/1 (the -2 level). However, as the volume split is further reduced to 3/1 and 2/1, more water will appear in the underflow and efficiency should pass through a maximum at some point. Since essentially no oil was present in the cyclone overflow (0.10%) at a volume split of

FIGURE IV-7 EFFECT OF OIL/WATER RATIO ON CYCLONE EFFICIENCY

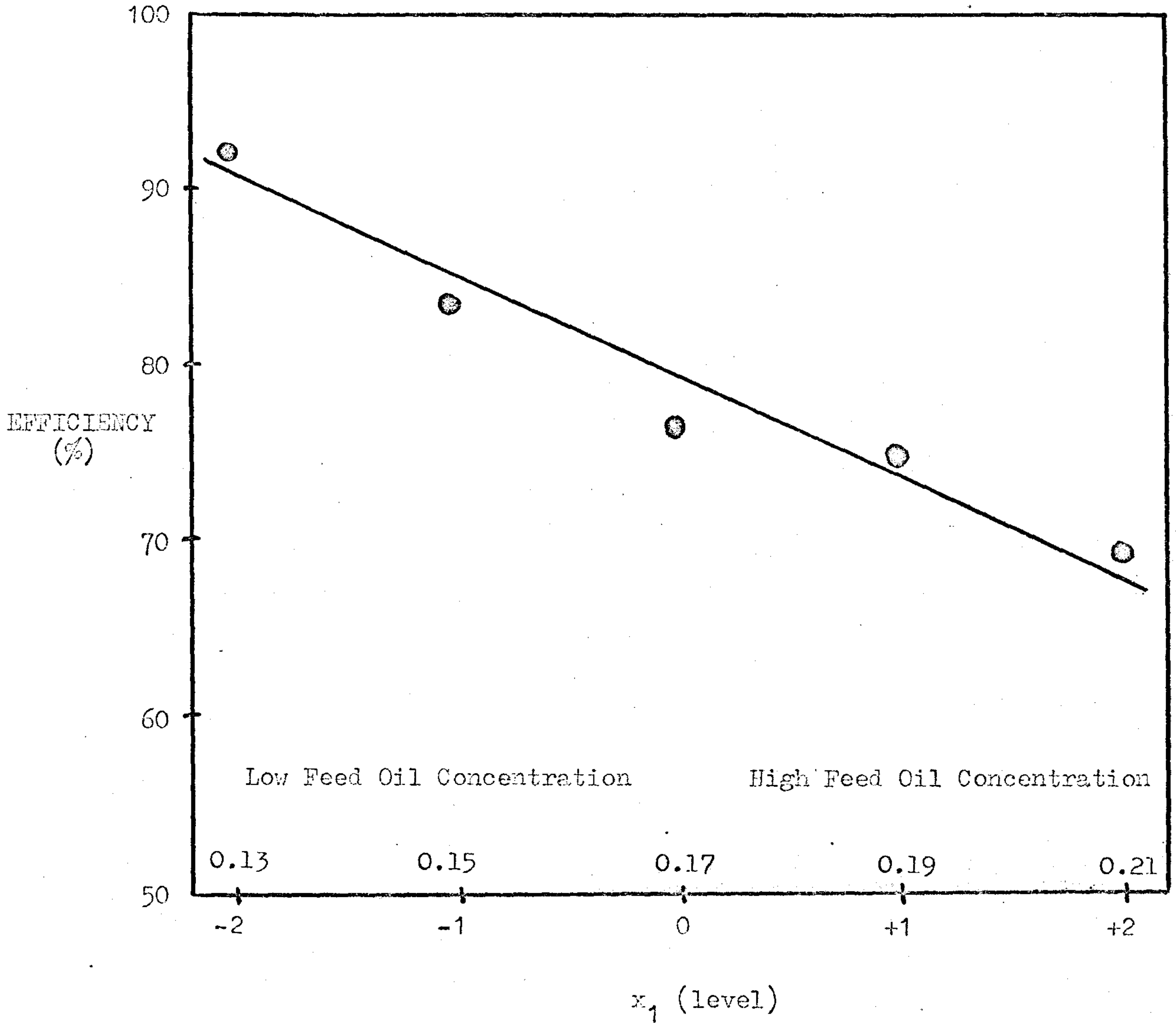

Data at zero levels for x_2 and x_3

TABLE IV-5 OIL PERCENTAGE IN CYCLONE OVERFLOW AS A FUNCTION OF OIL/WATER RATIO, ASSUMING 15% WATER IN THE UNDERFLOW

LEVEL OF x_1	OBSERVED % OIL IN OVER-FLOW	CALCULATED % OIL IN OVERFLOW
-2	.65	0.10
-1	2.02	1.36
0	3.25	3.00
+1	3.78	4.82
+2	5.57	6.46

x_2 and x_3 at zero level

FIGURE IV-8 EFFECT OF VOLUME SPLIT ON CYCLONE EFFICIENCY

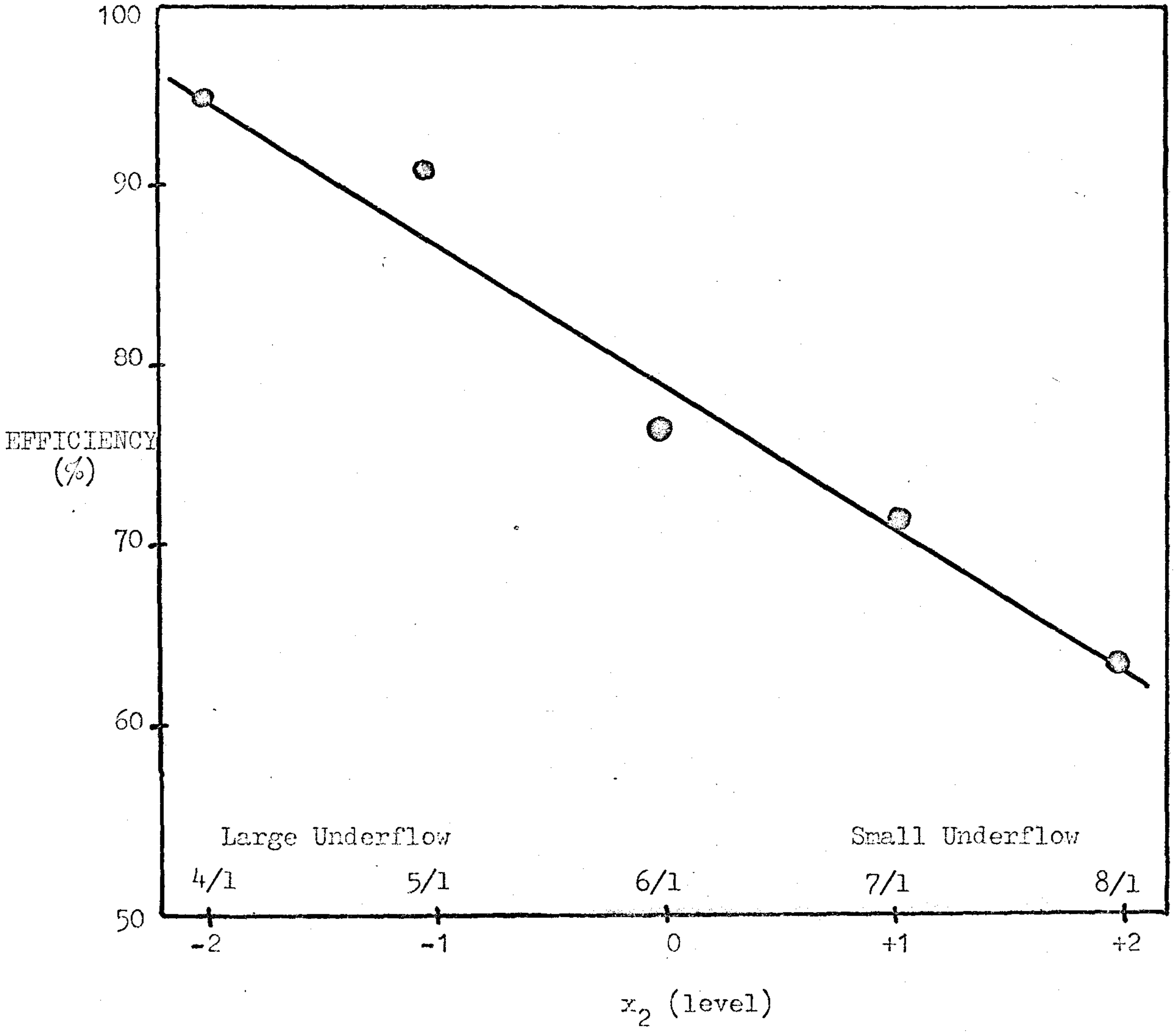

Data at zero levels for x_1 and x_3

TABLE IV-6 OIL PERCENTAGE IN CYCLONE OVERFLOW AS A FUNCTION OF VOLUME SPLIT, ASSUMING 15% WATER IN UNDERFLOW

LEVEL OF x_2	OBSERVED OIL CONCENTRATION VOLUME %	CALCULATED OIL CONCENTRATION VOLUME %
-2	0.06	0.10
-1	1.10	0.63
0	3.25	3.00
+1	4.69	4.67
+2	5.50	5.91

x_1 and x_3 at zero level

4/1, further reducing volume split will result in even less oil in the overflow. Efficiencies for volume splits of 3/1 and 2/1 (-3 and -4 levels) can then be calculated. These calculations are summarized in Table IV-7, and the efficiencies are plotted in Figure IV-9. Cyclone efficiency is seen to pass through a maximum for a volume split of 4/1 (-2 level).

This is easily explained. The underflow was seen never to be pure oil, but always a mixture of oil drops in water. Although the underflow rate equals the oil feed rate (all oil assumed to be separated) at a volume split of 5.8/1, the underflow always contains water, so at this volume split some oil goes to the overflow. When all the oil can go out the underflow, efficiency should reach a maximum, which is roughly at a volume split of 4/1. This is similar to the argument of Simkin and Olney (S-3) who point out that cyclone efficiency is a maximum when that phase which is in the largest quantity is also purest. This can be deduced from the efficiency definition,

$$E_s = \frac{Q_2}{Q_1}\left[\frac{y_2 - y_1}{1 - y_1}\right] + \frac{Q_3}{Q_1}\left[\frac{y_1 - y_3}{y_1}\right]$$

since the first term is the largest, and since the efficiency is relatively insensitive to changes in y_3 because the second term is small. Efficiency would seem to be a maximum when y_2 was approximately unity.

This section has shown that for maximum overall cyclone efficiency, there is an optimum volume split. Unfortunately, this volume split can not be predicted because the oil wets the glass cyclone wall and because there is no drop-drop coalescence.

If the feed drop size distribution is known, a mixture of solid

TABLE IV-7 EFFICIENCY CALCULATIONS FOR VOLUME SPLIT AT THE -3 AND -4 LEVELS

VARIABLES	VOLUME SPLIT 3/1	VOLUME SPLIT 2/1
	-3 LEVEL OF VOLUME SPLIT	-4 LEVEL OF VOLUME SPLIT
Q_1, IGPM	4.042	4.042
Q_2, IGPM	3.032	2.695
Q_3, IGPM	1.010	1.347
y_1	0.855	0.855
y_2	1.00	1.00
y_3	0.411	0.560
Efficiency %	88.0	78.2

Assuming no oil in overflow, underflow is all feed oil plus water not going out overflow.

Q_{oil} = 0.594 IGPM

Q_{water} = 3.448 IGPM

FIGURE IV-9 EFFECT OF VOLUME SPLIT ON CYCLONE EFFICIENCY FOR VOLUME SPLIT DECREASED TO 2/1 (-4 LEVEL)

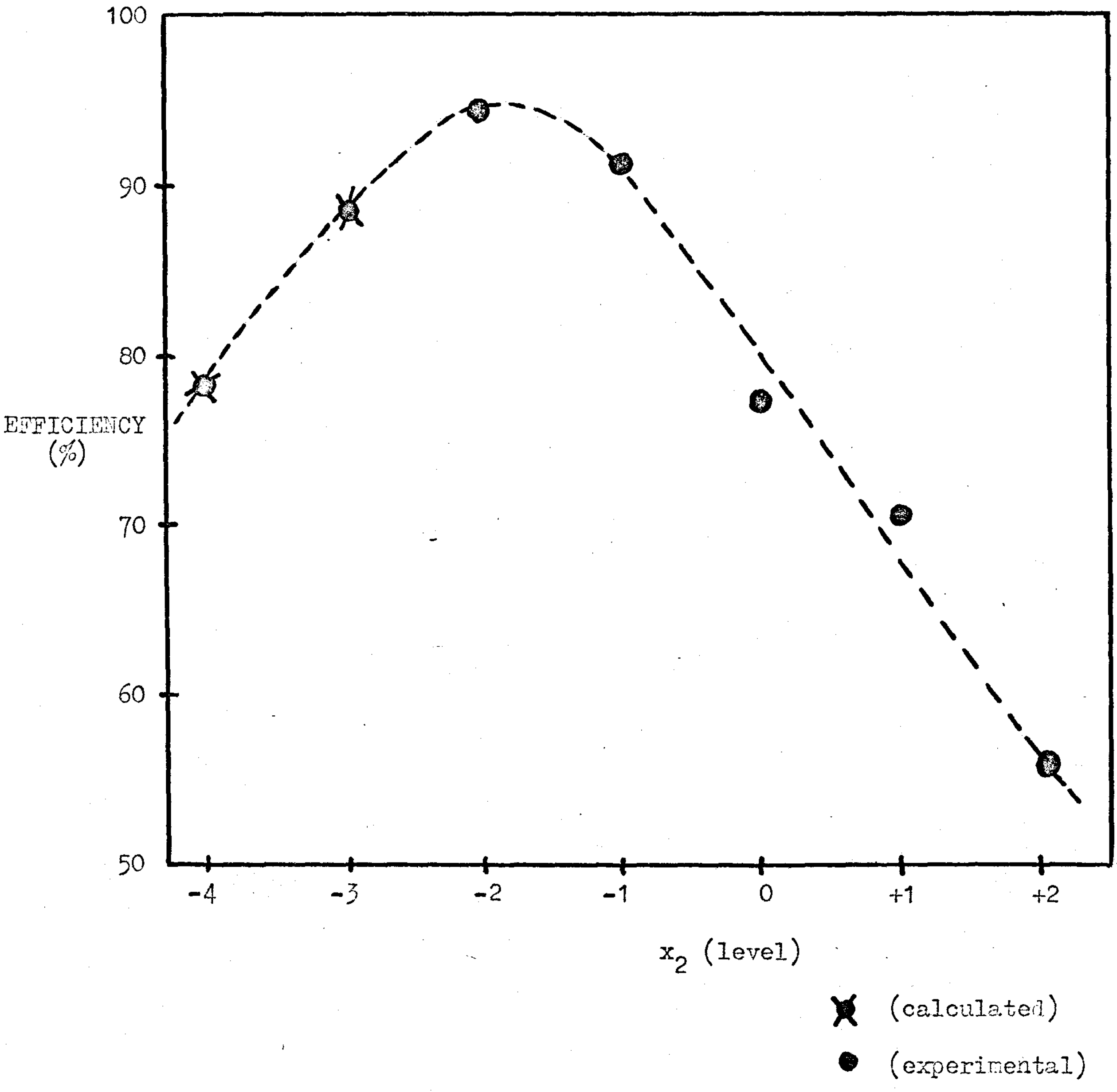

x_1 and x_3 at zero level

Feed 0.855 volume fraction water

spheres can be made having the same size distribution. The spheres may be a factor of 10 or 20 larger in diameter, but if the void space for this mixture is determined experimentally, this void fraction may be used to estimate the water that will appear at the underflow.

IV·c <u>Summary</u>

This work was not intended to be exhaustive, but rather it was used as a means to study those few cyclone operating variables that were felt to be most important for a liquid/liquid feed. No quantitative statements regarding the applicability of the results of this work to other cyclones can be made since only one cyclone of one particular design was used, with only one liquid/liquid system. However this work has brought out several points, and they will be briefly touched on.

Using an oil which does not wet the cyclone walls means water will always appear at the cyclone underflow because the oil is always dispersed as drops. If the heavy oil wets the cyclone walls, it is possible that pure oil may appear at the underflow.

A 'dirty' liquid/liquid system means no drop-drop coalescence. Therefore, the amount of water in the underflow will depend on the drop size distribution. If there is drop-drop coalescence, the amount of water in the underflow will be decreased as the underflow rate is decreased.

Surprisingly, no short circuit flow was observed in this work. (Short circuit flow is the by-passing of feed from the feed inlet, across the cyclone roof and down the vortex finder wall to the overflow.) The presence of short circuit flow would be indicated by large overflow oil concentrations. Perhaps the inlet feed pressure was not large enough to cause short circuiting in this work.

V CONCLUSIONS

V CONCLUSIONS

Conclusions reached from the drop size measurement work are now given.

1. Various volume ratios of carbon tetrachloride in water were passed at a constant velocity through a mixing valve whose opening was measured by the pressure drop across it. The mixing valve served to convert the feed pressure energy into new drop surface energy. The pressure drop across the mixing valve, for a constant flow rate, is a measure of the change in drop surface energy. It was found that a linear relation existed between the mixing valve pressure drop and the volume/surface diameter $\langle D_p \rangle_{32}$ of the drop size distribution. The oil/water ratio effect on $\langle D_p \rangle_{32}$ was not statistically significant at the 95% confidence level. A linear relationship between mixing valve pressure drop and $\langle D_p \rangle_{32}$ was also obtained by Simkin and Olney (S-3), and Holland _et al_ (M-4) found that the oil/water ratio was also not important in determining $\langle D_p \rangle_{32}$.

2. The drop size distributions obeyed the log-normal law, but as the pressure drop across the mixing valve was increased, the large drops were broken up. This resulted in two log-normal distributions. At the largest mixing valve pressure drop, however, the two distributions could still be represented by one log-normal distribution.

Conclusions reached from the cyclone separation study are given below.

1. When a feed mixture of carbon tetrachloride in water at a particular oil/water ratio and drop size distribution is sent to a hydrocyclone

operating at a given volume split, the efficiency of separation could be experimentally determined. A linear relation was found to exist between the separation efficiency and the above three variables. Interactions between the variables were found not to be statistically significant at the 95% confidence level.

2. The three variables can be listed in decreasing order of importance for the range of variables studied as:

a.) volume split

b.) oil/water ratio

c.) drop size distribution

3. The underflow was always found to be a mixture of oil droplets in water, and never pure oil. This suggested no drop-drop coalescence in the hydrocyclone. A $(D_p)_{50}$ value was calculated using available correlations, and by assuming a constant void space between droplets at the underflow, and by assuming no short circuit flow, the cyclone separation could be predicted. The overflow drop size distribution was also predicted and it compared closely with the overflow distribution measured.

The assumption of no short circuit flow is justifiable because its existence would lead to larger overflow oil concentrations than those observed. Kelsall (K-1) found that 15% of his feed short circuited.

4. In this work, it was found that $(D_p)_{50}$ was about 25 microns. Only about 5% of the total number of drops observed in the feed distributions were less than this size, and therefore $(D_p)_{50}$ was not found to be very important. Withdrawing less oil at the underflow than the amount in

the feed was important, and this was controlled by the volume split.

NOMENCLATURE

NOMENCLATURE

A	=	drop interfacial area per unit volume of mixture
A'	=	weighting factor in chi-square test
C_D	=	drag coefficient
D	=	inside diameter
$\langle D_g \rangle$	=	geometric mean diameter
D_p	=	particle diameter
$\langle D_p \rangle_{20}$	=	mean surface diameter
$\langle D_p \rangle_{30}$	=	mean volume diameter
E_s	=	hydrocyclone efficiency (defined in A3)
F_c	=	centrifugal force
F_D	=	drag force
g	=	gravitional acceleration
L	=	height of cyclone
L_i	=	height of imaginary cone (Figure (A4-2))
P	=	pressure
ΔP_t	=	total cyclone pressure drop
Q	=	flow rate
r	=	radius
V	=	velocity
V_i	=	inlet velocity in cyclone at mean radius of entry
V_C	=	tangential fluid velocity near cyclone wall in the feed inlet section
V_T	=	tangential velocity

V_R = radial velocity

v_t = particle terminal velocity

$\langle D_p \rangle_{32}$ = volume/surface diameter for spherical drops

y = volume fraction water

Greek Letters

σ_g = standard deviation of log-normal drop size distribution

ρ_s = particle density

ρ_c = continuous phase density

μ_c = continuous phase viscosity

ϕ = volume fraction dispersed phase per unit volume of mixture

μ = micron

Subscripts

1 = at cyclone inlet

2 = at cyclone overflow

3 = at cyclone underflow

C = cyclone (ie D_C = cyclone diameter)

c = continuous phase

s = solid phase

p = particle

Other

$\langle \; \rangle$ = average

BIBLIOGRAPHY

BIBLIOGRAPHY

A-1 Andreas, J.M. et al J.Phys.Chem. 42 1001 (1938).

B-1 Bergman, W.E. et al "Liquid Cyclone Cuts Cost of Treating Drilling Fluids" Oil and Gas J. (Oct. 15) 114-116 (1956).

B-2 Bradley, D. "Theoretical Correlation of the Efficiency of Hydraulic Cyclones" AERE-CE/M 211 (1957)

B-3 Bradley, D. "The Hydraulic Cyclone as a Liquid-liquid Contactor and Separator" AERE-CE/M 177 (1957).

B-4 Bradley, D. "A Theoretical Study of the Hydrocyclone" Ind.Chem. 34 473 (1958)

B-5 Bradley, D. and D.J. Pulling "Flow Patterns in the Hydraulic Cyclone ..." Trans.Inst.Ch.Engrs 37 34-45 (1959)

B-6 Bressee, J.C. "Design and Performance of a Dual-Clone Liquid Separator" ORNL-CF-56-3-171, (1956).

C-1 Cerny, J. "Hydrocyclone Performance in the Solvent Recovery System of the Thorex Pilot Plant" ORNL-CF-58-3-8, (1958).

C-2 Clayton, W. "The Theory of Emulsions" pg. 136, Blakiston, Philadelphia (1935).

C-3 Crowe, E.L. et al "Statistics Manual" Dover, New York (1960).

D-1 Dahlstrom, D.A. Mining Transactions 184 331 (1949).

D-2 Dahlstrom, D.A. and J.J. Moder C.E.P. 48 (2) 75-88 (1952).

D-3 Dallavalle, J.M. "Micrometrics", pg. 60, Pitman, New York (1948).

D-4 Darby, G.M. "Classification in Hydrocyclones" Ceramic Bulletin 34 (9) 287-290 (1955).

D-5 Davies, J.T. "Mass Transfer and Interfacial Phenomena" Adv.in Chem.Eng. Vol.4 pg 36 (1963).

E-1 Ellefson, R.R. M.Sc. Thesis, Northwestern (1953).

G-1 Gwyn, J.E., E.J. Crosby, and W.R. Marshal,Jr. "A Consideration of Bias in Particle-Size Analyses by the Count Method" I.E.C.Fund. 4 204-8 (1965).

H-1 Herdan, G. "Small Particle Statistics" Academic Press, London (1960).

H-2 Hitchon, J.W. "Cyclones as Liquid-liquid Contactor-Separators" AERE-CE/R 2777 (1959).

H-3 Hodgson, T.D. Ph.D. Thesis, Swansea (1966).

H-4 Hughes, R.R. et al "Flash Vaporization" C.E.P. 49 (2) 78-87 (1953).

H-5 Hunter, J.S. "Some Applications of Statistics to Experimentation" C.E.P. Symposium Series 56 (#31) 10-26 (1960).

K-1 Kelsall, D.F. "A Study of the Motion of Solid Particles in a Hydraulic Cyclone" Trans.Inst.Ch.Engrs 30 87-103 (1952).

K-2 Kelsall, D.F. "A Further Study of the Hydraulic Cyclone" Chem. Eng. Sci 2 254-272 (1953).

K-3 Klein, F.G. M.Sc. Thesis, Northwestern (1951).

K-4 Kriijgsman, C. "Results of Experimental and Full Scale Operation of Hydrocyclones" Chem. Ing. Tech. 23 (22) 540-2 (1951).

K-5 Kottler, F. "The Distribution of Particle Sizes" J.Franklin Inst. 250 419-441 (1950).

L-1 Lilge, E.O. "Hydrocyclone Fundamentals" Bull.of Inst.Minning and Met. 71 288 (1962).

L-2 Lindner, E. "On the Separation of Solid Particles from Liquids by Hydrocyclones" Monthly Tech. Review 2 (1) 5-12 (1958).

L-3 Linton, M. and K.L. Sutherland "Second International Conference on Surface Activity", Vol.1, pg. 495.

M-1 Mason, S.G. and M.A. Nawab "The Viscosity of Dilute Emulsions" Trans.Faraday Soc. 54 (431 1-12 (1958).

M-2 Mason, S.G. and C.E. Chaffey "Energy Dissipation in Emulsion Drops in Shear Flow" J.Colloid and Interface Sci. 21 (2) 254-5 (1966).

M-3 McCarroll, S.J. "Cyclone Classification and Thickening at Manganese, Inc." Mining Congress J. (July) 50-51 (1956).

M-4 McDonough, J.A. et al "Formation of Interfacial Area in Immiscible Liquids by Orifice Mixers" A.I.Ch.E.J. 6 (4) 615-618 (1960).

✓M-5 Mitzmager, A. and J. Mizrahi "Correlation of the Pressure Drop Through Small Cyclones Operating with Dilute Pulps of Various Liquids" Trans.Inst.Chem.Engrs 42 T 152-7 (1964).

✓ M-6 Mizrahi, J. "Separation Mechanisms in Dilute Pulp Hydrocyclone Classifiers" Brit.Chem.Eng. 10 (10) 686-692 (1965).

M-7 Molyneux, F. "Extraction in the Hydraulic Cyclone" Chem.and Process Eng. 502-510.

M-8 Mugele, R.A. and H.D. Evans "Droplet Size Distribution in Sprays" I.E.C. 43 (6) 1317-1324 (1951).

O-1 Olney, R.B., Personal Communication, March 4, 1966.

O-2 Osipow, L.I. "Surface Chemistry" pg. 309 Rheinhold, New York (1962).

R-1 Rekemeyer, P.C. et al Monthly Progress Report, ORNL-CF-56-11-143 (1956)

R-2 Rietema, K. Chem.Eng.Sci. 15 298-325 (1961).

S-1 Sauter, J. "Determining Size of Drops in Fuel Mixture of Internal Combustion Engines" Zeitschrift des Vereines deutscher Ingenieure, July 31, 1926, 1040-1042.

S-2 Siggia, S. and J.G. Hanna "Analysis of Three Component Systems Containing Two Mutually Immiscible Components" Anal.Chem. 21 (9) 1086-1089 (1949).

S-3 Simkin D.J. and R.B. Olney "Phase Separation and Mass Transfer in a Liquid-liquid Cyclone" A.I.Ch.E.J. 2 (4) 545-551 (1956).

S-4 Simms, R. "High Speed Contactor" ORNL-CF-59-10-136 (1959).

S-5 Sleicher, C.A., Jr. "Maximum Stable Drop Size in Turbulent Flow" A.I.Ch.E.J. 8 (4) 471-77 (1962).

T-1 Tengbergen, H.J. and K. Rietema "Efficiency of Phase Separations" 23-32, Cyclones in Industry, Elsevier, Amsterdam (1961).

T-2 Tepe, J.B. and K.W. Woods U.S.A.E.C. Report A.E.C.D. 2864 (Jan.1943).

T-3 Ter Linden, A.J. "Cyclone Dust Collectors" Engineering (Feb.18) 165-168 (1949).

V-1 Van Rossum, J.J. "Separation of Emulsions in a Cyclone" Cyclones in Industry (ed. Rietema) pg. 110-117, Elsevier, New York (1961).

V-2 Van Slyke, W.R. "Heavy-Media Cyclones in Iron Ore Beneficiation" Mining Congress J. 48 (Jan.) 41-45 (1962).

W-1 Whatley, M.E. "Liquid Cyclone Contactor" U.S. Patent 3,052,361 (1962).

W-2 Wise, M.E. "Converting a Number Distribution of Particle Size into One for Volume or Surface Area" Philips Res.Rep. 9 231-237 (1954).

Y-1 Yancey, H.F. "Cyclone Washers for Fine Coal" Coal Age (Dec.) 118-121 (1958).

Y-2 Yeh, G.C. et al "Phase Volume Relationship at the Point of Phase Inversion in Liquid Dispersions A.I.Ch.E.J. 10 (2) 260-265 (1964).

Y-3 Yoshioka, N. and Y. Hotta Chem.Eng. (Japan) 19 632 (1955).

APPENDIX 1 PHYSICAL PROPERTY DETERMINATION

A1 PHYSICAL PROPERTY DETERMINATION

A1·a The Need for Pure Liquids

For a liquid/liquid feed to a hydrocyclone, there may be two separation mechanisms operating: sedimentation, and coalescence. Since coalescence is very sensitive to impurities, an attempt is made here to show the effect of impurities on the physical properties of the carbon tetrachloride/water system used.

Properties measured were:

(1) Density

(2) Refractive Index

(3) Viscosity

(4) Interfacial Tension

(5) Mutual Solubility

A1·b Physical Property Measurements

A1·b·1 Density

Densities were found for pure carbon tetrachloride (spectroscopic grade) and for distilled water, besides for the liquids used in the cyclone. The liquids were placed in flasks which were immersed in a water bath at 25°C. Then a 10 ml. specific gravity bottle was filled with the liquid of interest at 25°C and quickly weighed using an analytical balance.

Densities measured are in Table A1-1.

A1·b·2 Refractive Index

An Abbey refractometer connected to a 25°C water bath, with

TABLE A1-1 TABLE OF THE DENSITY, REFRACTIVE INDEX AND VISCOSITY OF THE CARBON TETRACHLORIDE/WATER SYSTEM

LIQUID	DENSITY @ 25°C gm/ml.	REFRACTIVE INDEX @ 25°C	VISCOSITY @ 25°C cp.
Distilled water	0.9971	1.3338	0.8937
* Tank water	0.9974	1.3338	0.8937
Pure Carbon tetrachloride	1.58621	1.4582	0.910
Tank Carbon tetrachloride	1.58315	1.4582	0.915

* 'Tank' refers to the liquid used in the hydrocyclone study.

white light, was used to determine the liquid refractive indices.

Refractive indices are in Table A1-1.

A1·b·3 Viscosity

An Ostwald viscometer, thoroughly cleaned with chromic acid, and immersed in a water bath at 25°C, was used to measure viscosities.

The viscosity of the fluids was calculated by relating the measured efflux times to the efflux times for a reference material through the following relationship:

$$\frac{\mu_1}{\mu_2} = \frac{\rho_1 t_1}{\rho_2 t_2}$$

where μ = viscosity

ρ = density

t = time for the liquid level to fall between two reference marks on the viscometer

The Handbook of Physics and Chemistry gives the viscosity of water at 25°C as $\mu_1 = 0.8937$ cp.

Therefore, from the densities and the efflux times, the viscosities can be calculated, and are given in Table A1-1.

A1·b·4 Interfacial Tension

The experimental apparatus for determination of interfacial tension by the pendant drop method is best described by Figure A1-1. The method entails measuring two diameters of the drop, d_e and d_s. This is shown in Figure A1-2. From these two diameters, the interfacial tension can be calculated from the table given by Andreas (A-1).

Aside from a slight fuzziness at the drop edge on the

FIGURE A1-1 EQUIPMENT FOR INTERFACIAL TENSION MEASUREMENTS

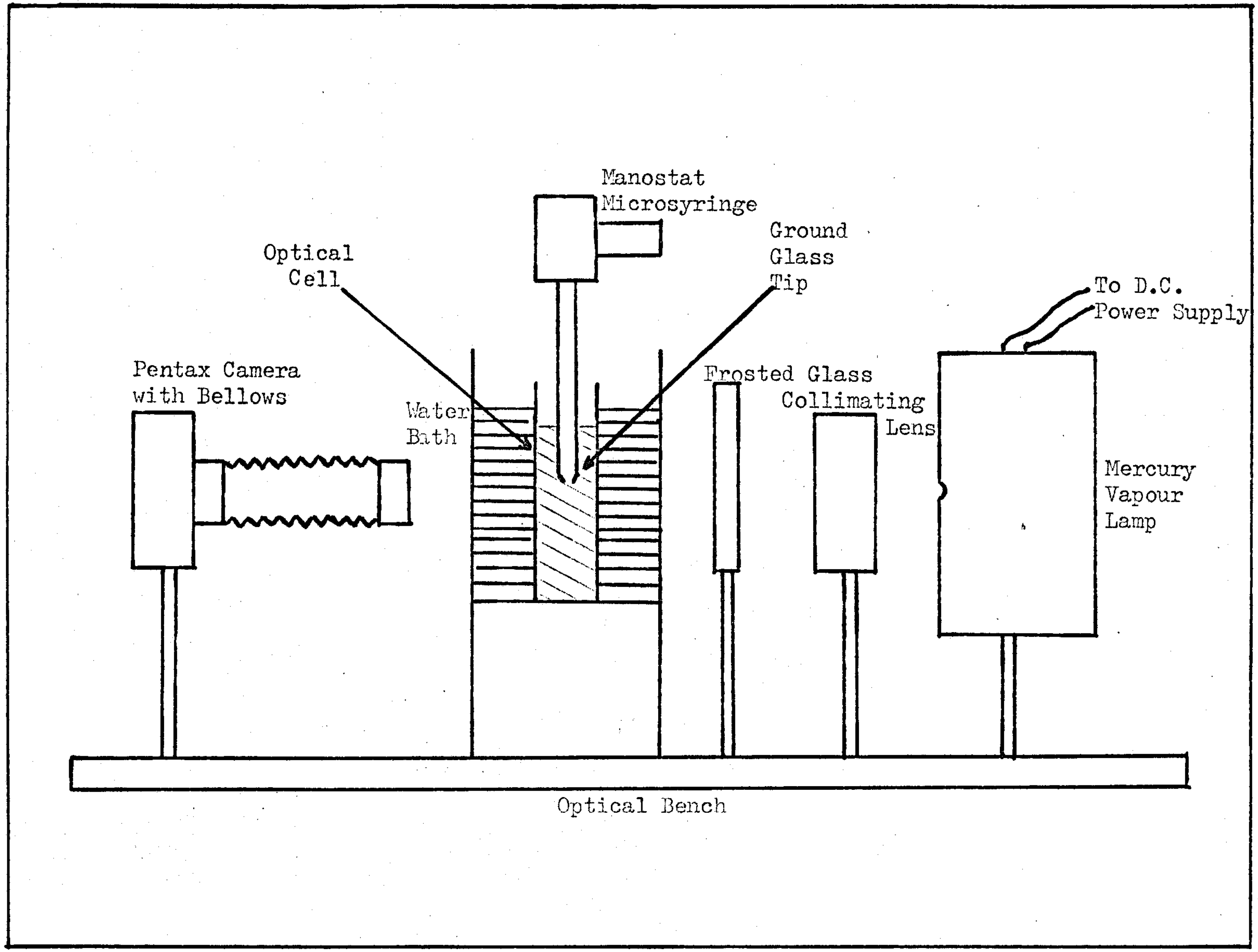

FIGURE A1-2 KEY DIAMETER MEASUREMENTS FOR THE PENDANT DROP METHOD

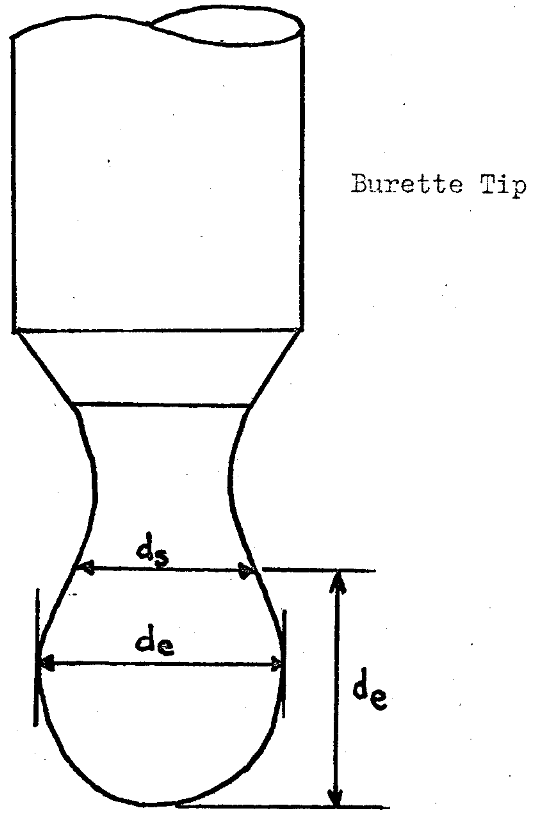

photographic negative, this method is capable of giving very accurate results. Drops of different sizes were used, and the effect of aging was studied.

Data are given in Table A1-2.

Drop aging over 0 to 30 seconds appeared to have no effect on the interfacial tension. Calculation of the standard deviation, s, defined by:

$$s = \left[\frac{1}{n-1} \sum_{i=1}^{n} (x_i - \bar{x})^2 \right]^{1/2}$$

where n = number of observations

x_i = an observation

$\bar{x}$ = the arithmetic average of all the observations

gives an average (weighted) value of 1.0 dyne/cm. The confidence interval for (a) pure carbon tetrachloride in distilled water, and (b) tank carbon tetrachloride in tank water may then be calculated using

$$\text{confidence interval} = t_{\alpha/2,n-1}\left[\frac{s}{\sqrt{n}}\right]$$

where α = 100 - confidence interval

n = number of observations

$t_{\alpha/2,n-1}$ = Student 't' value (see Crowe (C-3) page 47)

Then, for the pure system, (a),

$\bar{x}$ = 41.6 dynes/cm.

α = 5 (95% confidence level)

n = 7

s = 1.0 dyne/cm.

$t_{.025,6}$ = 2.447 (C-3)

TABLE A1-2   INTERFACIAL TENSIONS OF THE LIQUIDS USED

		Interfacial Tension, dynes/cm.				
		DISTILLED WATER IN AIR 24.2°C	PURE CARBON TETRACHLORIDE IN DISTILLED WATER, 25°C		TANK CARBON TETRACHLORIDE IN DISTILLED WATER, 25°C	TANK CARBON TETRACHLORIDE IN TANK WATER, 25°C
Aging	10 sec.	74.6	42.75	40.7	39.1	39.4
	20 sec.	74.6	42.75	40.7	40.1	39.4
	30 sec.	72.7	-	40.7	38.2	37.6
Fresh Drop	5 seconds	76.6	41.25	42.3	38.0	37.6
Overall Average		74.6	41.6		38.9	38.5
Standard Deviation s		1.6	0.98		0.97	1.04
$\bar{s}$		1.6	1.0			

then

$$x = 41.6 \pm 2.447 \left[\frac{1.0}{\sqrt{7}} \right]$$

$$= 41.6 \pm 0.9 \text{ dynes/cm.}$$

Similarly for the tank system, (b),

$$x = 38.5 \pm 3.182 \left[\frac{1.0}{\sqrt{9}} \right]$$

$$= 38.5 \pm 1.1 \text{ dynes/cm.}$$

Also, a statistical test on the means of (a) and (b) can be made using

$$t = \frac{\left| \bar{x}_a - \bar{x}_b \right|}{\bar{s}(x) \sqrt{1/n_a + 1/n_b}}$$

t = Student t value

$\bar{x}_a, \bar{x}_b$ = the two means = 38.5 and 41.6 dynes/cm.

$\bar{s}(x)$ = pooled standard deviation = 1.0 dynes/cm.

n_a, n_b = number of observations in each mean

= 4 and 7

Thus,

$$t = \frac{3.1}{1 \times .63} = 4.92$$

Using Appendix Table 3 of Crowe (C-3) for a 5% significance level, $t_{.025,9} = 2.262$. Since the calculated $t > 2.262$, it may be concluded with 95% confidence that there is a significant difference between the interfacial tension for the pure liquids and that for the tank liquids. Therefore, the tank fluids are contaminated with an agent that affects the surface behavior.

A1.b.5 Solubilities

Both the water and carbon tetrachloride were together in the settling tank for about 2 months prior to taking data. Extraction of the water phase with hexane and measurement of the hexane refractive index showed no carbon tetrachloride present in the hexane.

Titration of the carbon tetrachloride with Karl Fischer Reagent showed no water present.

A1·c A Measure of the Presence of Surface Active Agents

Some further means of illustrating the amount of contamination present in the liquid/liquid system was needed, since drop-drop coalescence would be greatly inhibited if surface active agents were present (H-3). The following procedure was used to detect the presence of surface active agents.

Surface active agents affect the drag of a drop. A drop with no surface layer (no surface active agents) will circulate, according to Linton and Sutherland (L-3). The presence of a monolayer on the drop surface resists drop circulation and may reduce the rate of fall for a circulating drop of the same diameter (D-5). To test for the presence of surface active agents in this work, the free fall velocity of oil drops of a known size was measured.

A burette with its tip immersed in a column of distilled water 18 inches high, and at 28°C, was used to form the drops. Calculations showed that the drop reached its terminal velocity almost immediately upon release from the burette tip. Problems were encountered in getting a constant drop size, and the drops did not fall in a straight line.

The range of data given in Table A1-3 is for 20 drops formed

TABLE A1-3 TERMINAL VELOCITIES OF PURE AND CONTAMINATED CARBON TETRACHLORIDE DROPS IN WATER

	PURE CARBON TETRACHLORIDE IN DISTILLED WATER	TANK CARBON TETRACHLORIDE IN DISTILLED WATER
drop volume (ml.)	0.036 - 0.037	0.030 - 0.034
drop radius (cm.)	0.206 - 0.208	0.193 - .202
measured v_t (fps)	0.728 - 0.735	0.645 - 0.650

one after the other. Calculation of the terminal velocity using Newton's Law for D_p = 0.40 cm. gives $v_t \doteq 0.86$ feet/sec. for a solid sphere. This terminal velocity is greater than the velocities measured for both liquid systems, and is probably due to the drops not falling in a straight line. The clean system seems to form larger drops which fall faster than drops from the dirty system. This test for surface active agents is therefore inconclusive.

APPENDIX 2 EXPERIMENTAL DETAILS

A2 EXPERIMENTAL DETAILS

A2·a Sampling Procedure

The underflow and overflow samples were obtained directly by placing sampling flasks under both streams. This avoided the problems of not getting a representative sample when fluid is bled off, and of changing the pressure drop across the cyclone when bleeding off a sample.

A2·b Overflow Analysis

The method selected for the overflow sample analysis is considered first, and then an example calculation is given.

A2·b·1 Method of Analysis of Overflow

Since the overflow carbon tetrachloride (oil) concentration was expected to be < 5 volume %, the method of analysis had to be sensitive to small changes in overflow oil concentration. The method decided upon was extraction of the carbon tetrachloride from the water using hexane, and then analysis of the hexane plus oil by refractive index. A dipping refractometer capable of measuring refractive index to an accuracy of 1 in 10^6 was used. Reproducibility of this procedure was less than 5% in error.

A calibration curve giving refractive index at 25°C as a function of the percent volume carbon tetrachloride in hexane is given in Figure A2-1.

To further illustrate the method, an example calculation is now given.

FIGURE A2-1 REFRACTIVE INDEX OF HEXANE-CARBON TETRACHLORIDE MIXTURES AT 25°C

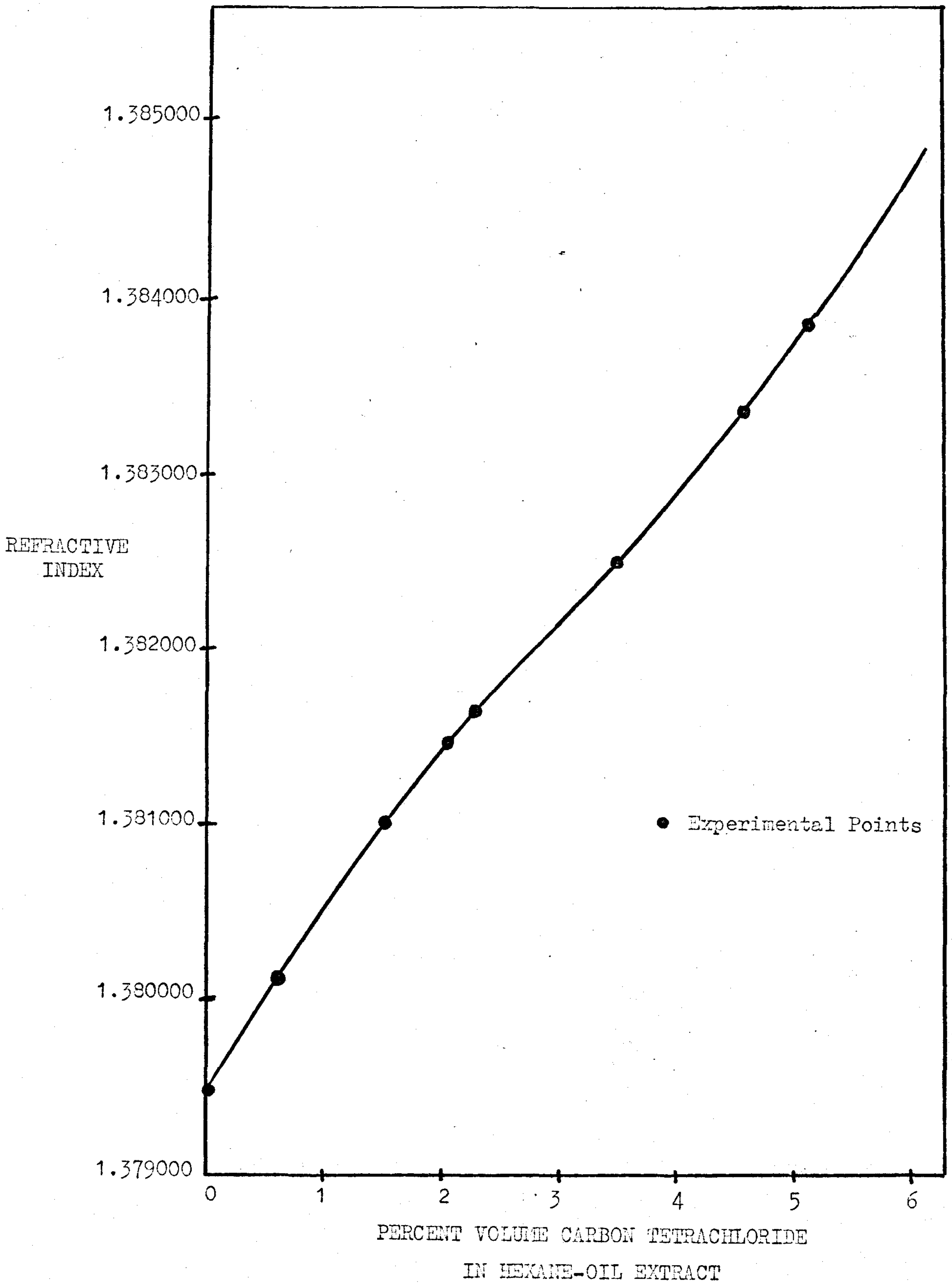

A2·b·2 Example Calculation of the Overflow Oil Concentration for Trial 6

Sample volume = 89 ml

First extract volume = 74.5 ml = V_2

Second extract volume = 63.5 ml = V_3

Refractive index at 25°C of V_2 was 1.382974

Refractive index at 25°C of V_3 was 1.379410

Using the calibration curve, V_2 is 4.1 volume % oil and V_3 is 0% oil.

Therefore, the volume of carbon tetrachloride in the sample is

$$\frac{4.1}{100} \times 74.5 = 3.06 \text{ ml}$$

and so the sample is $\frac{3.06}{89} \times 100 = 3.44$ volume % carbon tetrachloride.

A2·c Underflow Analysis

The method of determining the underflow composition is considered first, and then an example calculation is performed.

A2·c·1 Method of Analysis of Underflow

The previous method employing refractive index could not be used since the necessary prism for the dipping refractometer was not available. A gas chromatograph was rejected as being too time consuming to calibrate. The method finally selected is called turbidimetric analysis (S-2).

Turbidimetric analysis can be used when there are three liquids A,B, and C, where A and B are immiscible and C is miscible with both. For this work, A,B, and C are, respectively, carbon tetrachloride, water, and acetic acid. The method consists of adding a known weight of acetic acid to a known weight of a mixture of carbon tetrachloride and water, whose composition is unknown. Enough acetic acid is added to give a one phase mixture. This mixture is then titrated with water until two phases appear. It is then possible to calculate back to the original sample composition. Reproducibility of this procedure is less than 5% in error.

A solubility diagram for the ternary system employed is given in Figure A2-2, and a representation of turbidimetric titration is given in Figure A2-3. There the unknown concentration is at 1; acetic acid is added to yield a one-phase mixture at 2. Titration with water follows a line joining 100% water with point 2. This intersects the immiscible curve at the "end point" 3. To further illustrate the method, an example calculation is now given.

A2·c·2 Example Calculation of the Underflow Water Concentration for Trial 6

Sample weight	=	102.79 grams
Acetic acid added	=	104.64 grams
Water used to give end point	=	0.50 grams

Therefore, total sample weight is 207.93 grams.

The percent weight acetic acid may now be found.

$$\% \text{ weight acetic acid} = \frac{104.64}{207.93} \times 100 = 50.3\%$$

The calibration curve (Figure A2-2) shows that for 50.3% acetic acid, the equilibrium mixture is 6.1% water and 43.6% carbon tetrachloride.

FIGURE A2-2 SOLUBILITY CURVE FOR THE TERNARY LIQUID SYSTEM WATER-ACETIC ACID-CARBON TETRACHLORIDE AT 25°C

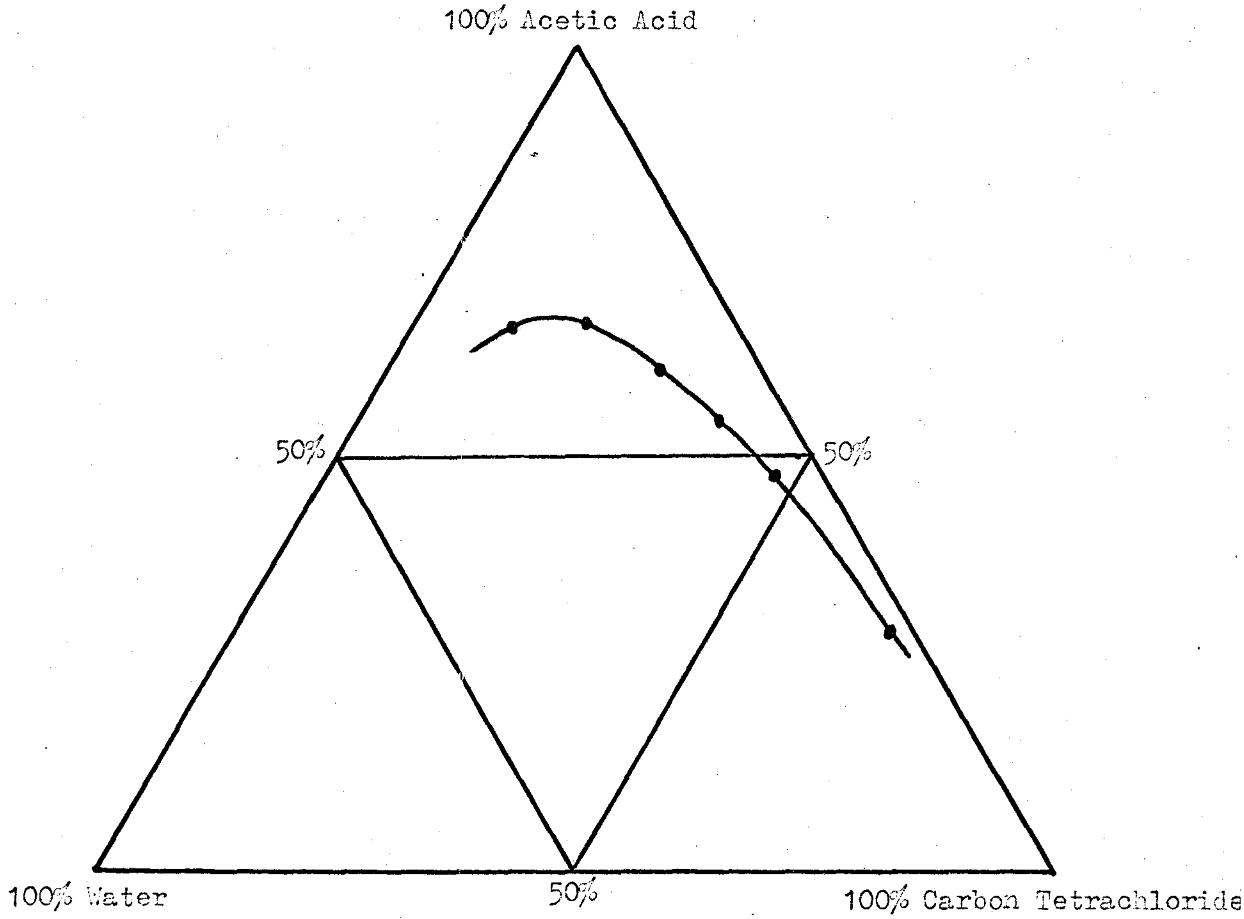

● Experimental points

All concentrations are weight percent.

FIGURE A2-3 STEPS IN TURBIDIMETRIC TITRATION

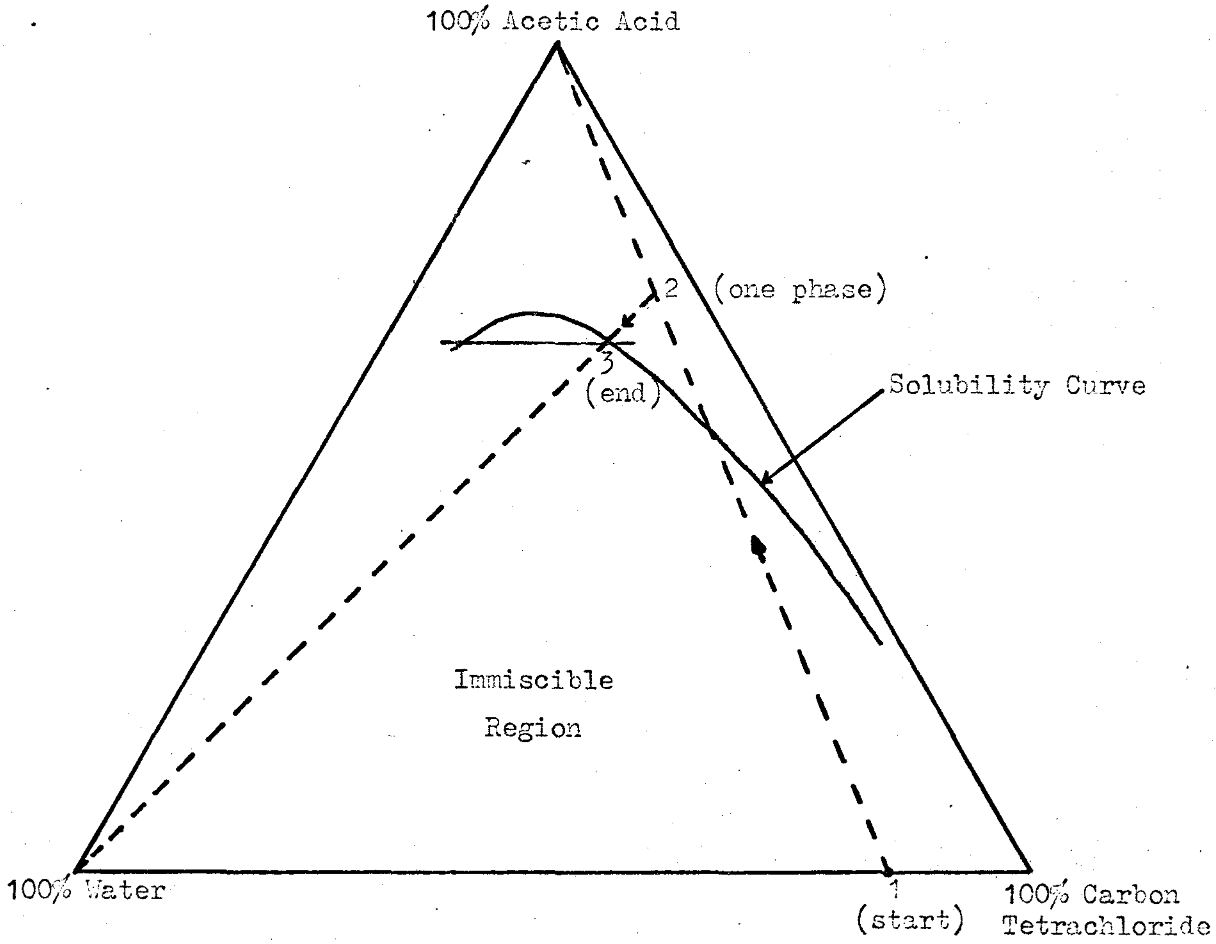

Therefore, the weight of water is $\frac{6.1}{100} \times 207.93 = 12.69$ grams

Water added in titration was 0.50 grams

Initial water in sample was 12.19 grams

The volume of oil in the original sample was then $\frac{102.79 - 12.19}{1.583} = 57.20$ ml.

Therefore the sample volume was $57.20 + 12.19 = 69.39$ ml.

and the percent volume water was $\frac{12.19}{69.39} \times 100 = 17.58\%$.

A2·d Rotameter Calibration

The calibration curves for the 0-10 USGPM rotameters, calibrated in their lower ranges at $25 \pm 2°C$, are given in Figures A2-4 and A2-5. Calibrations were checked periodically, and the data were reproducible to within $\pm 2\%$.

A2·e Photographic Details

To give the details necessary to follow the experimental technique, this section first considers those steps leading up to taking a photograph. The second part of this section presents the steps involved in going from the photograph in the camera to the final drop size distribution.

A2·e·1 Taking a Photograph of a Dispersion

Since the oil settled out and coalesced very rapidly when the pumps were shut off, the method used here, of necessity, allows a photograph of a dispersion to be taken without disturbing the dispersion.

A light source consisted of an electrical apparatus connected to a lamp. This apparatus, whose schematic diagram is shown in Figure A2-6, allowed an electrical pulse of 5 kilovolts and of 10 micro-second duration to flash the lamp.

Since the subject was the dispersion inside the pipe, the optical

FIGURE A2-4 ROTAMETER CALIBRATION CURVE FOR WATER AT 25°C

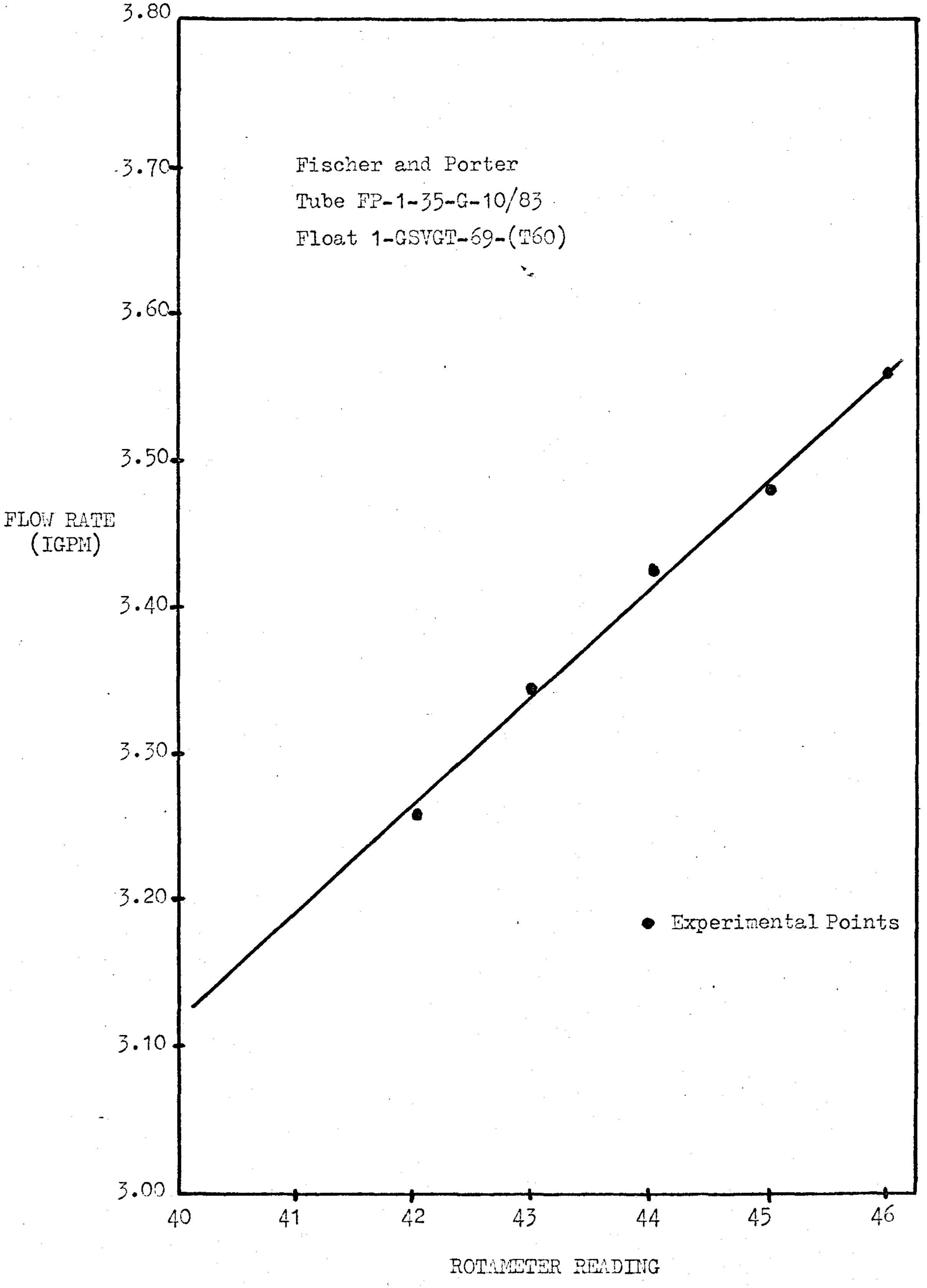

FIGURE A2-5 ROTAMETER CALIBRATION CURVE FOR CARBON TETRACHLORIDE AT 25°C

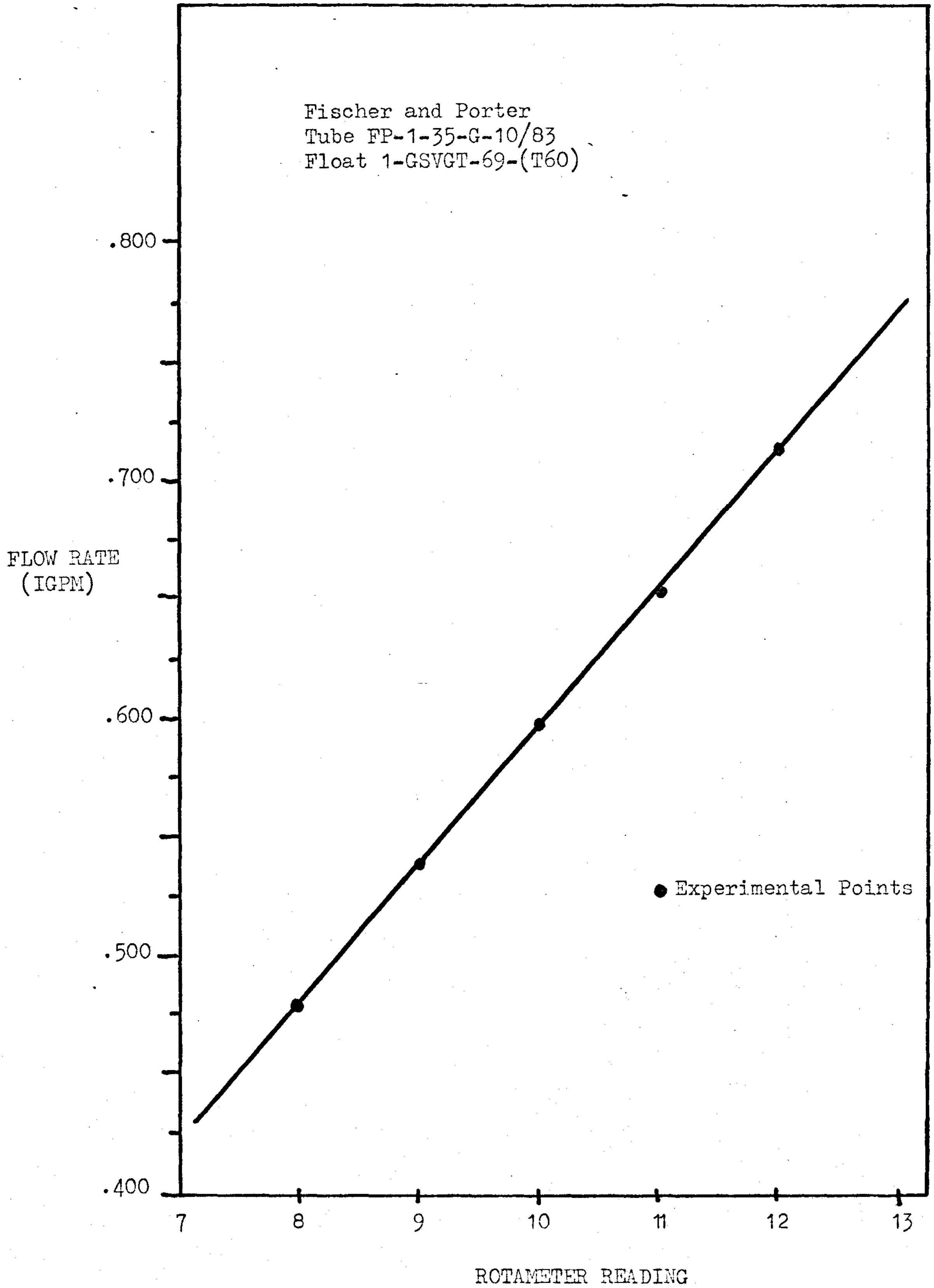

FIGURE A2-6 SCHEMATIC DIAGRAM OF FLASH UNIT

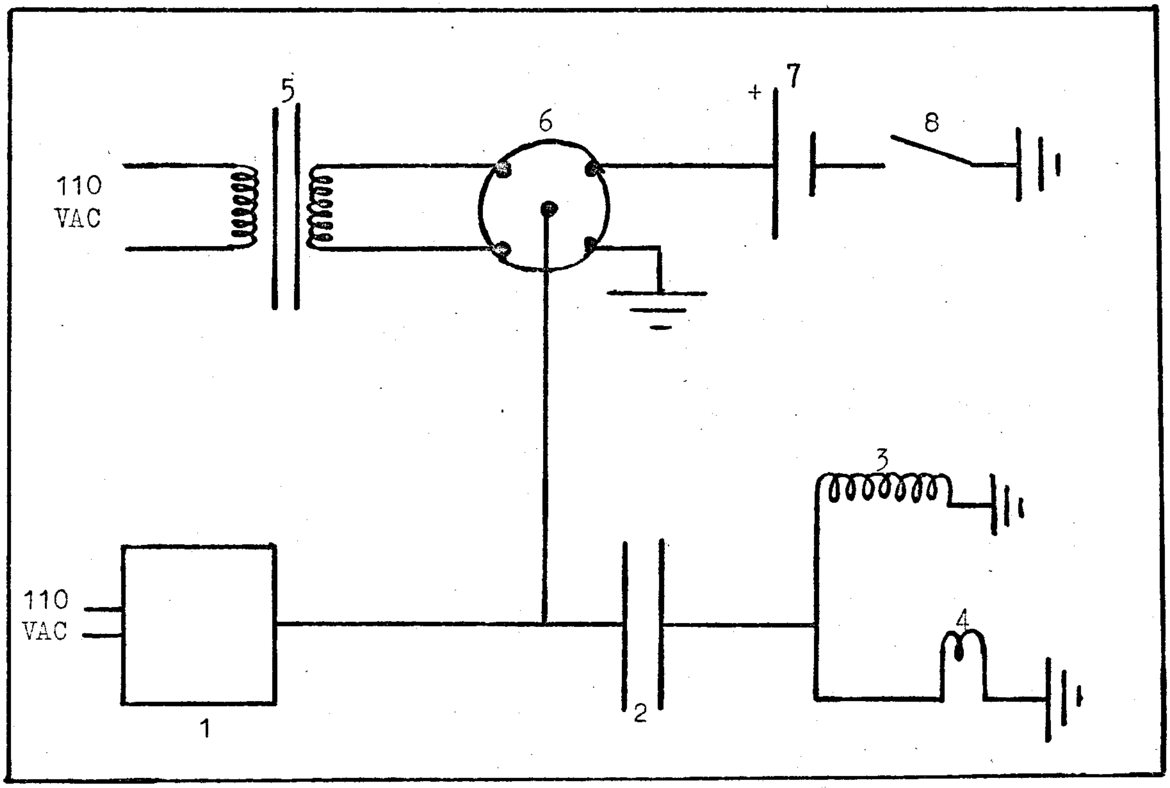

1. 0-18 KV. Power Supply
2. Capacitor
3. Coil
4. Flash Lamp
5. Filament Transformer
6. 5C22 Thyratron
7. 300 Volt Battery
8. Switch

cell shown in Figure A2-7 was used. This cell allowed the light source to illuminate the dispersion and also prevented any distortion of the drop images. Figure A2-7a shows the components present in the optical cell cross section. Figure A2-7b shows schematically how the optical cell corrects for the curved glass wall.

The camera, using two bellows and one set of extension tubes, was positioned so that the camera lens was about one inch from the optical cell. The film used was Kodak Panatomic-X 35 mm. film of ASA 32 film speed. This film possesses an extremely fine grain emulsion.

To take a photograph, the room lights were darkened, the camera shutter opened, and the light source flashed so that the dispersion flowing through the optical cell was 'caught'.

A2·e·2 Obtaining the Drop Size Distribution of a Dispersion from a Photograph

The film first must be developed, then the negative printed. From this print a drop size distribution may be obtained. Since the short duration of the light pulse left the film under-exposed, the developing procedure tried to achieve maximum contrast. Acufine developer used with the film for 5 minutes at 70°F gave reasonable negatives, although contrast was still poor.

For printing, Agfa high-contrast megatype photographic paper was preferred for use, but was not always available. Consequently, the low contrast megatype paper was often used. This paper was light weight and easily used with the Zeiss particle size analyzer. For maximum print contrast, the enlarger was "stopped down" for minumum light, and the photographic paper exposed for about 20 seconds. This

FIGURE A2-7a,b OPTICAL CELL

FIGURE A2-7a

Schematic Diagram of Optical Cell Components

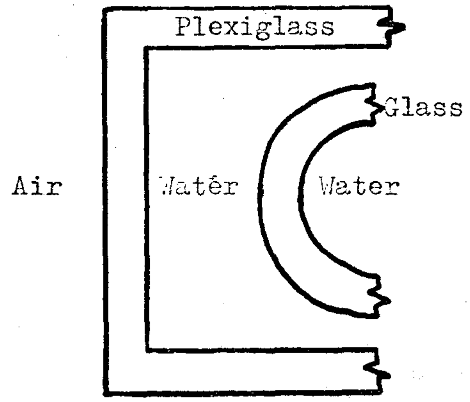

FIGURE A2-7b

Operation of the Optical Cell

Undistorted Image of Drop

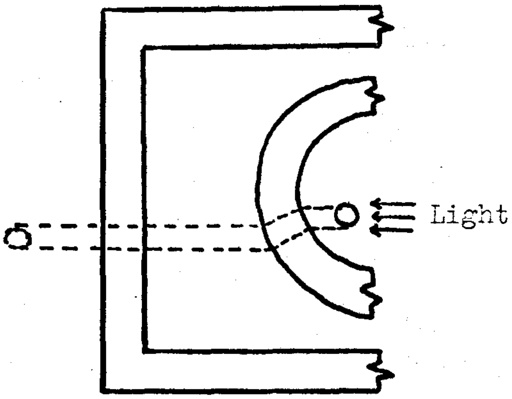

resulted in a burning-in of the drop images. Ansco 'Vividol' and 'Acid Fixer' were then used as recommended for the print developing.

For printing, the enlarger-to-paper distance was adjusted to give an overall drop magnification of 40.7 X. The negative itself was already at 5X magnification because of the bellows and extention tubes used on the camera.

Sample photographs of the feed dispersion are given in Figure A2-8.

A Zeiss particle size analyzer was used with the print to determine the drop size distribution. This instrument has 48 size intervals ranging from 1.20 mm to 27.71 mm, divided exponentially, as shown in Figure A2-9. About 500 to 2000 drops were counted and sized for each dispersion. The analyzer punched a hole in each drop as it was measured so that the drop would not be remeasured. The data contained in the 48 size intervals were then plotted on log-probability paper to conveniently report the drop size distribution.

A2·f <u>Details of the Hydrocyclone and its Auxilary Equipment</u>

A description of the equipment is considered first, followed by details on the equipment construction.

A2·f·1 <u>Equipment Description and Operation</u>

The equipment description follows the flow sheet given in Figure A2-10.

Equipment specification and suppliers are given in Table A2-1.

The two liquids were discharged separately from two centrifugal pumps, sent through two globe vlaves used to throttle the discharge, and through two rotameters.

FIGURE A2-8 SAMPLE PHOTOGRAPHS OF THE FEED DISPERSION
Oil/Water Ratio = 0.1722

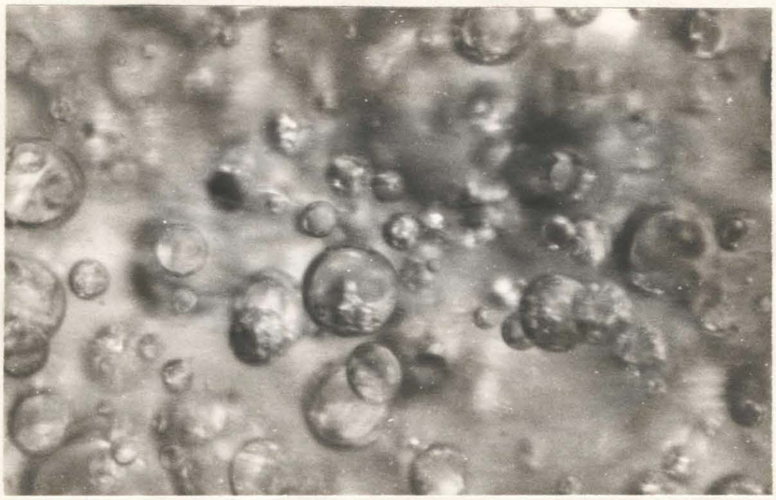

P = 17.65 mm. Hg

P = 52.95 mm. Hg

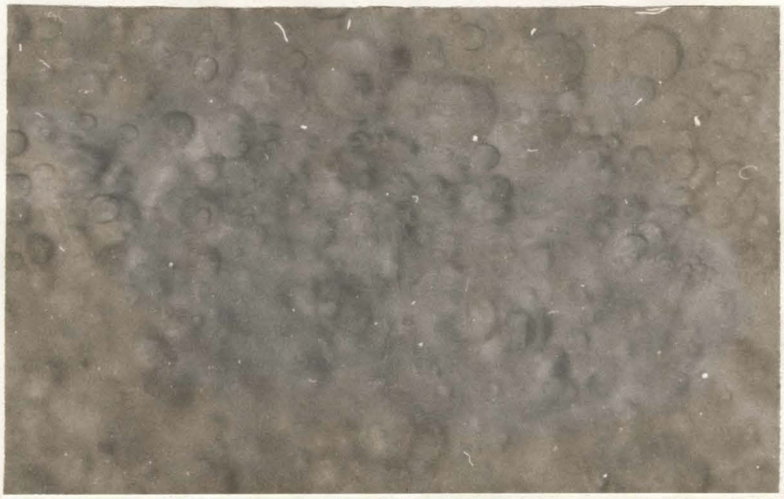

P = 88.25 mm. Hg

FIGURE A2-9 DETAILS OF ZEISS PARTICLE SIZE ANALYZER

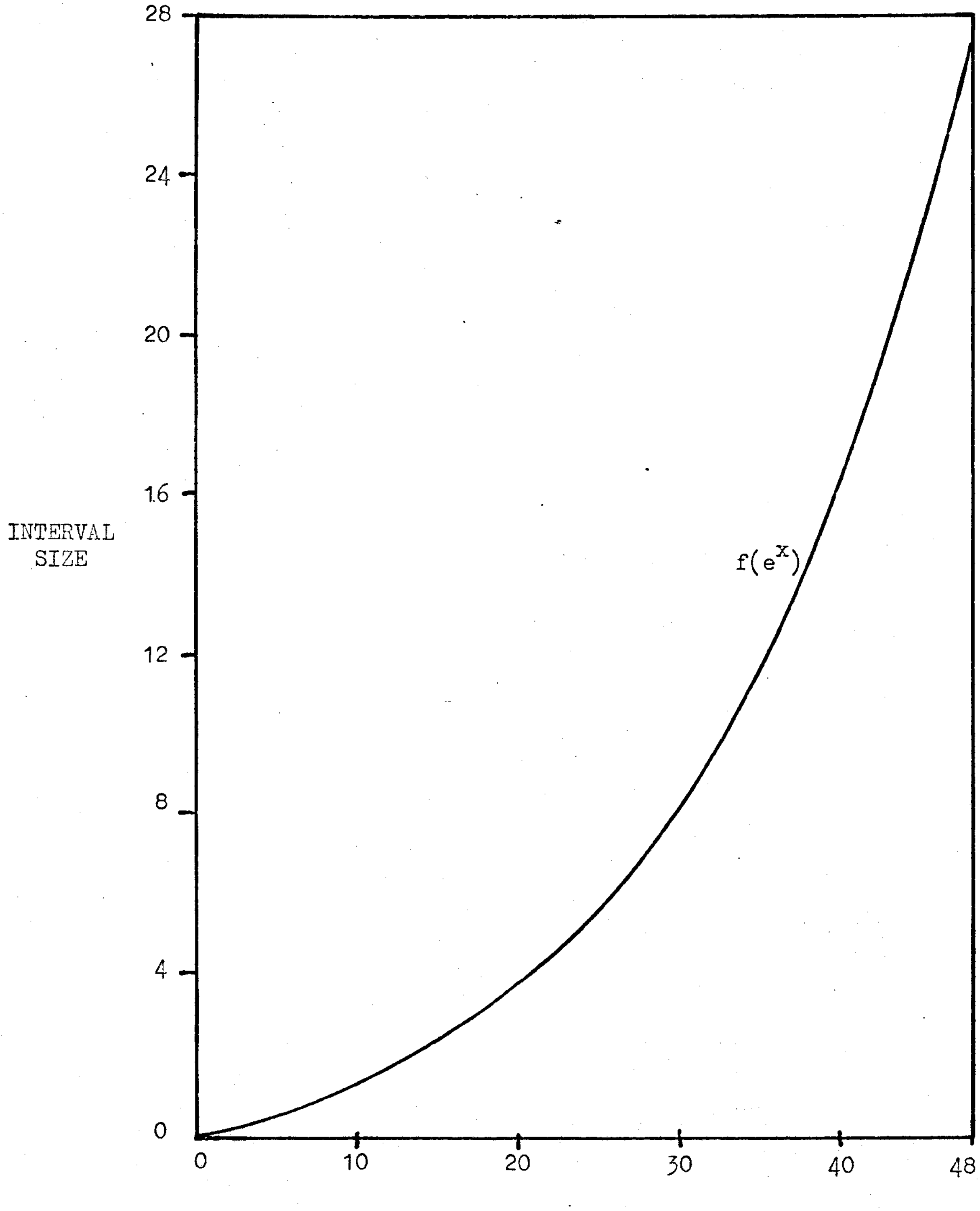

FIGURE A2-10 OVERALL FLOW SHEET

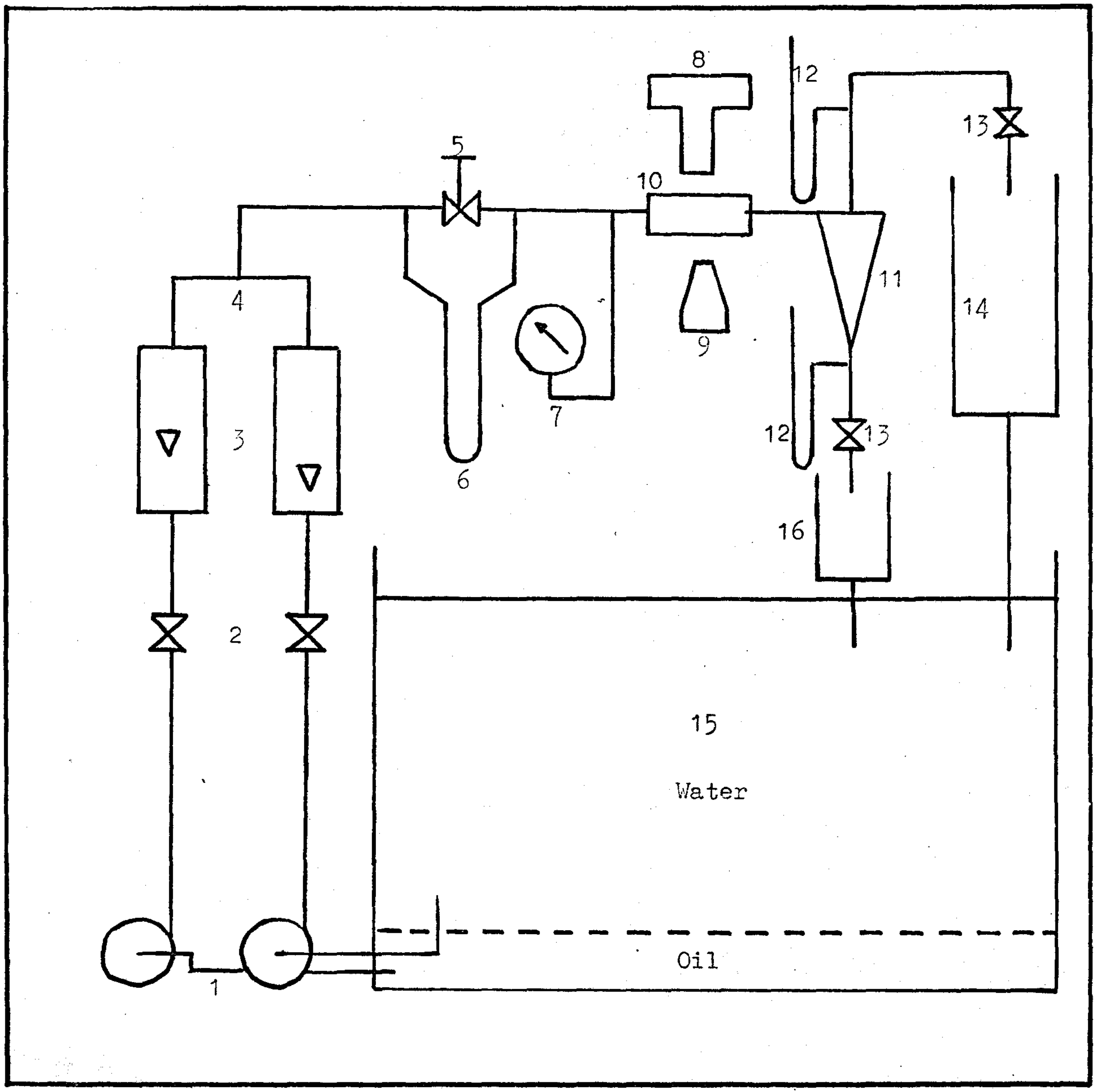

1. Feed Pumps
2. Throttle Valves
3. Rotameters
4. Mixing Tee
5. Mixing Valve
6. Manometer
7. Inlet Pressure Gage
8. Camera
9. Flash Lamp
10. Optical Cell
11. Hydrocyclone
12. Manometers
13. Cyclone Valves
14. Overflow Tank
15. Reservoir
16. Underflow Tank

The liquids were then mixed at the mixing tee. The dispersion then passed through a gate valve which changed the drop size distribution, depending on the valve opening. The pressure drop acoss this valve was registered by a mercury manometer.

Inlet feed pressure was shown by a Bourdon pressure gage, and the dispersion was photographed in the optical cell. The dispersion then passed directly into the glass hydrocyclone. The overflow liquid pressure was registered by a mercury manometer, and the overflow rate was controlled by a globe valve (in operation this valve was fully open). Finally, the overflow discharged into an overflow tank which was used to measure the overflow rate. This tank emptied into the reservoir.

The cyclone underflow pressure was registered by a mercury manometer, and the flow rate was controlled by a gate valve. The underflow then discharged into a large glass beaker which was used to measure the underflow rate. This beaker then emptied into the reservoir.

A2.f.2 <u>Equipment Construction</u>

The reservoir was a 150 Imperial gallon combination holding tank and decanter which allowed oil droplets in the water phase to separate before the liquids were recycled. (In practice the overflow was collected in the overflow tank to prevent the water phase from becoming cloudy with unsettled oil drops.) This reservoir was roughly 3 feet on a side, with three sides of plate glass, and the bottom and other side made of type 304 stainless steel. The glass was glued to strips of right-angled stainless steel on the outside edge of the glass. To prevent the carbon tetrachloride from dissolving this adhesive the inside edges of the glass were sealed with Dow Corning RTV-733 fluorosilicone cement. This adhesive was found to be completely oil resistant for a period of about three months. It was also sufficiently elastic to take up the shear between the glass and stainless steel as the room temperature changed.

The optical cell construction is shown in Figure A2-11. Its middle plexiglass section was square to correct for distortion. Drain holes were provided for adding water to surround the glass tube. The glass tube was connected to the stainless steel feed line using Swagelok connectors with teflon ferrules.

The cyclone was constructed from 2 inch I.D. glass pipe. Its dimensions, relative to D_C are:

$$\frac{D_1}{D_C} = \frac{D_2}{D_C} = \frac{D_3}{D_C} = 0.23$$

$$\frac{L_2}{D_C} = 1.0$$

$$\frac{L}{D_C} = 4.15$$

$$\theta = 10^\circ$$

These dimensions conform to the optimum cyclone dimensions given by Simkin and Olney (S-3) for liquid/liquid cyclones, and to those given by Rietema (R-2) for solid/liquid cyclones. A photograph of the feed inlet section and cyclone is given in Figure A2-12.

FIGURE A2-11 OPTICAL CELL CONTRUCTION

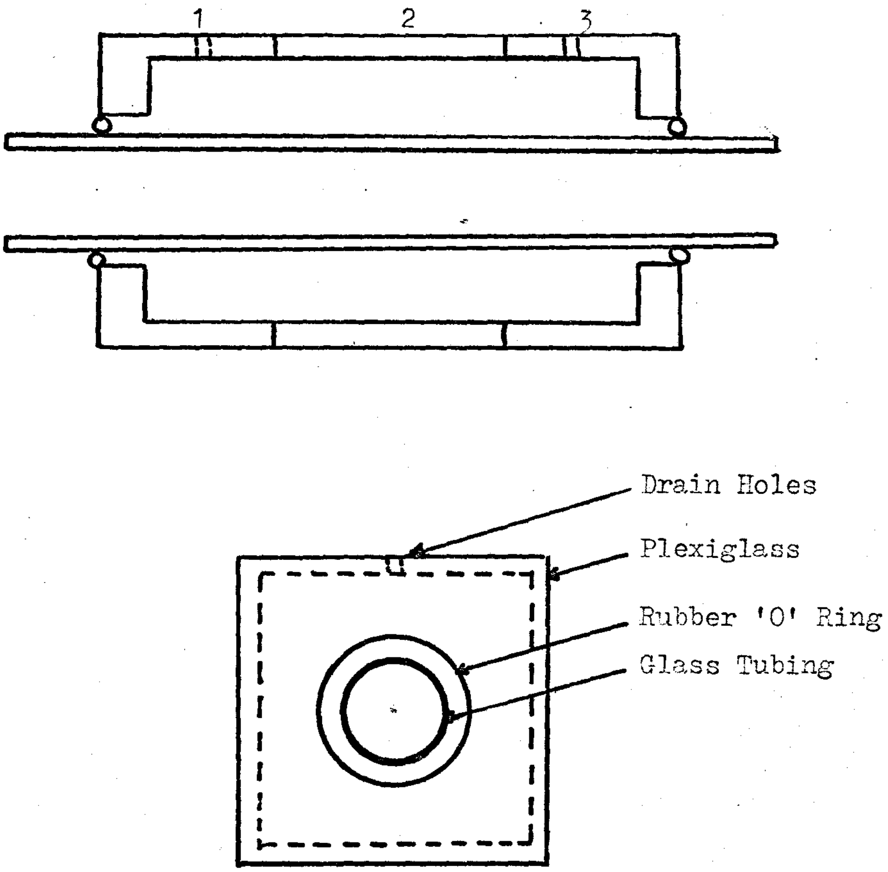

NOTES

1. Sections 1 and 3 are of circular inside cross section

2. Section 2 is of square cross section

FIGURE A2-12 PHOTOGRAPH OF FEED INLET AND HYDROCYCLONE

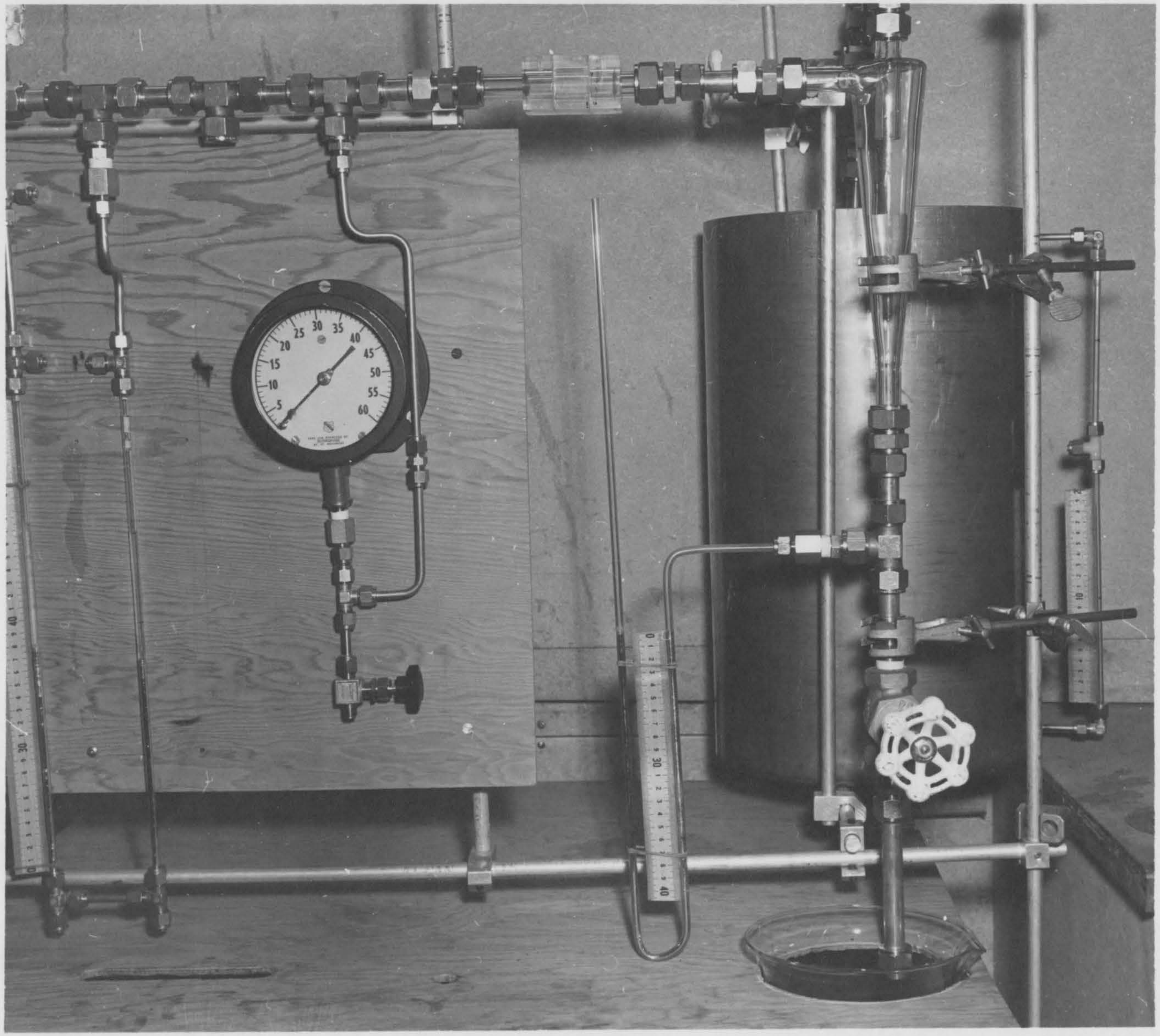

TABLE A2-1 EQUIPMENT SPECIFICATIONS AND SUPPLIERS

EQUIPMENT	SPECIFICATIONS	SUPPLIER
Feed Pumps	10 USGPM @ 80 feet Head - 3600 rpm 316 Stainless Steel	Hayward-Gordon 50 Chauncy Ave. Toronto 18, Ont.
Rotameters	0-10 USGPM 316 Stainless Steel and Teflon	Fischer-Porter 1110 A Wilson Ave. Downsview, Ont.
1" & 5/8" O.D. Tubing	Type 304 Stainless Steel	Atlas Alloy Metal Sales 215 Lakeshore Rd. Toronto 2, Ont.
Mixing Valve	Gate Valve, ½" Orifice 316 Stainless Steel	Niagara Valve 102 Parkdale Ave.N. Hamilton, Ont.
Other Valves	Globe & Gate Valves ½" Orifice 316 Stainless Steel	Niagara Valve 102 Parkdale Ave.N. Hamilton, Ont.
Swagelok Fittings	Type 316 Stainless Steel	Niagara Valve 102 Parkdale Ave.N. Hamilton, Ont.
Pressure Gage	0-60 p.s.i. 316 Stainless Steel	Thomson-Gordon Ltd. 200 Queen St.N. Hamilton, Ont.

TABLE A2-1 (continued)

Camera	ASAHI S1a 35 mm. Camera with 55 mm. Focal Length Lens	PhotographyDept. Eng. Bldg. McMaster University Hamilton, Ont.
Glass Cyclone	See Appendix 2 for dètails	Glass Blower McMaster University Hamilton, Ont.
Reservoir	316 Stainless Steel, RTV 733 Silicone Cement	Machine Shop Eng. Bldg. McMaster University Hamilton, Ont.
Carbon Tetrachloride	Reagent Grade	Fisher Scientific 184 Railside Road Don Mills, Ont.
Flexible Tubing	Teflon 1" I.D.	Warehouse Plastic Sales 571 Gerrard Street Toronto 8, Ont.
Capacitor	Electrolytic 15KV. Breakdown, 0.1 mfd.	E. Turner Electrical Const. Ltd. Chilton Works High Wycombe Buchshire, England
Power Supply	0 to 18 KV.	B.R.H. Associates P.O. Box 214, Stat. Q Toronto 7, Ont.
Thyratron	5C22 15KV. Breakdown	Zentronics Limited 66 Orfus Road Toronto 19, Ont.

APPENDIX 3 TREATMENT OF DATA

A3 TREATMENT OF DATA

A3·a Feed Drop Size Distributions

First the mixing valve had to be calibrated. This calibration consisted of relating the mixing valve pressure drop to some measure of drop size distribution. Chapter 4 mentions that the $\langle D_p \rangle_{32}$ diameter was chosen.

Details of the photographic procedure and the drop counting method are given in Appendix 2.

A3·a·1 Statistical Design

A statistical experiment design with both variables at 5 levels was used. It was a central composite design for two independent variables; x_1 = mixing valve pressure drop and x_2 = oil/water ratio, the dependent variable being $\langle D_p \rangle_{32}$. This design is shown in Table A2-1, for both coded and uncoded levels along with the data obtained.

Attempts were made to use the geometric standard deviation as the dependent variable, since the geometric mean diameter varied little ($\langle D_p \rangle_g = 95 \pm 20 \mu$).

However, a more significant correlation was obtained with $\langle D_p \rangle_{32}$ as the dependent variable.

A3·a·2 Controlling the Variables

Since the feed flow rate was kept constant, an increase in the oil flow rate necessitated a decrease in the water flow rate. The total flow rate actually ranged from 4.02 to 4.09 IGPM (or a

TABLE A3-1 STATISTICAL EXPERIMENT DESIGN FOR TWO INDEPENDENT VARIABLES AT FIVE LEVELS AND RESULTING VOLUME/SURFACE DIAMETER

RUN	CODED		UNCODED		$\langle D_p \rangle_{32}$ μ
	x_1	x_2	x_1 mm.Hg	x_2 Oil/water volume ratio	
1	0	0	52.95	0.1722	212.1
2	0	0	52.95	0.1722	223.2
3	-1	-1	35.30	0.1534	293.9
4	1	-1	70.60	0.1534	220.2
5	-1	1	35.30	0.1920	274.3
6	1	1	70.60	0.1920	195.3
7	0	0	52.95	0.1722	230.5
8	0	0	52.95	0.1722	199.6
9	2	0	88.25	0.1722	162.0
10	-2	0	17.65	0.1722	304.0
11	0	2	52.95	0.2110	226.1
12	0	-2	52.95	0.1341	220.0

Note

1.) Pressures are corrected for liquid in manometer lines

2.) Standard deviation of observations at the centre point is 13.5 μ.

velocity of 7.85 to 8.00 f.p.s.). The mixing valve pressure drop was adjusted to the desired value by changing the mixing valve setting. The pressure drops quoted in Table A3-1 have been corrected for carbon tetrachloride that collected in the manometer lines above the mercury.

A3·a·3 Calculation of $\langle D_p \rangle_{32}$

The cumulative number-size distributions found by the Zeiss particle size analyzer were plotted on log-probability paper (Figures A3-1 to A3-12). Since a relatively small number of drops (500 to 2000) were counted per distribution, the correction of Gwyn et al (G-1) must be applied to each distribution before the volume surface diameter $\langle D_p \rangle_{32}$ can be calculated. To use this correction, each distribution must be log-normally distributed. A chi-square test done in section A3·a·5 considers this point.

The Zeiss analyzer reports the number of drops existing between two size ranges. Gwyn et al define new diameters based on each size interval diameter as follows. For example,

mean area diameter for an interval $$d^2_{5-6} = \frac{d_5^{\,2} + d_6^{\,2}}{2}$$

mean volume diameter for an interval $$d^3_{5-6} = \frac{d_5^{\,3} + d_6^{\,3}}{2}$$

where d_5 and d_6 are the size interval limits of interval 5.

Surface area of drops of size in interval 5 $= \pi n_5 d^2_{5-6}$

and volume of drops of size in interval 5 $= \frac{\pi}{6} n_5 d^3_{5-6}$

where n_5 = number of drops in interval 5.

These volumes and areas are summed for each interval to give the total

FIGURES A3-1 to A3-12

DROP SIZE DISTRIBUTIONS FOR

RUNS 1 to 12

FIGURE A3-1

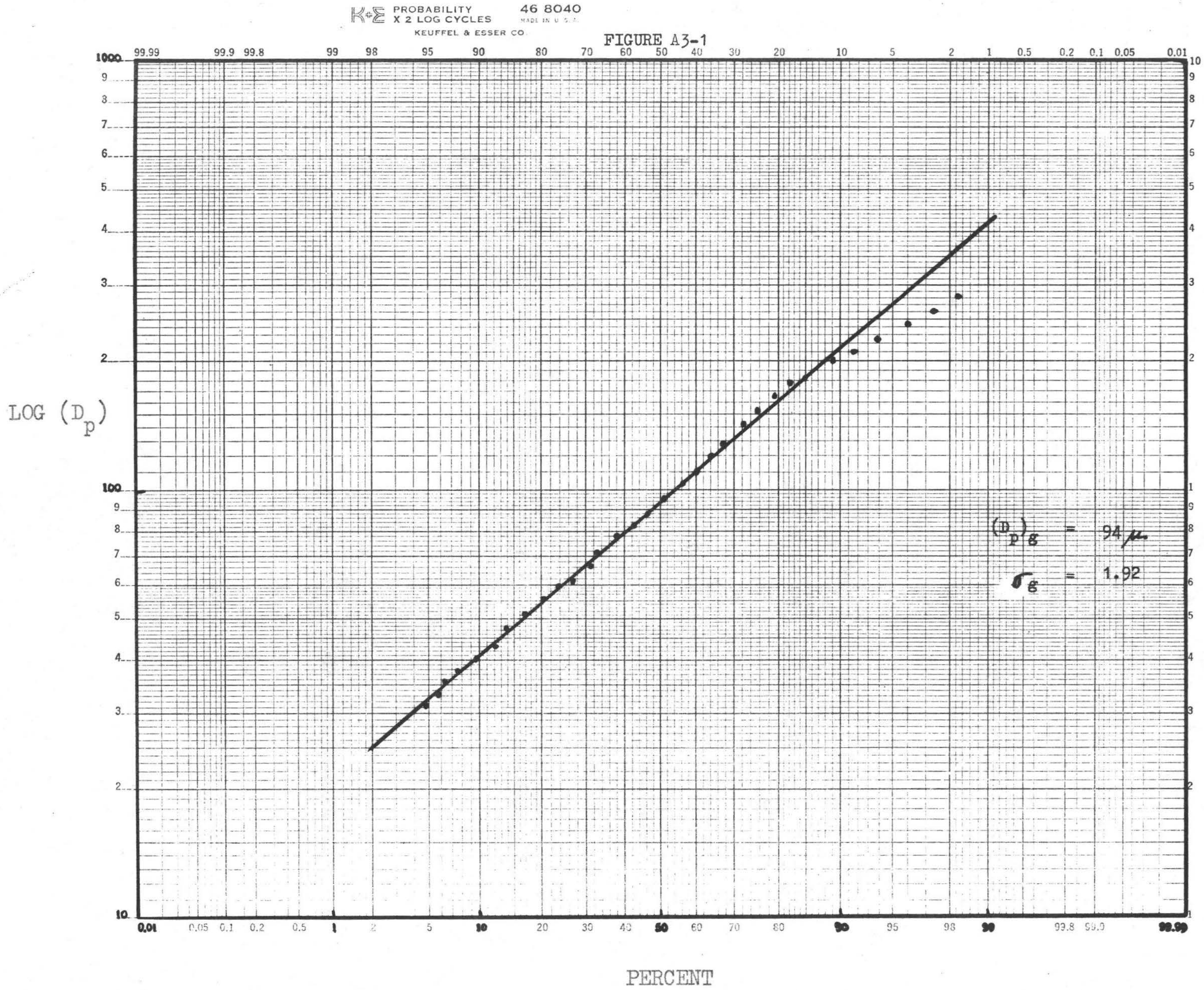
K+E PROBABILITY X 2 LOG CYCLES 46 8040
KEUFFEL & ESSER CO.
LOG (D_p)
PERCENT
$(D_p)_g$ = 94 μ
σ_g = 1.92

FIGURE A3-2

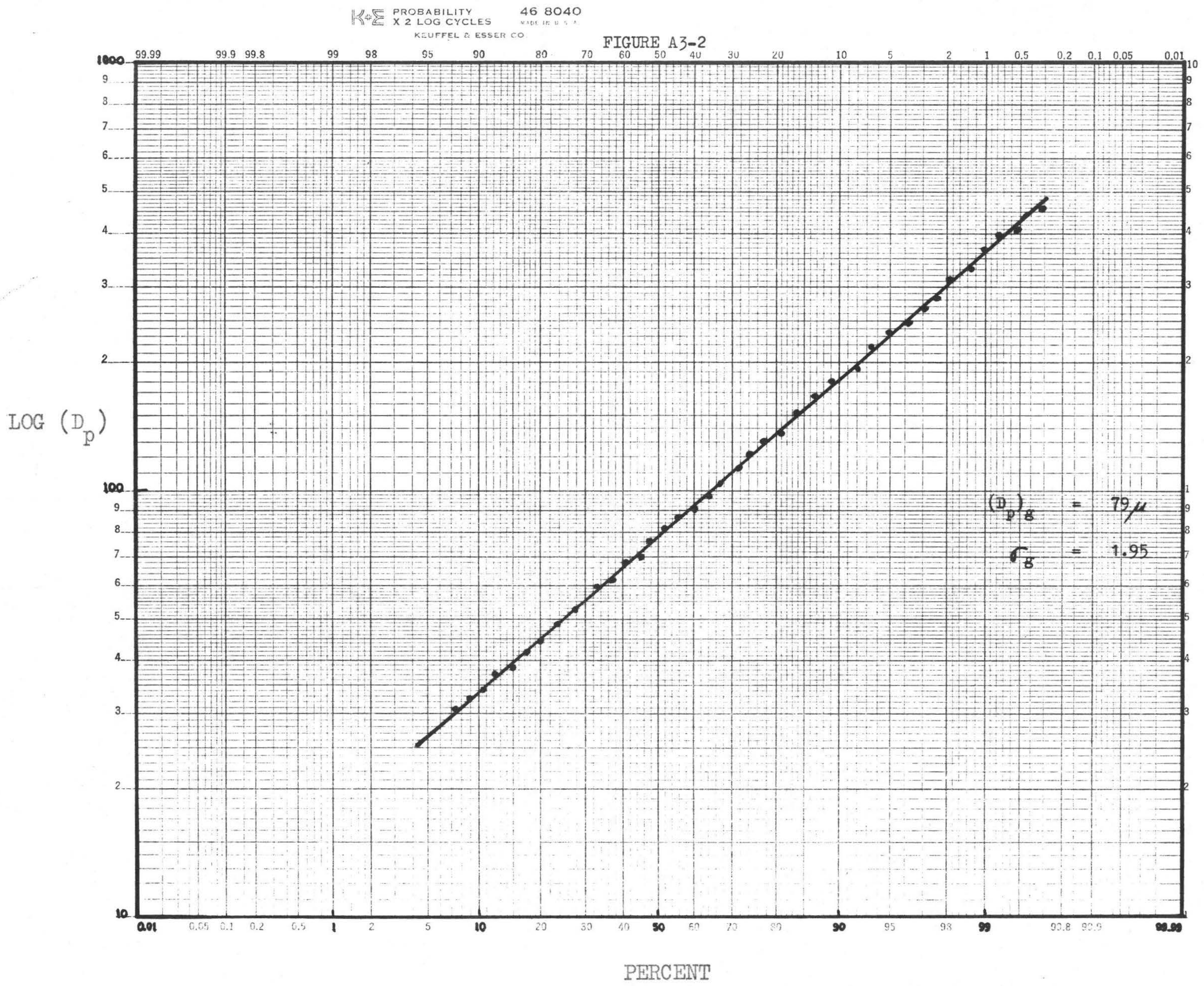

K+E PROBABILITY X 2 LOG CYCLES 46 8040
KEUFFEL & ESSER CO.
LOG (D_p)
PERCENT
(D_p)_g = 79 μ
σ_g = 1.95

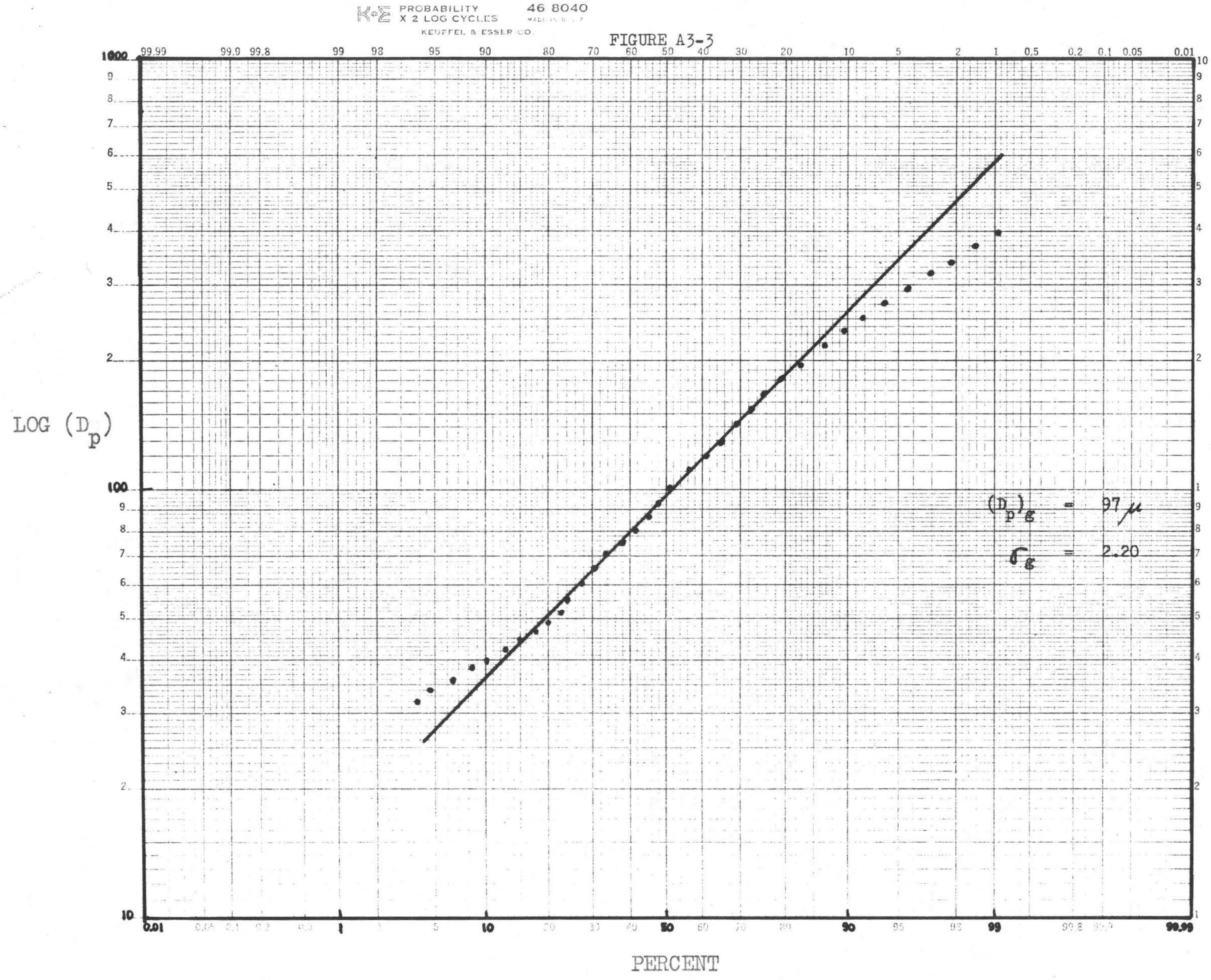
K+E PROBABILITY X 2 LOG CYCLES 46 8040
KEUFFEL & ESSER CO.
FIGURE A3-3
LOG (D_p)
PERCENT
$(D_p)_g$ = 97 μ
σ_g = 2.20

FIGURE A3-4

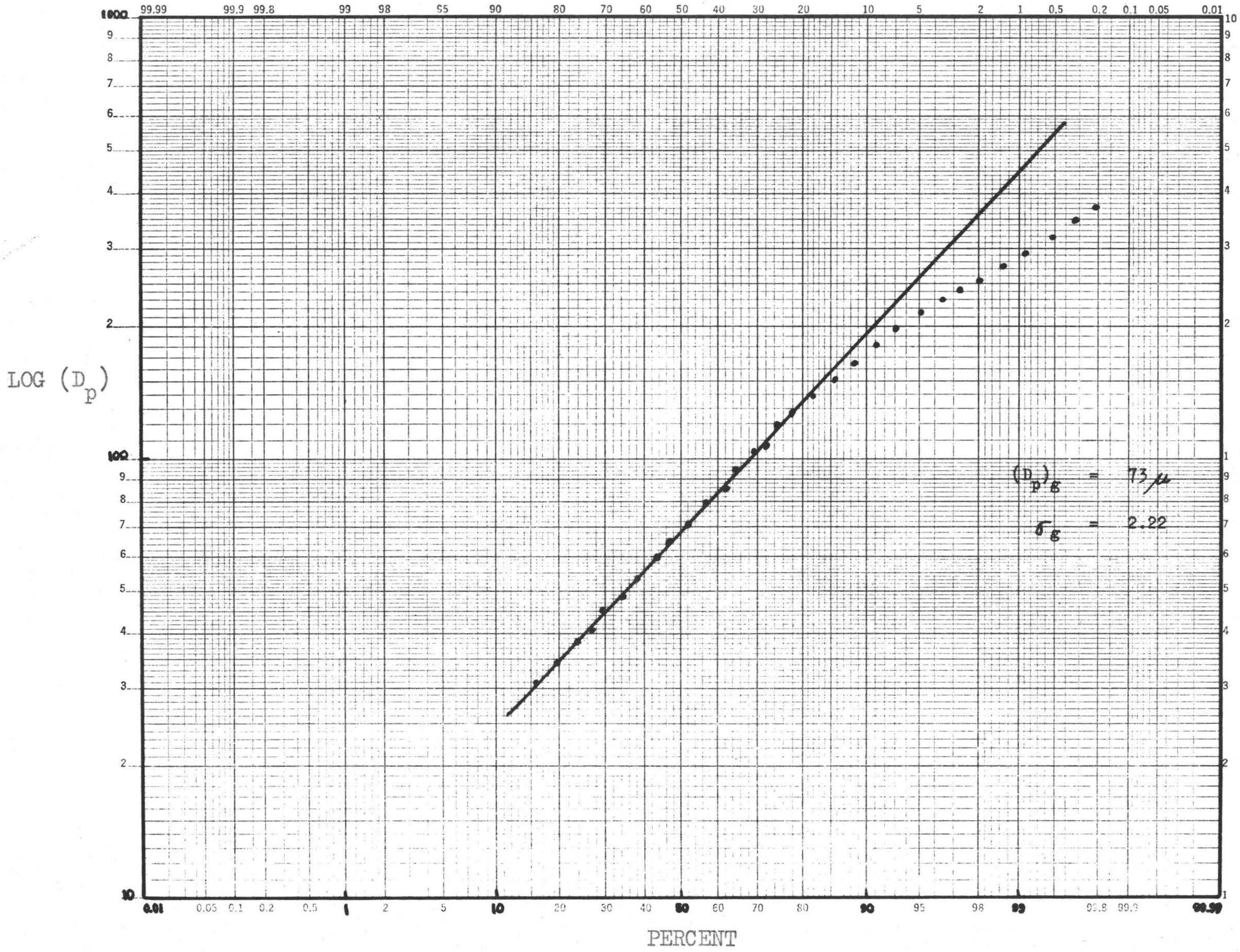

FIGURE A3-5

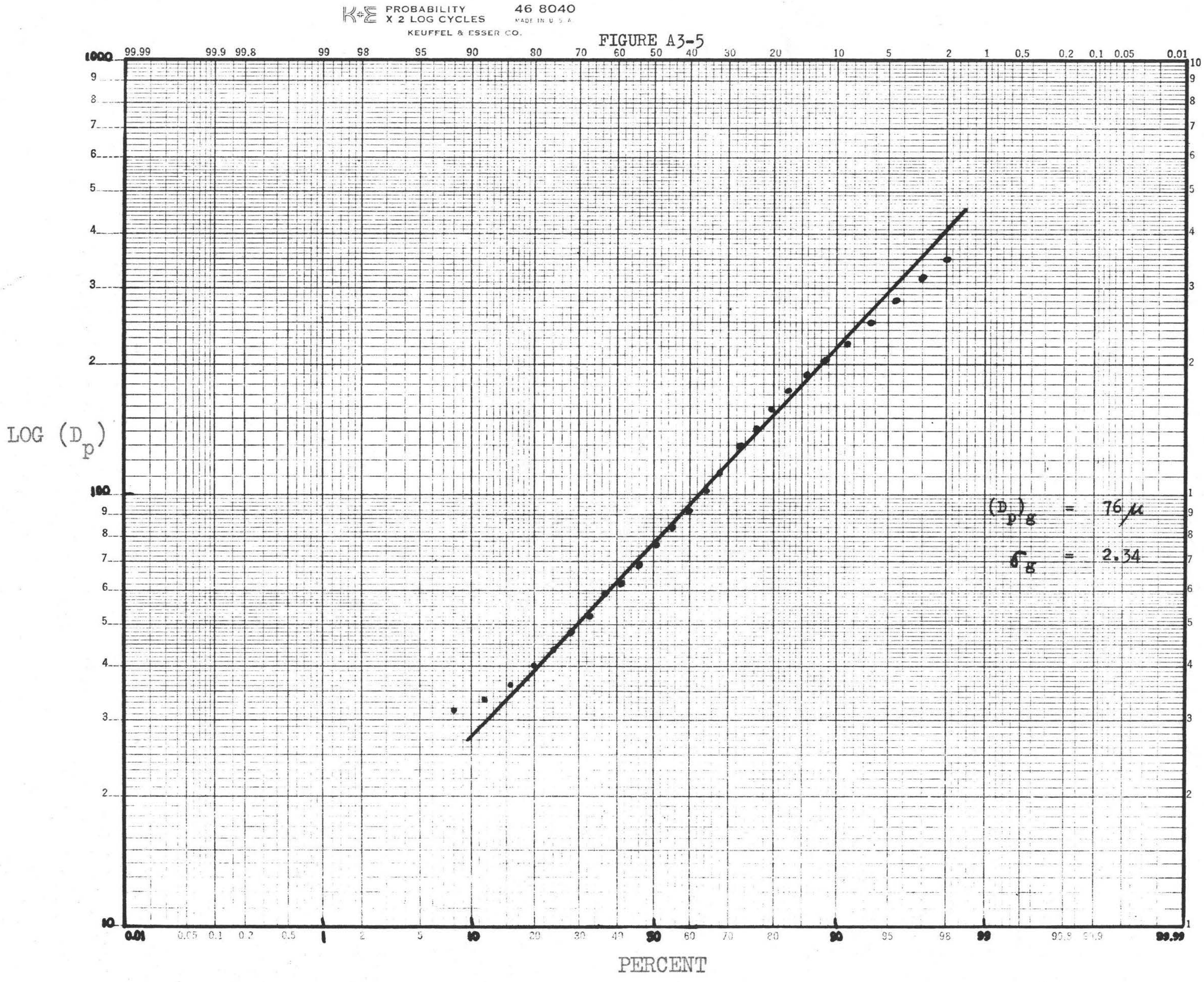
LOG (D_p)
PERCENT
$(D_p)_g$ = 76 μ
σ_g = 2.34
PROBABILITY X 2 LOG CYCLES 46 8040
KEUFFEL & ESSER CO.

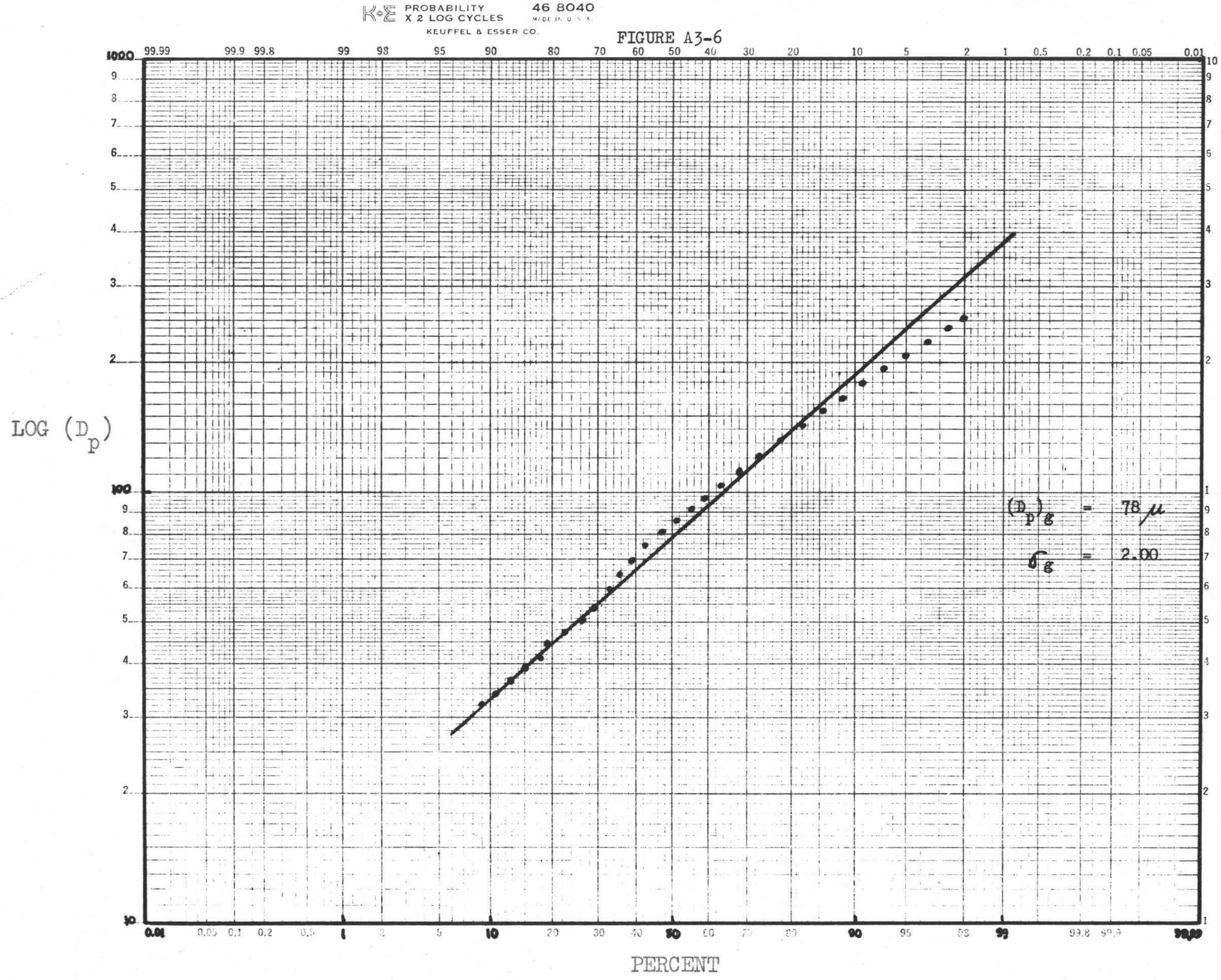
K+E PROBABILITY X 2 LOG CYCLES
46 8040
MADE IN U.S.A.
KEUFFEL & ESSER CO.
LOG (D_p)
PERCENT
(D_p)_g = 78 μ
σ_g = 2.00

FIGURE A3-6

FIGURE A3-7

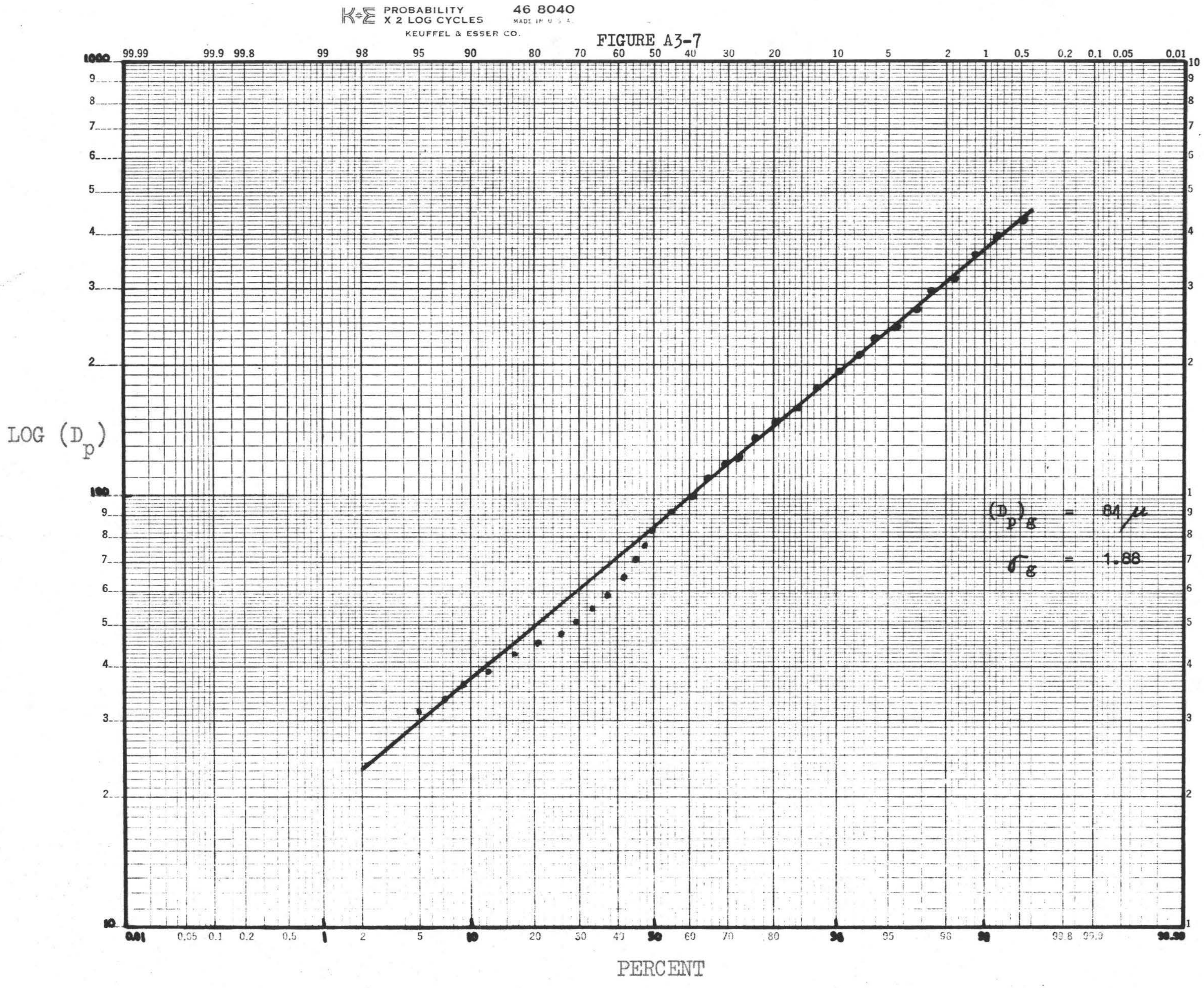

K+E PROBABILITY X 2 LOG CYCLES 46 8040
KEUFFEL & ESSER CO.
LOG (D_p)
PERCENT
$(D_p)_g$ = 84 μ
σ_g = 1.88

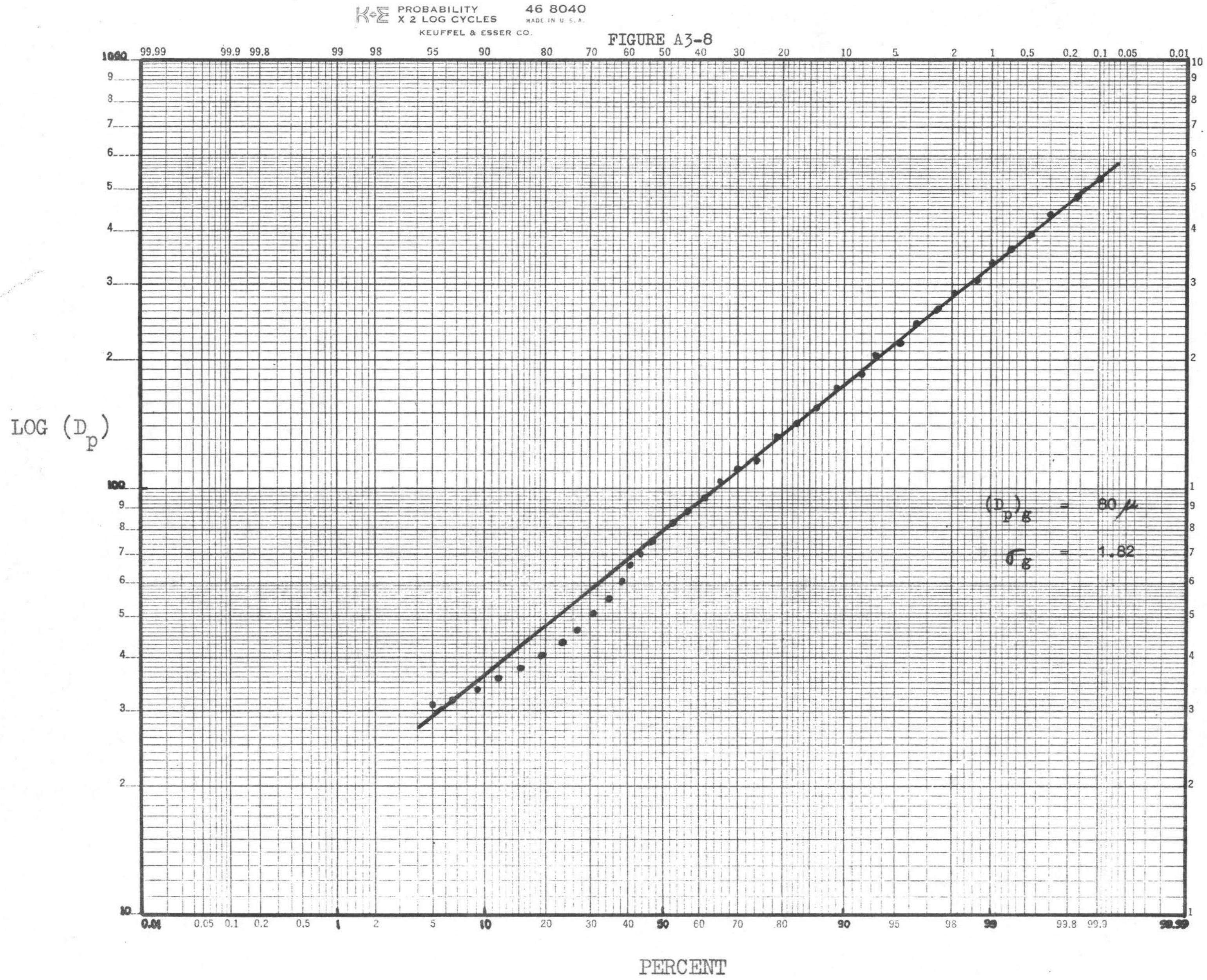

K+E PROBABILITY X 2 LOG CYCLES 46 8040
KEUFFEL & ESSER CO.
LOG (D_p)
PERCENT
$(D_p)_g$ = 80 μ
σ_g = 1.82

FIGURE A3-8

FIGURE A3-9

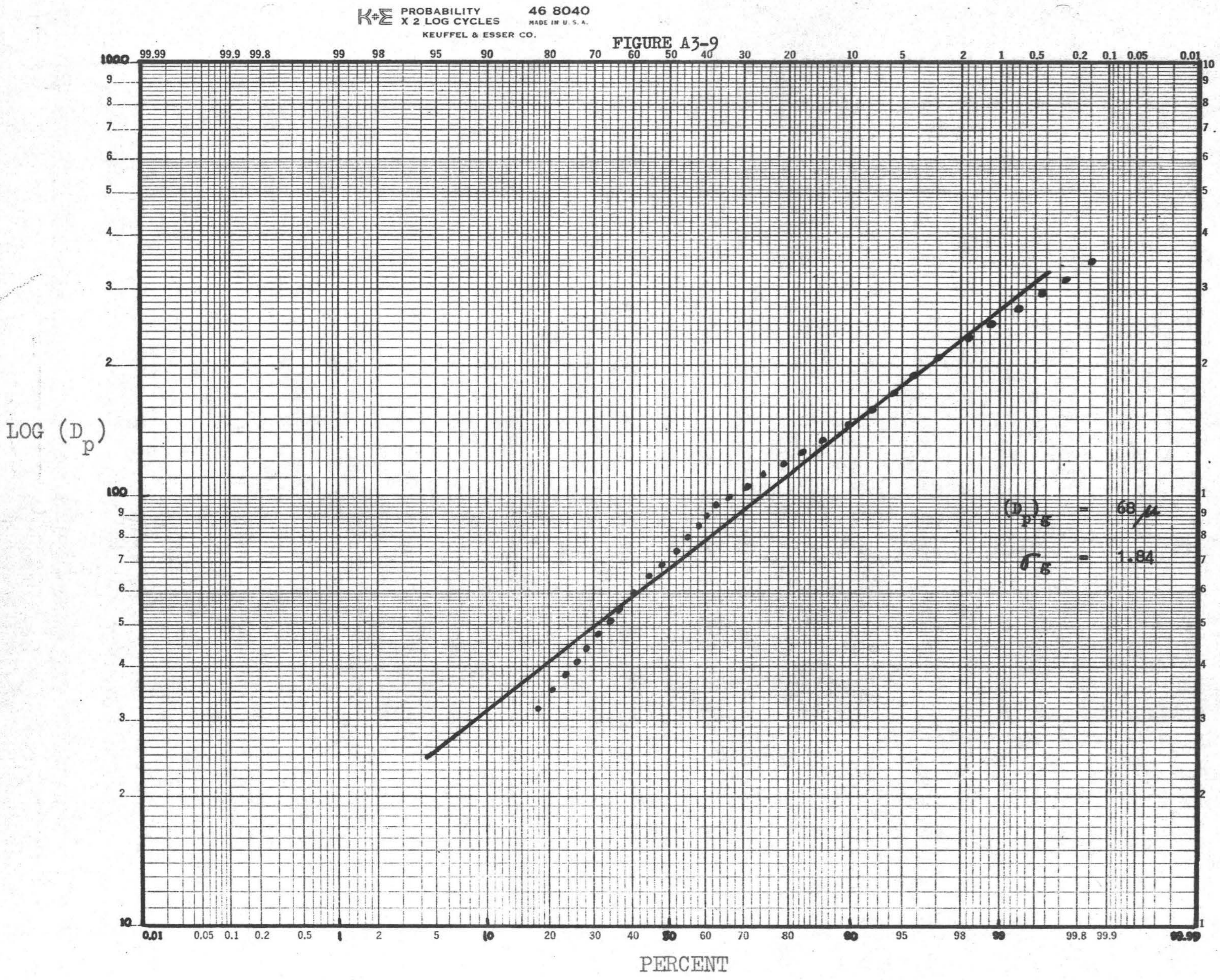
K+E PROBABILITY X 2 LOG CYCLES 46 8040
KEUFFEL & ESSER CO.
LOG (D_p)
$(D_p)_g$ = 68 μ
σ_g = 1.84
PERCENT

FIGURE A3-10

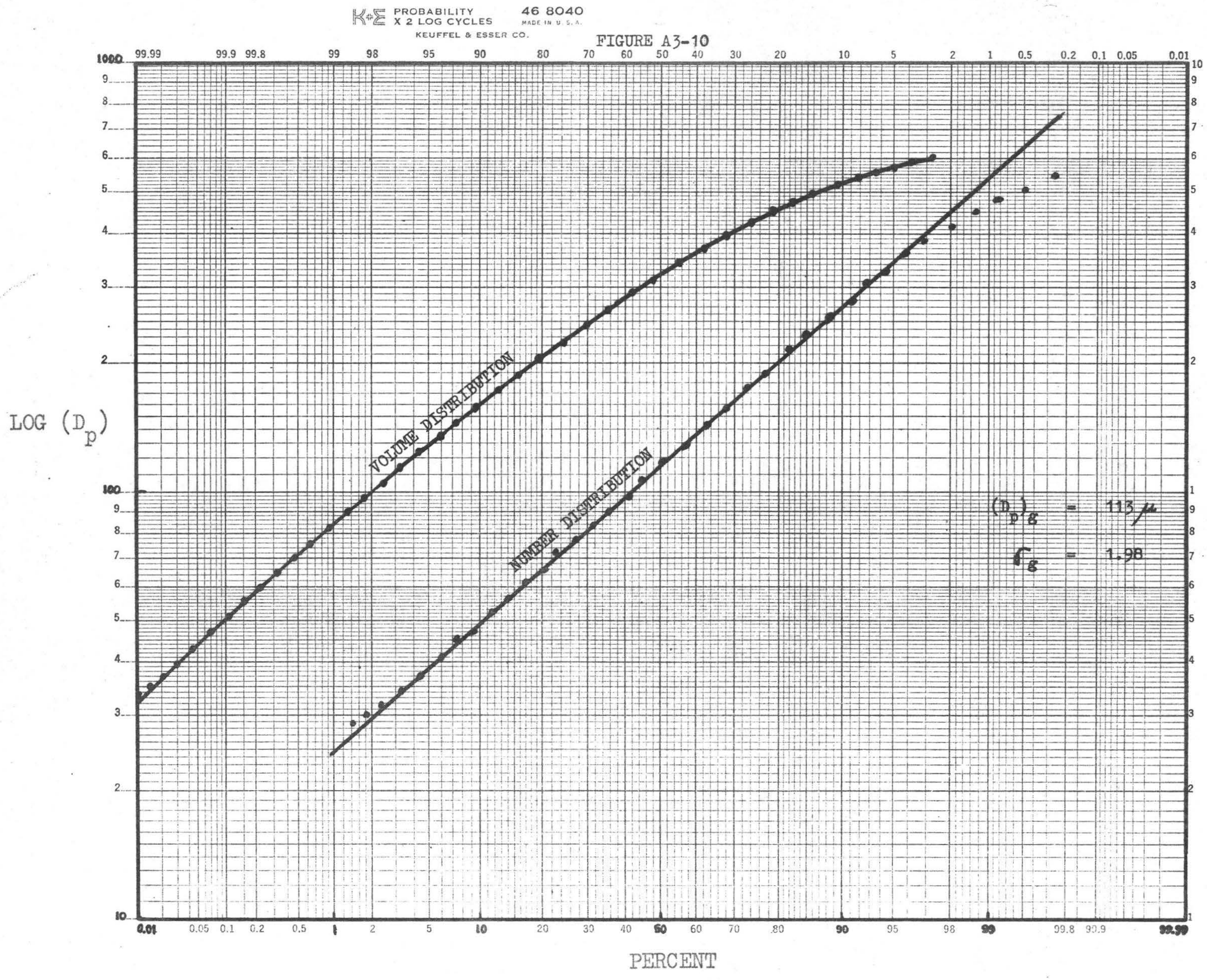

K+E PROBABILITY X 2 LOG CYCLES 46 8040
KEUFFEL & ESSER CO.
LOG (D_p)
PERCENT
VOLUME DISTRIBUTION
NUMBER DISTRIBUTION
(D_p)_g = 113 μ
σ_g = 1.98

K+E PROBABILITY X 2 LOG CYCLES 46 8040 MADE IN U.S.A.
KEUFFEL & ESSER CO.

FIGURE A3-11

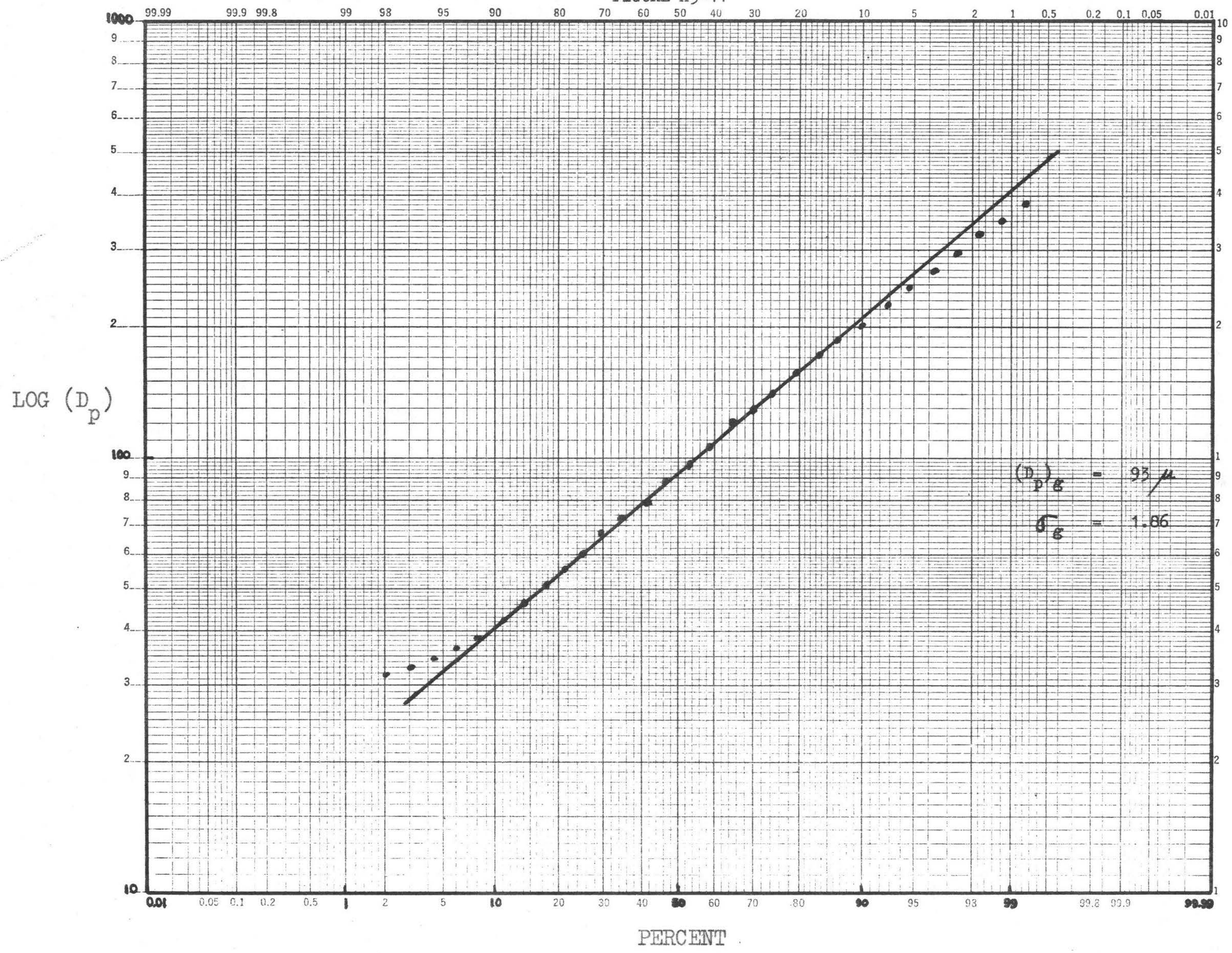

FIGURE A3-12

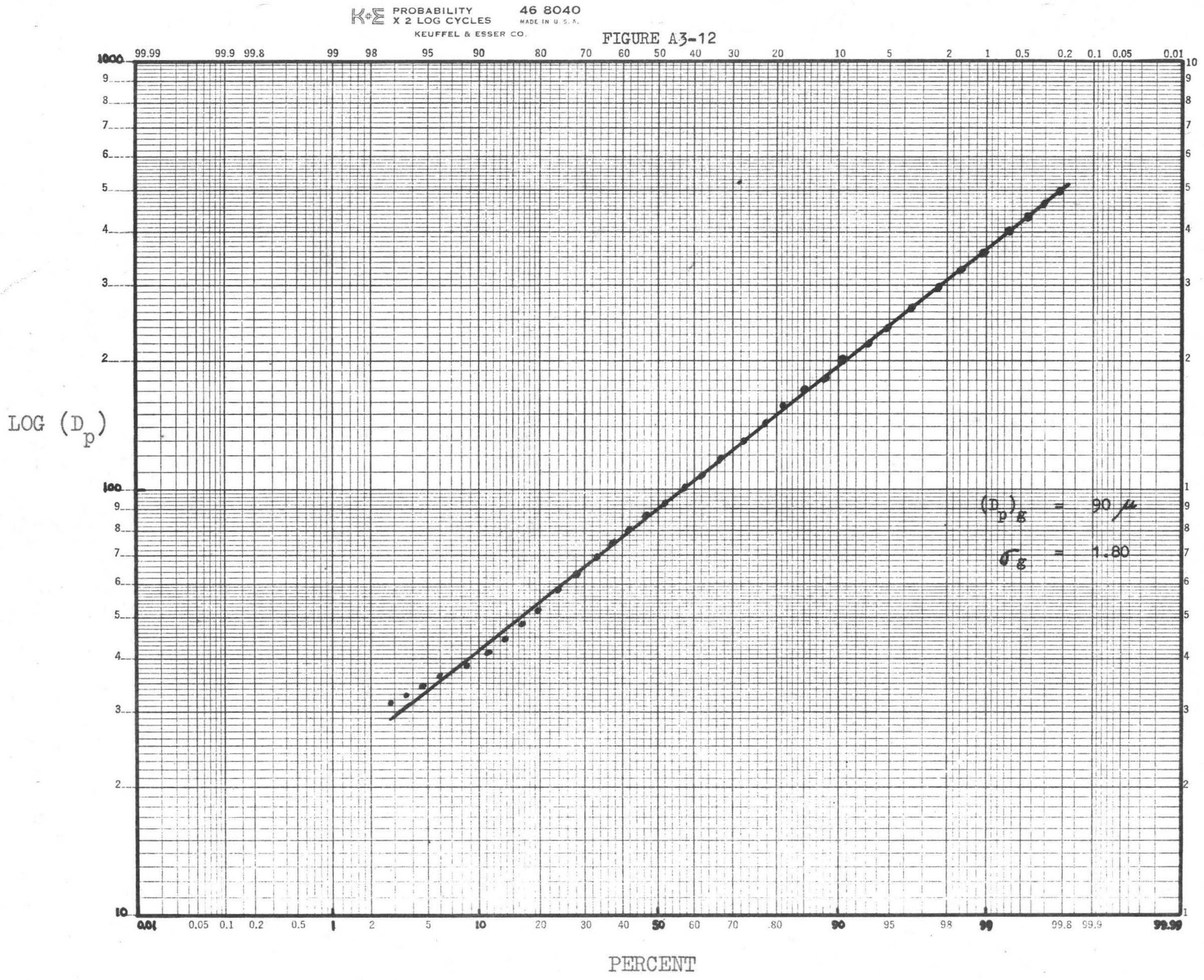
K+E PROBABILITY X 2 LOG CYCLES
46 8040
MADE IN U.S.A.
KEUFFEL & ESSER CO.
LOG (D_p)
PERCENT
(D_p)_g = 90 μ
σ_g = 1.80

volume and total area for that run. It is apparent that the proper diameter to use for each interval is weighted, depending on its use. The run volumes and areas and the number of drops counted for each run are given in Table A3-2.

According to Gwyn et al, there are drops in the distribution which are larger than the largest drops observed in the photographs. These larger drops, although having a low frequency, will markedly affect the total drop areas and volumes given in Table A3-2.

A sample calculation of $\langle D_p \rangle_{32}$ for run 1 will now be given.

From Figure A3-1

geometric number mean diameter $\langle D_p \rangle_g$ = 94 μ

geometric standard deviation (σ_g) = 1.92

$\log \langle D_p \rangle_g = 1.972$

$\log \sigma_g = 0.282$

Actual number of drops counted = 1,990

Then the expected value of the probability for the largest observed size is $\frac{1,990}{1,991} = 0.9995$

The term probability means that a fraction 0.9995 of all drops are smaller then this largest observed size. From Figure 1 of Gwyn et al. a drop of this probability lies 3.27 $(\log \sigma_g)$ above $\log \langle D_p \rangle_g$, on a number basis.

For a log-normal distribution, σ_g is the same, regardless of whether the distribution is plotted on a number (N), area (S), or volume (V) basis. The geometric means for these three bases are related by Equation 1.

TABLE A3-2 MEASURES OF DROP VOLUMES, AREAS, AND NUMBERS FOR EACH RUN

RUN	VOLUME $\Sigma n_i d_i^3$ $\mu^3 \times 10^{-8}$	AREA $\Sigma n d_i^2$ $\mu^2 \times 10^{-8}$	NUMBER Σn_i
1	0.6794	0.3433	2000
2	0.2802	0.1398	1000
3	0.6361	0.2493	1100
4	0.3633	0.1955	1600
5	0.7665	0.3288	2000
6	0.2712	0.1546	1200
7	0.1520	0.0747	500
8	0.2402	0.1293	1000
9	0.1410	0.0940	1000
10	0.7543	0.2789	1000
11	0.3545	0.1705	1000
12	0.6950	0.3321	2000

$$\log\left(\langle D_p\rangle_g\right)_S = \log\left(\langle D_p\rangle_g\right)_N + 4.606 \left(\log \sigma_g\right)^2 \qquad \ldots.\ 1$$

$$\log\left(\langle D_p\rangle_g\right)_V = \log\left(\langle D_p\rangle_g\right)_N + 6.909 \left(\log \sigma_g\right)^2$$

where $\left(\langle D_p\rangle_g\right)_S$ = geometric mean diameter for a distribution plotted on an area basis, for example.

Then the logarithm of the expected value of the largest observed size on an area basis, $\log\left(E\left(D_{p_L}\right)_S\right)$ lies a distance ϵ_1 above the log of the area mean. The value ϵ_1 is given by

$$\epsilon_1 = \left(3.27 - 4.606 \log \sigma_g\right)\right) \log \sigma_g$$

$$= 0.556 \qquad \text{(see Figure A3-13)}$$

Then, $\log\left(E\left(D_{p_L}\right)_S\right) = 1.972 + 0.556 = 2.528$

and $E\left(D_{p_L}\right)_S = 338\ \mu$

Figure A3-13 shows that the above calculation has located point A on the number distribution. Point A has a probability of 0.976, which is the same as the probability of the largest observed size, on an area basis.

Similarly, the logarithm of the expected value of the largest observed size on a volume basis $\log\left(E\left(D_{p_L}\right)_V\right)$ lies a distance ϵ_2 above the log of the volume mean. The value $_2$ is given by

$$\epsilon_2 = \left(3.27 - 6.909 \left(\log \sigma_g\right)\right) \log \sigma_g = 0.3725$$

Then, $\log\left(E\left(D_{p_L}\right)_V\right) = 1.972 + 0.3725 = 2.3445$

and $E\left(D_{p_L}\right)_V = 220\ \mu$

This point B on Figure A3-13. The probability at this point is 0.908.

FIGURE A3-13 SUMMARY OF CORRECTION CALCULATIONS USED TO CALCULATE $\langle D_p \rangle_{32}$

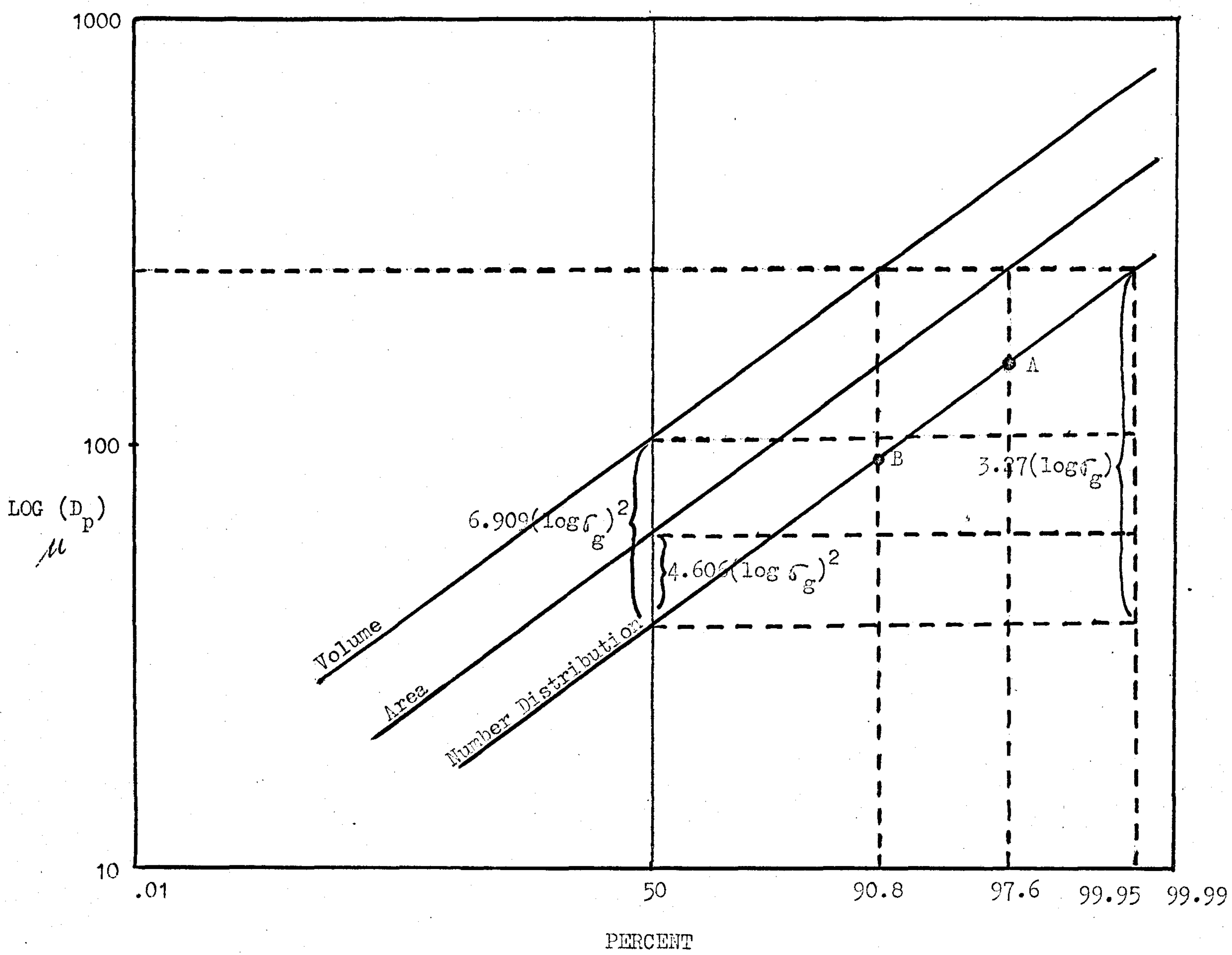

Now the volumes and areas previously calculated can be corrected.

$$\text{Total drop surface area} = \frac{\pi \times 0.3433 \times 10^8}{0.976} = \frac{\pi \times 0.352 \times 10^8}{} \mu^2$$

$$\text{Total drop volume} = \frac{\pi \times 0.6794 \times 10^{10}}{6 \times 0.908} = \frac{\pi \times 0.748 \times 10^{10}}{6} \mu^3$$

Then
$$\langle D_p \rangle^3_{30} = \frac{6}{\pi} \times \frac{\pi \times 0.748 \times 10^{10}}{6 \times 1991} = 0.3755 \times 10^7 \ \mu^3$$

$$\langle D_p \rangle^2_{20} = \frac{1}{\pi} \times \frac{\pi \times 0.352 \times 10^8}{1991} = 0.1767 \times 10^5 \ \mu^2$$

and
$$\langle D_p \rangle_{32} = \frac{3755. \times 10^3}{17.67 \times 10^3} = 212.1 \ \mu$$

A comparison of this value with a calculated value of 197.9 μ by the definition, Equation (4) Chapter 2, illustrates the importance of the correction proposed by Gwyn et al.

A3.a.4 Cumulative Drop Size Distributions

The cumulative number distributions for runs 1 to 12 are in Figures A3-1 to A3-12. An inspection of the data points shows that they are well fitted by the log normal distribution, except for run 9. The predominant feature of most of the distributions is the existence of tails at the ends of the line.

As far as the tail at the small sizes is concerned, it was found that changing drop size observers changed the tail, and left the rest of the distribution unchanged. Thus observer judgement and poor photograph contrast are to blame.

One interesting point about log-normal distributions is that the cumulative number, surface and volume distributions are all parallel on log-probability paper. This is well illustrated by

Figure A3-10. The tail at the upper end of the number distribution markedly affects the volume distribution by the 50% probability point, because the large drops containing about 50% of all the volume are not log-normally distributed.

The tail at the upper end of the distribution illustrates the concept of an "upper-limit size" as presented by Mugele and Evans (M-8). It seems that the mixing valve tends to break up the large drops. Thus the percentage of the smaller drops in the distribution increases (and still follows a log-normal distribution) while the percentage of large drops decreases. This is shown quite markedly by Figure A3-9, for the run with a large pressure drop across the mixing valve (run 9).

Both Mugele and Evans, and Irani and Callis (I-1) give procedures for obtaining straight lines on log-probability paper when such an upper limit size is apparent. These methods remove the actual physical interpretation of the distributions and put them on a mathematical basis which seems to have little meaning. While it is evident from Figure A3-9 that there is an upper limit size, rather then use the Mugele--Evans or the Irani--Callis procedures, a straight line was drawn by eye through the data. To test whether this line adequately represents the data was determined by the χ^2 test given in the next section.

A3.a.5 <u>The χ^2 Test on a Drop Size Distribution</u>

The use of the χ^2 test for distributions plotted on log-probability paper is thoroughly discussed by Kottler (K-5). He points out that the probability scale is stretched at its ends and therefore the deviation of a distribution from a straight line at the ends of the line must be weighted before an accurate estimate of χ^2 can be obtained.

The probability scale is really a representation of the cumulative normal distribution and is defined by

$$P = \int_{-\infty}^{z} \frac{1}{\sqrt{2\pi}} e^{\frac{-z^2}{2}} dz$$

When z = 0, P = 0.50, and this is the centre point on the probability scale. To determine the weighting factor to use in the χ^2 test, consider the equation

$$\delta P = A' \delta z$$

where A' is the weighting factor. The value of A' for a few different probabilities is given in Table A3-3. Table A3-3 shows that the probability scale is greatly distorted at high (or low) probabilities.

The χ^2 test gives an indication of the deviation of a distribution from a straight line. Suppose run 9 is considered, and its distribution is represented by a line with $\langle D_p \rangle_g = 68\,\mu$, and $\sigma_g = 1.84$.

Let $$\chi^2 = \sum_{i=1}^{n} \frac{(o_i - e_i)^2}{e_i}$$

where o_i is the observed value of the probability at some drop size i, and e_i is the expected value of the probability at the same size, as given by the straight line. For log-probability plots, $(o_i - e_i)$ must be weighted, depending on the probability value. Let the observed probability value determine the weighting factor to be used.

Table A3-4 gives the details for the χ^2 calculation. The

TABLE A3-3 VALUES OF THE WEIGHT A' AT DIFFERENT PROBABILITIES

P	δP	δz	A'	A'/A'_{50}
0.5000	.0040	.01	0.400	1.00
0.6026	.0038	.01	0.380	.952
0.7019	.0036	.01	0.360	.900
0.8023	.0028	.01	0.280	.698
0.9015	.0017	.01	0.170	.426
0.9901	.0003	.01	0.030	.075
0.9951	.0001	.01	0.010	.025

TABLE A3-4 A χ^2 CALCULATION FOR RUN 9

1	2	3	4	5	6	7
DROP SIZE μ	OBSERVED PROBABILITY	EXPECTED PROBABILITY	$\lvert 2-3 \rvert \times 7$	$\frac{(4)^2}{(3)}$	PROBABILITY P %	WEIGHT
32	18.1 %	10.0	5.26	2.770	18	.650
41	26.7	20.0	5.52	1.520	27	.825
50	33.9	30.0	3.61	.433	34	.925
61	42.9	42.9	0	--	43	.975
70	48.4	52.5	4.10	.318	48	1.00
79	55.3	60.0	4.59	.348	55	.975
90	63.3	68.5	4.95	.355	63	.950
103	70.4	76.0	4.62	.280	70	.825
110	74.6	79.5	3.80	.181	75	.775
125	87.7	85.0	1.50	.027	83	.650
143	88.4	90.0	0.80	.007	88	.500
152	90.7	91.5	0.32	.001	91	.400
162	92.0	93.0	0.375	.001	92	.375
			$\Sigma = 6.241$			

calculated value of χ^2 is 6.241, for 13 - 1 = 12 degrees of freedom. At the 95% confidence level and 12 degrees of freedom, the table value of χ^2 (see Crowe (C-3)) is 21.03, well above the calculated χ^2. This means that the measured drop size distribution for run 9 is not unlike that represented by a straight line with $\langle D_p \rangle_g = 68$ and $\sigma_g = 1.84$.

One point that should be made clear is that this is not necessarily the best line that could be drawn. By trial and error, or least squares, the χ^2 value can be made even smaller by other lines. However the slope and position of the best line will not change radically from those given here. Therefore, even though the distribution for run 9 is really two distributions, it can be well approximated by a straight line, and the corrections of Gwyn <u>et al</u> based on a log-normal distribution can be applied.

All the remaining drop distributions do not show such marked deviation from straight lines and it would seem reasonable then that their calculated χ^2 would be much less than the table value, inspite of the presence of tails.

A3.a.6 <u>Statistical Treatment of the Drop Size Distribution Data</u>

The second order polynomial given in equation (2)

$$\langle D_p \rangle_{32} = b_o x_o + b_1 x_1 + b_2 x_2 + b_{11} x_1^2 + b_{12} x_1 x_2 + b_{22} x_2^2 \quad \ldots\ 2$$

was fitted to the data for the coded variable levels given in Table A3-1, using least squares. The resulting equation with the coefficients evaluated is

$$\langle D_p \rangle_{32} = 229.3 - 37.09 x_1 - 2.69 x_2 - 1.32 x_1 x_2 + 3.64 x_1^2 + 1.68 x_2^2 \quad \ldots\ 3$$

To evaluate how well this equation represents the data, some statistical measures should be considered.

The sum of squares of the deviations of observations y_i from their overall mean $\langle y \rangle$ can be broken into two parts

$$(y_i - \langle y \rangle)^2 = (y_i - y_i')^2 + (y_i' - \langle y \rangle)^2$$

where y_i' is the predicted value given by the regression equation. This expression can also be written as

$$s_y^2 = s_{y/x}^2 + s_{y'}^2$$

where $s_{y'}^2 = (y_i' - \langle y \rangle)^2 / (n - 1)$

$= $ variance accounted for by the regression equation

$s_{y/x}^2 = $ variance not accounted for by the regression equation (standard error of estimate)

$s_y^2 = $ total variance of y_i about the mean $\langle y \rangle$.

A correlation coefficient can now be defined as

$$r_{y/x} = +\sqrt{\frac{s_{y'}^2}{s_y^2}}$$

This correlation coefficient ranges from a value of zero for no correlation, to a value of one for all observation, y_i, lying exactly on the regression plane. Observations always have random error associated with them, so that $r_{y/x}$ is almost never zero or one. Its statistical significance should therefore be tested.

Although the correlation coefficient may be significant, some of the regression coefficients in the regression equation may not be significant. This can be checked by first calculating the standard errors of the partial regression coefficients. For b_j

$$s_{b_j} = s_{y/123\ldots k} \sqrt{ne_{jj}}$$

where $s_{y/123\ldots k}$ is the standard error of estimate, n is the number of observations in the sample, and e_{jj} is the value of the diagonal element in the inverse matrix for the normal equations (see Crowe (C-3) page 171).

A Student 't' test can be performed to see if b_j is significantly different from zero. The calculated t value for b_j is

$$t = \frac{b_j}{s_{b_j}}$$

and this t value may be compared with the table value of t.

The significance of equation 3 may now be determined. The multiple correlation coefficient can be calculated from

$$r_{y/123\ldots k} = \sqrt{1 - \frac{(n - k - 1)\, s^2_{y/123}}{(n - 1)\, s^2_y}}$$

where k = number of independent variables

n = number of observations

and where

$$s^2_{y/123\ldots k} = \frac{1}{n - k - 1} \sum_{i=1}^{n} (y_i - y_i')^2$$

and

$$s^2_y = \frac{n \sum y_i^2 - (\sum y_i)^2}{n\,(n-1)}$$

Using these formulae and the data from Table A3-1, it was found that:

$$s^2_y = 1{,}780. \qquad n = 12$$

$$s^2_{y/12} = 424.9 \qquad k = 2$$

and

$$r_{y/12} = 0.910$$

The statistical significance of the multiple correlation coefficient is determined by comparing it with the table value (see (C-3), page 241) at the 95% confidence level, for k + 1 variables and n - k - 1 degrees of freedom. Then,

$$k + 1 = 3$$

$$n - k - 1 = 9$$

and

$$r_{table} = 0.697$$

Therefore the calculated value of r is significant at the 95% confidence level. (There are only 5 chances in 100 that $r \gtrsim 0.697$ could have arisen due to random error alone.) Equation 3 satisfactorily represents that data, but the statistical significance of its regression coefficients must be checked. Table A3-5 gives the standard errors for each of the regression coefficients, and the calculated Student 't' value. If the calculated t value for each coefficient is larger than the table value given at the 95% confidence level for n - k - 1 degrees of freedom (see (C-3), page 231), the regression coefficient is statistically different from zero. Then, at the 95% confidence level

$$n - k - 1 = 9$$

$$t_{table} = 2.262$$

Only b_1 is significant.

The procedure to follow when a partial regression coefficient

TABLE A3-5 STUDENT 't' VALUES FOR THE PARTIAL REGRESSION COEFFICIENTS (DROP SIZE CORRELATION)

COEFFICIENT	STANDARD ERROR	STUDENT 't' VALUE
b_1	5.950	6.233
b_2	5.950	0.452
b_{12}	10.306	0.129
b_{11}	4.463	0.815
b_{22}	4.463	0.375

$$t_{table} = 2.262$$

is not statistically significant is:

1) retain the term.

2) calculate a new regression equation (preferrably on a new sample of observations), omitting observations on the insignificant variable.

3) discard the term and use the regression equation as it was.

If procedure one is decided against, then procedure two is the proper method. If the experimental design was orthogonal (as it was here) then procedures two and three are equivalent.

Procedure two was decided upon since a new linear regression equation based on the uncoded levels of mixing valve pressure drop (x_1) was desirable. Using least squares to fit a linear relation to the data resulted in

$$\langle D_p \rangle_{32} = 324.64 - 1.69\, x_1$$

where

$$\langle D_p \rangle_{32} = \text{volume/surface dia., } (\mu)$$

$$x_1 = \text{mixing valve } \Delta P, \text{ (mm. } H_g\text{)}$$

The statistics are

$$r_{y/x} = 0.7427 \qquad r_{table} = 0.576$$

$$s_b = 0.4823$$

$$t_b = \frac{1.69}{0.482} = 3.50 \qquad t_{table} = 2.228$$

The correlation is statistically significant at the 95% confidence level, and the slope (1.69) is statistically different from zero, at the 95% level.

A significant correlation between a measure of the drop size distribution, $\langle D_p \rangle_{32}$, and the mixing valve pressure drop has been obtained.

A3·b Hydrocyclone Separation

In attempting to separate two immiscible liquids from one another, the efficiency of the separation will depend in part on the drop size distribution. This variable was correlated with an easily measured parameter (mixing valve pressure drop) in (a) part. From the literature, it appeared that the volume split in the cyclone was also important. Finally, the oil/water ratio should play a significant part in determining separation efficiency since it determines the load that the cyclone must operate under, if the feed flow rate is kept constant.

A3·b·1 Statistical Design

A statistical central composite experiment design for three independent variables at five levels was used. The variables were; x_1 = oil/water ratio (in feed), x_2 = volume split (overflow rate/underflow split), and x_3 = $\langle D_p \rangle_{32}$ (Sauter mean diameter of the feed). The experiment design, for coded and uncoded levels, and the resulting cyclone efficiencies are given in Table A3-6. (To distinguish between runs 1 to 12 used in measuring drop size distributions, let the efficiency work be designated as TRIALS 1 to 20.)

A3·b·2 Controlling the Variables

The oil/water ratio was controlled simply by adjusting the pump discharge throttle valves until the desired rotameter readings were reached. The mixing valve pressure drop (determining $\langle D_p \rangle_{32}$) was easily changed by adjusting the mixing valve opening.

The adjustment of the volume split was difficult since it could

TABLE A3-6 STATISTICAL EXPERIMENT DESIGN FOR THREE INDEPENDENT VARIABLES AT FIVE LEVELS, AND THE RESULTING CYCLONE EFFICIENCIES

TRIAL	CODED LEVELS			UNCODED LEVELS			OBSERVED EFFICIENCY (%)
	x_1	x_2	x_3	oil/water ratio x_1	volume split x_2	$\langle D_p \rangle 32$ x_3 (μ)	
1	-1	-1	-1	.1534	5/1	284.1	95.66
2	1	1	1	.1920	7/1	284.1	67.58
3	1	-1	1	.1920	5/1	207.8	79.55
4	-1	1	1	.1534	7/1	207.8	70.85
5	0	0	0	.1722	6/1	218.6	80.60
6	0	0	0	.1722	6/1	218.6	76.76
7	1	1	1	.1920	7/1	207.8	65.41
8	-1	-1	1	.1534	5/1	207.8	91.69
9	-1	1	-1	.1534	7/1	284.1	75.90
10	1	-1	-1	.1920	5/1	284.1	94.99
11	0	0	0	.1722	6/1	218.6	75.74
12	0	0	0	.1722	6/1	218.6	76.46
13	-2	0	0	.1341	6/1	218.6	91.96
14	2	0	0	.2110	6/1	218.6	69.89

TABLE A3-6 (continued)

15	0	-2	0	.1722	4/1	218.6	94.16
16	0	2	0	.1722	8/1	218.6	64.54
17	0	0	-2	.1722	6/1	304.0	84.25
18	0	0	2	.1722	6/1	162.0	74.05
19	0	0	0	.1722	6/1	218.6	78.63
20	0	0	0	.1722	6/1	218.6	80.35

not be measured directly. Since the cyclone overflow valve was always open, the volume split was altered by changing the underflow valve opening. By placing plugs in the overflow and underflow tanks, and recording the times for these tanks to fill up between two reference marks, the volume split could be determined. Usually three re-settings of the underflow valve were necessary before the desired volume split was attained.

A3·b·3 Calculation of Cyclone Efficiency

Since the cyclone flow rates (Q_1, Q_2, Q_3) were all known, and sample analyses determined the volumetric compositions y_2 and y_3, the separation efficiency could be calculated from

$$E_s = \frac{Q_2}{Q_1}\left[\frac{y_2 - y_1}{1 - y_1}\right] + \frac{Q_3}{Q_1}\left[\frac{y_1 - y_3}{y_1}\right]$$

The sample compositions for all 20 Trials are given in Table A3-7. Since two samples were taken for each y_2 and y_3 measurement, two efficiencies could be calculated for each trial. The efficiencies in Table A3-6 are thus an average of two efficiencies.

A3·b·4 Pressure Drop Acoss the Cyclone

Flow rate to the hydrocyclone was kept constant. However, changing the volume split changed P_1, P_2, and P_3. For the sake of completeness, these pressures were measured and are also recorded in Table A3-7. The pressures are corrected for liquids in the manometer lines.

A3·b·5 Statistical Treatment of the Cyclone Separation Data

This subsection follows a similar form to the statistical treatment of part (a). The data were fitted to a second order

TABLE A3-7 CYCLONE OUTLET SAMPLE COMPOSITIONS AND PRESSURES FOR ALL TRIALS

TRIAL	PRESSURES mm.Hg			COMPOSITIONS (% VOLUME) WATER			
	P_1	P_2	P_3	y_2 (1)	y_2 (2)	y_3 (1)	y_3 (2)
1	290	103	176	100.0	99.68	17.02	17.58
2	295	122	203	94.40	94.37	14.31	14.28
3	295	111	183	96.70	96.90	19.80	19.95
4	300	124	199	96.00	96.10	20.50	20.43
5	295	116	190	96.80	97.60	17.80	18.35
6	295	116	190	96.56	96.50	17.83	17.58
7	300	124	204	94.05	94.17	18.90	17.90
8	290	103	174	99.36	99.36	22.42	21.30
9	295	120	199	96.84	96.54	14.87	14.62
10	290	109	181	99.68	99.53	14.67	15.47

TABLE A3-7 (Continued)

11	295	118	196	96.49	96.18	17.20	17.23
12	295	116	190	96.48	96.47	18.27	18.02
13	295	115	170	99.38	99.32	20.95	20.08
14	300	120	199	94.56	94.30	16.32	15.89
15	295	98	170	99.94	99.94	23.80	23.75
16	305	126	208	94.67	94.33	16.35	16.60
17	295	115	190	97.60	97.76	13.29	13.21
18	310	116	198	96.32	96.02	21.41	21.90
19	295	116	194	96.93	96.71	16.53	17.12
20	290	111	190	97.28	96.96	17.00	17.32

TABLE A3-7 (Continued)

NOTES:

1.) Pressures are corrected for the presence of water and carbon tetrachloride in pressure lines.

2.) Compositions give component mass balances to within 13%.

3.) Overall mass balances agreed within 5%.

4.) Standard deviation of observations at the centre point is 2.10%.

5.) Solubility in the opposite phase was negligible in each case.

6.) Temperature constant at 25°C ± 2°C.

7.) Trials 5, 6, 11, 12, 19, 20 are replicate runs.

polynomial and its significance tested. Then a linear relationship among the variables was found and statistically tested.

A second order polynomial of the form given below was used to represent the data

$$E_s = b_o x_o + b_1 x_1 + b_2 x_2 + b_3 x_3 + b_{11} x_1^2 + b_{22} x_2^2 + b_{33} x_3^2 + b_{12} x_1 x_2 + b_{13} x_1 x_3 + b_{23} x_2 x_3$$

The constants for this polynomial were determined using an I.B.M. 7040 computer with a computer program written to solve the normal equations as given by Crowe (C-3). The resulting expression was

$$E_s = 79.45 - 4.419x_1 - 8.837x_2 - 2.939x_3 + 0.784x_1^2 + 0.390x_2^2 + 0.340x_3^2 - 0.119x_1x_2 - 1.074x_1x_3 + 1.524x_2x_3$$

The standard errors and the corresponding Student 't' values for the partial regression coefficients are given in Table A3-8. At a 95% confidence level and for 10 degrees of freedom, the tabulated t value is 2.228. Comparing this value with those in Table A3-8 shows that only b_1, b_2, and b_3 are significant. The multiple correlation coefficient for this equation was found to be

$$r_{y/123} = 0.954$$

For k + 1 variables (=4) and n - k - 1 degrees of freedom (=16), and at a 95% confidence level, $r_{table} = 0.615$. Therefore the regression equation in highly significant, even though the constants of the second order terms are not significant. This infers a linear relation.

TABLE A3-8 STUDENT 't' VALUES FOR THE PARTIAL REGRESSION COEFFICIENTS (SECOND ORDER EFFICIENCY CORRELATION)

COEFFICIENT	STANDARD ERROR	STUDENT 't' VALUE
b_1	0.810	5.458
b_2	0.810	10.914
b_3	0.810	3.630
b_{12}	1.145	0.104
b_{13}	1.145	0.938
b_{23}	1.145	1.331
b_{11}	0.646	1.213
b_{22}	0.646	0.604
b_{33}	0.646	0.526

$t_{table} = 2.228$

Although there is considerable scatter in the data for mixing valve pressure drop versus $\langle D_p \rangle_{32}$, the above second order regression equation shows that mixing valve pressure drop (x_3) is the least important of the three variables. Even though the difficulty of reproducing drop size distributions has seemingly been neglected in determining this second order equation, this error does contribute to the standard error of estimate of the separation data. Since x_3 is the least important of the three variables, its effect on the standard error of estimate is small.

A linear relation of the form given below was then fitted to the data

$$E_s = b_o x_o + b_1 x_1 + b_2 x_2 + b_3 x_3$$

Upon evaluating the constants, as before, this equation became

$$E_s = 79.45 - 4.419 x_1 - 8.837 x_2 - 2.939 x_3$$

The standard error of the partial regression coefficients and the calculated Student 't' values are given in Table A3-9. At a 95% confidence level and for 16 degrees of freedom, the tabulated t value is 2.120. Comparing this value with those for the partial regression coefficients shows that all coefficients are significant.

The multiple correlation coefficient was found to be

$$r_{y/123} = 0.959$$

and

$$r_{table} = 0.615$$

Therefore the linear regression is highly significant.

TABLE A3-9 STANDARD ERROR AND STUDENT 't' VALUES FOR THE PARTIAL REGRESSION COEFFICIENTS (LINEAR EFFICIENCY CORRELATION)

COEFFICIENT	STANDARD ERROR	STUDENT 't' VALUE
b_1	0.766	5.773
b_2	0.766	11.543
b_3	0.766	3.840

$t_{table} = 2.120$

A3.c <u>Summary of Appendix 3</u>

This appendix has given the experimental data on drop size distributions and hydrocyclone separations. It was found that the drop size distribution data can be correlated by a linear relation

$$\langle D_p \rangle_{32} = 324.64 - 1.69x_1$$

This correlation does not include the effect of oil/water ratio on $\langle D_p \rangle_{32}$ since the oil/water ratio was found to have no significant effect at the 95% significance level.

The cyclone separation data can be correlated by the equation

$$E_s = 79.45 - 4.419x_1 - 8.837x_2 - 2.939x_3$$

The second order terms were found to be not significant. The variables may be listed in decreasing order of importance as

x_2 = volume split

x_1 = oil/water ratio

x_3 = drop size distribution (mixing valve pressure drop)

APPENDIX 4 CONSIDERATION OF $(D_p)_{50}$

A4 CONSIDERATION OF $(D_p)_{50}$

In chapter 2 the concept of the $(D_p)_{50}$ size particle was briefly discussed. In this appendix, consideration will be given to methods of calculating $(D_p)_{50}$.

A4.a Stokes Law and the Hydrocyclone

A drop reaches its horizontal equilibrium position in the hydrocyclone when the drag force on the drop, due to the inward flow of liquid, equals the centrifugal force caused by the drop's circular path. If the radial velocity is known at all points, then this velocity can be set equal to the terminal velocity of a drop, and hence equilibrium envelopes can be calculated. An example of equilibrium envelopes for Kelsall's cyclone is given in Figure A4-1. However, to calculate the drop terminal velocity that equals the fluid radial velocity requires the use of either Stoke's Law (1) or Newton's Law (2), depending on the particle Reynold's Number, radial velocity, and tangential velocity.

$$v_t = \frac{(\rho_s - \rho_c)\, D_p^2\, V_T^2}{18\,\mu_c\, r_T} \quad \ldots\ldots\ldots\ldots\ldots\ldots 1$$

$$v_t = \sqrt{\frac{4\,(\rho_s - \rho_c)\, D_p\, V_T^2}{3\, C_D\, \mu_c\, r_T}} \quad \ldots\ldots\ldots\ldots 2$$

A4.b Calculation of $(D_p)_{50}$

There are five methods available for calculation of $(D_p)_{50}$. They will be discussed in turn. All methods are applicable to the

FIGURE A4-1 EXAMPLE OF DROP EQUILIBRIUM ENVELOPES (AFTER KELSALL (K-2))

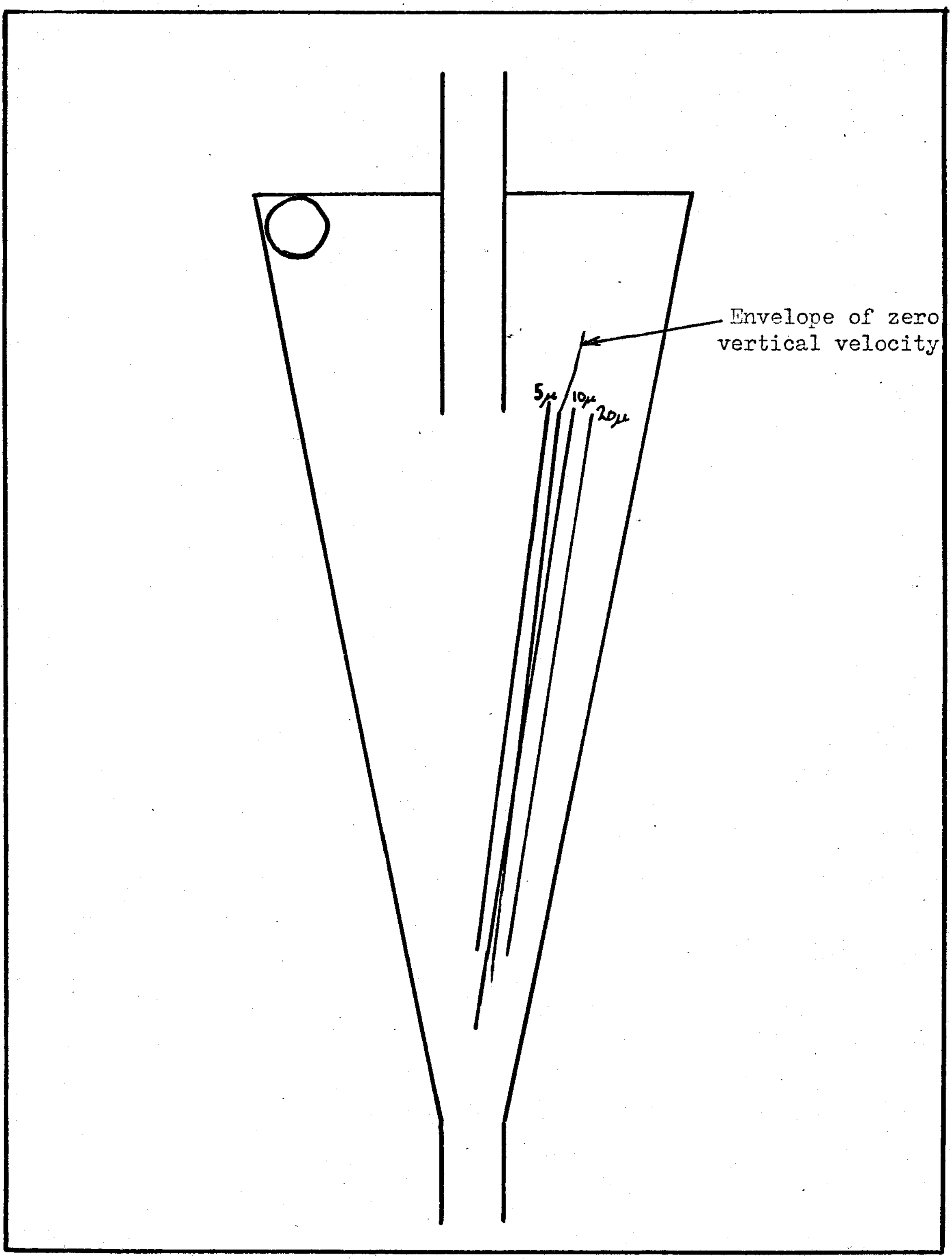

2 inch diameter cyclone used.

A4·b·1 Dahlstrom (D-1)

Dahlstrom presents an empirical equation that represents his data. It is

$$(D_p)_{50} = \frac{81\,(D_1\,D_2)^{0.68}}{(Q_1)^{0.53}} \left[\frac{1.73}{\rho_s - \rho_c}\right]^{0.5}$$

For Trial 6

$$Q_1 = 4.85 \text{ USGPM.}$$

$$D_1 = D_2 = 0.475 \text{ inches}$$

$$\rho_s = 1.583 \text{ gm./cc.}$$

$$\rho_c = 1.00 \text{ gm./cc.}$$

Then $(D_p)_{50} = 21.9\ \mu$

A4·b·2 Yoshioka and Hotta (Y-3)

These authors also present an empirical equation

$$(D_p)_{50} = \left[\frac{\mu_c}{\rho_s - \rho_c}\right] \frac{D_C^{0.1}\, D_1^{0.6}\, D_2^{0.8}}{Q_1^{0.5}}$$

For Trial 6

$$D_C = 0.146 \text{ feet}$$

$$\mu_c = 6.0 \times 10^{-4} \text{ lb./ft-sec.}$$

and

$$(D_p)_{50} = 21.4\ \mu$$

It should be noted that both the above equations are for cyclones with no valves on the outlets. The cyclone used in the present work had the overflow valve fully open so that its presence would have little effect on the cyclone operation.

A4·b·3 Lilge (L-1)

Lilge presents a method to calculate $(D_p)_{50}$ which is based on an empirical correlation of velocity profiles. The method is very long, and only the result is given here, for Trial 6.

$$(D_p)_{50} = 10.4\ \mu$$

This method does not assume Stokes Law and so involves a trial and error procedure. Lilge gives an equation for calculation of V_r, giving for this cyclone operation a valve V_r = 0.257 fps.

This V_r, when compared with the V_r from Bradley's work (to follow), is roughly three times larger.

A4·b·4 Rietema (R -2)

This author investigated many hydrocyclones of different designs. He gives the equation

$$Cy_{50} = \frac{(D_p)^2_{50}(\rho_s - \rho_c)\ L}{\mu_c}\ \frac{(\Delta p)_t}{\rho_c\ g}$$

where Cy_{50} is an empirical constant given by Figure 6 of his paper. For Trial 6, Cy_{50} = 6 and solving for $(D_p)_{50}$, it is found

$$(D_p)_{50} = 56\ \mu$$

Rietema has assumed Stokes Law to be applicable, and his derivation also assumes the presence of an air core. In the calculation, the $(\Delta p)_t$ given by Rietema's method for run 6 has been multiplied by 2, since the pressure drop in a cyclone with no air core is about twice the pressure drop when operating with an air core, for the same throughput (R-2).

A4·b·5 Bradley (B-2)

Since Bradley's derivation of an expression for $(D_p)_{50}$ is straight forward, it is given here, especially since it can be easily modified from the form he gives to a more generally applicable equation.

It is generally agreed that the tangential velocity in the outer region of the hydrocyclone is given by

$$V_T \, r^n = \text{constant} \qquad \text{(below the vortex finder and near the cyclone wall)}$$

where $\quad 1 \geq n \geq \text{zero}$

If the tangential velocity distribution in the outer region followed the law of conservation of angular momementun, n = 1. It has been found that n ranges from 0.4 to 0.8.

A velocity loss ratio α is defined as

$$\alpha = \frac{V_C}{\langle V_1 \rangle}$$

where V_1 is the velocity of the fluid in the inlet pipe and V_C is the fluid velocity at the feed inlet level in the hydrocyclone, near the cyclone wall.

The position of the envelope of zero vertical velocity (Figure A4-2) approximately coincides with the surface of a cone, drawn with base diameter equal to 2.3 D_2.

Now, assuming that all liquid passing to the overflow must cross through the side of this imaginary cone, the inward radial

FIGURE A4-2 LOCATION OF ZERO VERTICAL VELOCITY LOCUS

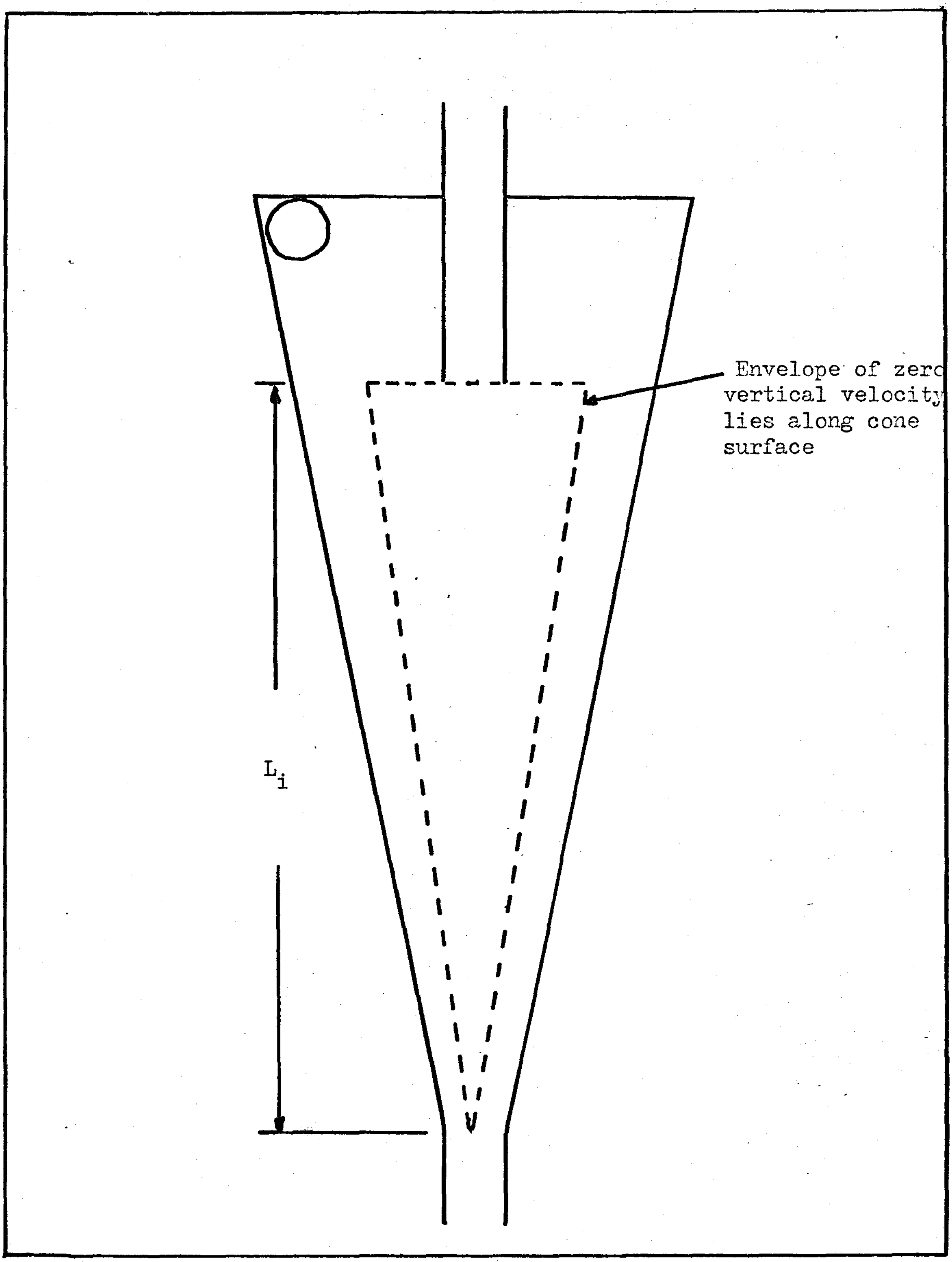

velocity can be written

$$V_r = \frac{Q_2}{(\pi/2)(2.3\ D_2)\ L_i} \quad \ldots\ldots\ldots\ldots\ldots\ 1$$

Bradley sets V_r equal to the terminal velocity v_t of a particle of size $(D_p)_{50}$, since V_r has been predicted at the envelope of zero vertical velocity.

Therefore

$$\frac{Q_2}{(\pi/2)(2.3\ D_2)\ L_i} = \frac{(\rho_s - \rho_c)(D_p)^2_{50}}{18\ \mu_c} \frac{(V_T)^2}{r_T} \quad \ldots\ldots\ 2$$

where in place of the gravitational acceleration, the centrifugal acceleration has been written. Here, V_T and r_T are the tangential velocity and radius at any point on the envelope of zero vertical velocity.

However,

$$V_T\ r_T^n = V_C\ r_C^n = \alpha \langle V_1 \rangle\ r_C^n$$

Therefore, $$V_T = \alpha \langle V_1 \rangle \left(\frac{r_C}{r_T}\right)^n$$

$$= \alpha \langle V_1 \rangle \left(\frac{D_C}{2.3 D_2}\right)^n, \text{ since } r_T = 2.3\ D_{2/2}$$

Since $$\langle V_1 \rangle = \frac{4\ Q_1}{\pi\ D_1^{\ 2}}$$

Then $$V_T = \frac{4 \alpha\ Q_1}{\pi\ D_1^{\ 2}} \left(\frac{D_C}{2.3\ D_2}\right)^n \quad \ldots\ldots\ldots\ldots\ldots\ 3$$

Substituting (3) into (2) and solving for $(D_p)_{50}$ yields

$$(D_p)_{50} = \sqrt{\frac{18\,\pi\,\mu_c\,Q_2}{16\,L_i(\rho_s - \rho_c)}}\left[\frac{2.3\,D_2}{D_c}\right]^n\left[\frac{D_1^{\,2}}{Q_1}\right] \ldots\ldots\ldots \quad 4$$

Since the particle Reynold's Number of $(D_p)_{50}$ may be > 1, Newton's Law should be used instead of Stokes Law. If Newton's Law is put into equation (2), then equation (5) results.

$$\frac{Q_2}{(\pi/2)(2.3\,D_2)(L_i)} = \sqrt{\frac{4(\rho_s - \rho_c)(D_p 50)(V_T^{\,2})}{3\,C_D\,\rho_c\,r_T}} \ldots\ldots \quad 5$$

Replacing V_T as before gives

$$\left[\frac{Q_2}{(\pi/2)(2.3\,D_2)(L_i)}\right]^2 = \left[\frac{4(\rho_s - \rho_c)(D_p)_{50}}{3\,C_D\,\rho_c\,r_T}\right]\left[\frac{4\,\alpha\,Q_1}{\pi\,D_1^{\,2}}\right]^2\left[\frac{D_c}{2.3\,D_2}\right]^{2n}$$

Solving for $(D_p)_{50}$ again results in

$$(D_p)_{50} = \frac{3\,C_D\,\rho_c\,r_T}{4(\rho_s - \rho_c)}\left[\frac{Q_2\,D_1^{\,2}}{(2.3\,D_2)(L_i)(\alpha)(2\,Q_1)}\right]^2\left[\frac{2.3\,D_2}{D_c}\right]^n \ldots\ldots \quad 6$$

where $$r_T = \frac{2.3\,D_2}{2}$$

A trial and error solution is necessary to equation (6), with three trials usually yielding a solution.

When equation (4) and equation (6) are solved for $(D_p)_{50}$, using the conditions of run 6, the results are

$(D_p)_{50} = 54\,\mu$ .... Equation 4

$(D_p)_{50} = 55\,\mu$ .... Equation 6

It may be seen that Stokes Law introduces negligible error, even in this case where Re particle = 1.7. For these calculations, values n = 0.8 and α = 0.5 were assumed. These are reasonable, according to Bradley (B-2).

A4·c <u>Measurement of $(D_p)_{50}$</u>

The wide variation in calculated $(D_p)_{50}$ dictated that an attempt should be made to measure $(D_p)_{50}$. The experimental procedure required photographing the overflow dispersion through the glass overflow pipe. Care was taken to position the camera so that it was focussed along the centre line of the pipe to avoid distortion, since the optical cell was not used here. The focal plane was moved into the pipe, away from the wall, to avoid any wall effect in the drop size distribution. Other experimental details can be found in Appendix 2. A sample photograph of the overflow dispersion is given in Figure A4-3.

When the drop size distributions that resulted were plotted on the basis of $n/\Delta x$ versus size x, where n = number of drops in size interval x_1 to x_2, $\Delta x = x_2 - x_1$, and x is the mid-interval size, the graphs in Figure A4-4 resulted. The feed drop size distribution is that expected for Trial 6 (photo series 16-b, photo #1). The second distribution is that for Trial 6 overflow. The third distribution is for the same conditions as Trial 6, but with an increased amount of liquid going to the underflow.

The most striking feature of these plots is that both overflow distributions show a very sharp peak which falls off rapidly to an $n/\Delta x$ of about 10. This is in contrast to the feed distribution which is quite full and rounded near its peak. Since the $(D_p)_{50}$ size

FIGURE A4-3 SAMPLE PHOTOGRAPH OF THE OVERFLOW DISPERSION

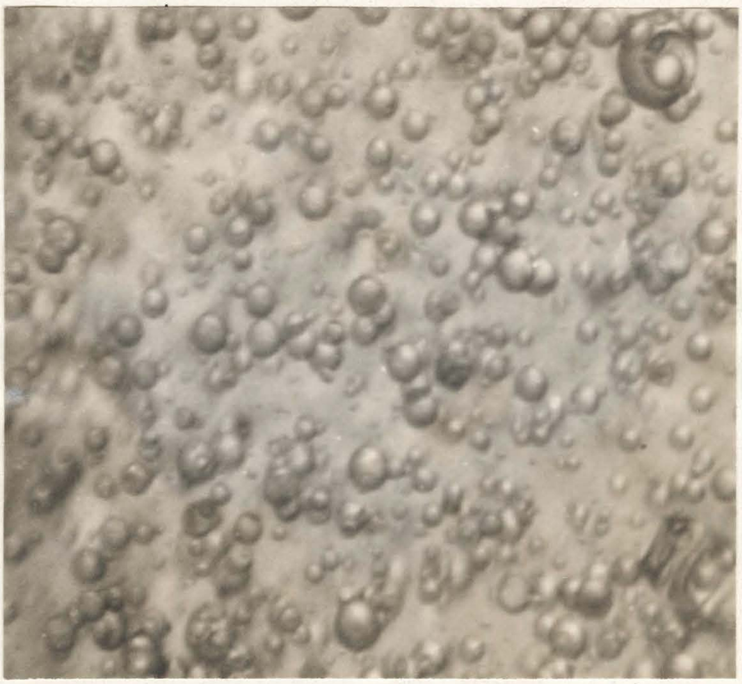

Photo Series 19-a-3 (#5)

FIGURE A4-4 FEED AND OVERFLOW DROP SIZE DISTRIBUTIONS FOR TRIAL 6, AND FOR A LARGER VOLUME SPLIT

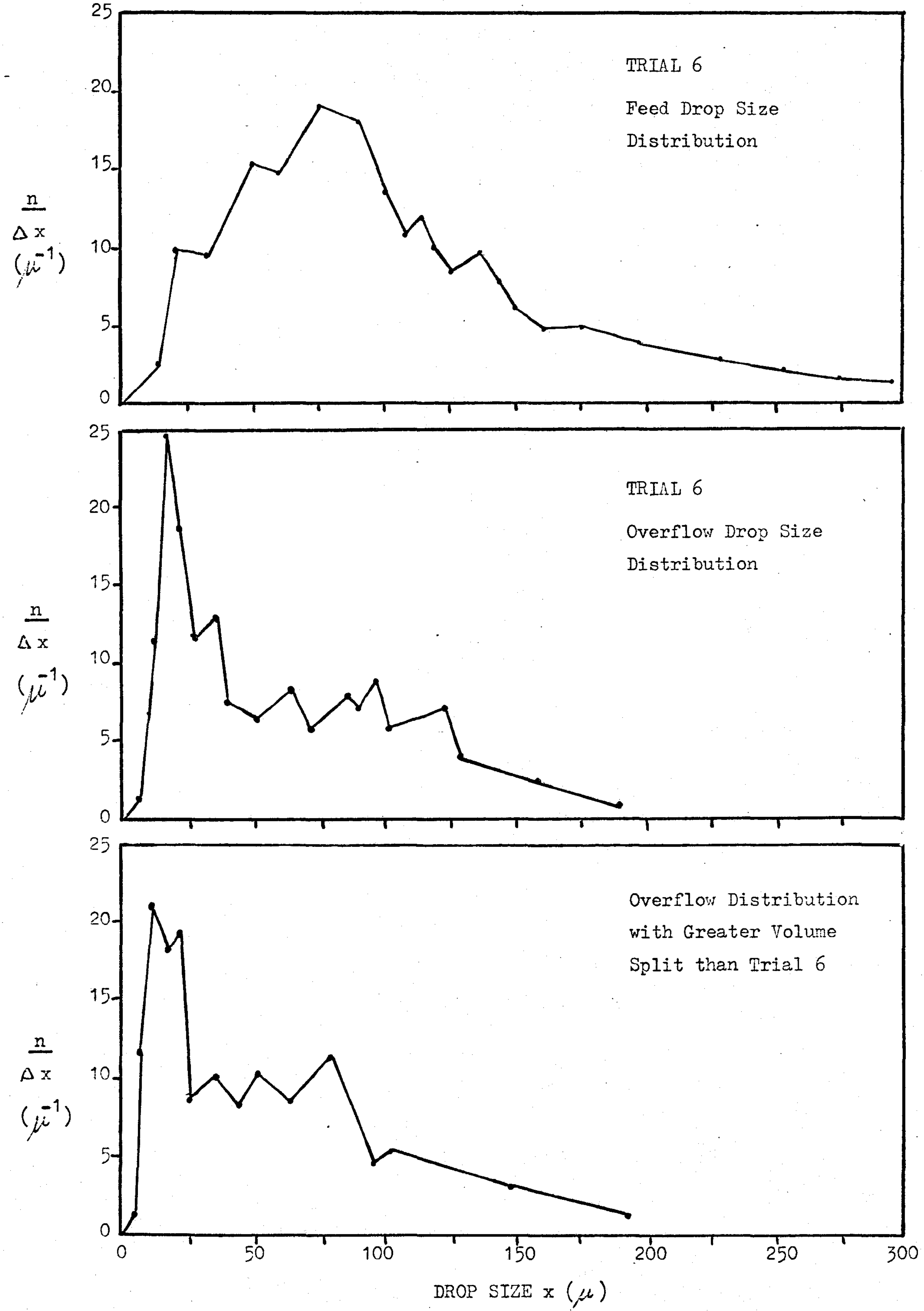

for a cyclone is theoretically that size at which the cyclone cut is sharpest, then $(D_p)_{50}$ should be easily locatable on a plot of the overflow drop size distribution. It is apparent from Figure A4-4 that $(D_p)_{50}$ is 20-25 μ. Further evidence that $(D_p)_{50}$ is between 20 to 25 microns has been presented in Chapter 4. The $(D_p)_{50}$ size does not seem to be sensitive to the volume split, and this is borne out by equation (6), which gives an insignificant change in $(D_p)_{50}$ when Q_2 is made smaller.

The results of this section can be summarized in Table A4-1.

A4·d <u>Hindered Settling</u>

The calculation of $(D_p)_{50}$ is based on the equivalence of F_d and F_c at the envelope of zero vertical velocity. This assumes no inter-particle influence. In sedimentation, it is known that groups of particles settle slower than if they were falling in the continuous medium with no other particles nearby. It would seem, then, that calculations of $(D_p)_{50}$ should contain a correction for this inter-particle influence. Kriijsman (K-4) and others have made the statement that particle flocculation in the cyclone is retarded by the high shearing stresses present. However, other than these qualitative statements, the matter was not persued.

A4·e <u>Summary of Appendix 4</u>

Both the Dahlstrom and the Yoshioka-Hotta equations for $(D_p)_{50}$ have predicted accurate values for $(D_p)_{50}$. The agreement between the experimental value of $(D_p)_{50}$ and Dahlstrom's equation is probably only coincidental since his equation is an empirical expression correlating $(D_p)_{50}$ values found for a particular solid/liquid feed. The Yoshioka-Hotta expression for $(D_p)_{50}$ has been derived using velocity profiles

TABLE A4-1 SUMMARY OF $(D_p)_{50}$ CALCULATIONS AND MEASUREMENTS

$(D_p)_{50}$ METHOD	$(D_p)_{50}$ (MICRONS)
Dahlstrom	22
Yoshioka *et al*	21
Lilge	10
Rietema	56
Bradley (eqn 4)	54
Eqn 6	55
Experimental Value	20 - 25

measured by a pitot probe. The $(D_p)_{50}$ value predicted by this expression should be close to the experimental value.

Most of the other equations for $(D_p)_{50}$ have predicted high values.

The use of Newton's Law to extend the range of applicability of Bradley's $(D_p)_{50}$ expression does not lead to any difference between the $(D_p)_{50}$ value predicted by his expression and the $(D_p)_{50}$ value predicted by the modified expression.

APPENDIX 5 DROP SIZE DISTRIBUTION CONSIDERATIONS

A5 DROP SIZE DISTRIBUTION CONSIDERATIONS

A5.a Introduction

The literature on particle size characterization was only briefly surveyed in chapter 2. This appendix discusses a few of the more pertinent topics that must be considered in particle size distribution work.

Since this work required the specification of a mean diameter to characterize the drop size distribution, a few definitions are considered first.

A5.b Definitions of Mean Diameter

First of all, if an infinite distribution of spherical particles is sampled, data consists of number of particles, n, in a given size interval, ΔD_p. Since there will be a smallest size D_{po} observed, and a largest size D_{pm} observed, and if the size intervals are very small, a mean volume diameter $\langle D_p \rangle_{30}$ can be defined as

$$\frac{\pi}{6} \langle D_p \rangle_{30}^3 \int_{D_{po}}^{D_{pm}} \frac{dn}{dD_p} \, dD_p = \frac{\pi}{6} \int_{D_{po}}^{D_{pm}} D_p^3 \frac{dn}{dD_p} \, dD_p \quad \ldots\ldots 1$$

Similarly, a mean surface diameter $\langle D_p \rangle_{20}$ can be defined as

$$\pi \langle D_p \rangle_{20}^2 \int_{D_{po}}^{D_{pm}} \frac{dn}{dD_p} \, dD_p = \pi \int_{D_{po}}^{D_{pm}} D_p^2 \frac{dn}{dD_p} \, dD_p \quad \ldots\ldots 2$$

Solving (1) and (2) for $\langle D_p \rangle_{30}^3$ and $\langle D_p \rangle_{20}^2$, and dividing these two mean diameters defines the volume surface diameter $\langle D_p \rangle_{32}$, or $\langle D_{sp} \rangle_{vs}$,

$$\langle D_p \rangle_{32} = \frac{\langle D_p \rangle_{30}^3}{\langle D_p \rangle_{20}^2} = \frac{\int_{D_{po}}^{D_{pm}} D_p^3 \frac{dn}{dD_p} \, dD_p}{\int_{D_{po}}^{D_{pm}} D_p^2 \frac{dn}{dD_p} \, dD_p} \quad \ldots\ldots\ldots\ldots\ldots\ldots \; 3$$

Since any particle size measurement involves finite size intervals, equation (3) can be expressed as

$$\langle D_p \rangle_{32} = \frac{\sum_{i=1}^{N} n_i \, D_{p_i}^3}{\sum_{i=1}^{N} n_i \, D_{p_i}^2} \quad \ldots \; 4 \; ,$$

where N size intervals are considered.

Sauter (S-1) defined a mean diameter as

$$\langle D_p \rangle_{vs} = \frac{6V}{A}$$

where V is the volume occupied by the particles and A is their surface area.

The $\langle D_p \rangle_{vs}$ for non spherical particles is defined as

$$\langle D_p \rangle_{vs} = \frac{6 \sum \alpha_v \, n_i \, D_{p_i}^3}{\sum \alpha_s \, n_i \, D_{p_i}^2}$$

where α_v and α_s are shape factors whose values depend on the particle material and the method of measuring D_{p_i}. For spheres, it may be seen that

$$\langle D_p \rangle_{vs} = \langle D_p \rangle_{32}$$

A5.c Sample Calculation on Literature Data

Having defined mean diameters, it is instructive to consider the effect of the Gwyn et al correction on some data. Gwyn et al gives the following data for a spray:

1) Number of particles measured $= 503$
2) Total Surface area $= 6154\ \mu^2 \ (= \sum n_i \, D_{p_i}^{\,2})$
3) Total Volume $= 37{,}252\ \mu^3 \ (= \sum n_i \, D_{p_i}^{\,3})$

Now calculate

$$\langle D_p \rangle_{20}^2 = \frac{\sum n_i \, D_{p_i}^{\,2}}{\sum n_i} = \frac{6154}{503} = 12.22\ \mu^2$$

$$\langle D_p \rangle_{30}^3 = \frac{\sum n_i \, D_{p_i}^{\,3}}{\sum n_i} = \frac{37{,}252}{503} = 74.10\ \mu^3$$

Then $$\langle D_p \rangle_{32} = \frac{74.10}{12.22} = \underline{6.06\ \mu}$$

This $\langle D_p \rangle_{32}$ is the value that is obtained using equation 4.

If the Upper Limit Equation of Mugele and Evans (M-8) is used, the following data result:

$(D_p)_{10} = 3.4\mu$

(10% of drop volume contained in drops smaller than this size, for the experimental drop size distribution)

$(D_p)_{50} = 7.6\mu$

$(D_p)_{90} = 14.2\ \mu$

and $(D_p)_m = 29.9\ \mu$ $\quad a = 2.94$

$u_{90} = 0.904$ $\quad \delta = 0.930$

$u_{50} = 0.341$

Since $\langle D_p \rangle_{32} = \dfrac{D_{pm}}{\left(1 + a\, e^{\frac{1}{4\delta^2}}\right)}$, inserting the numbers gives

$$D_{p\,32} = \underline{6.06\,\mu}$$

This agreement is no accident since Mugele and Evans have derived their method to give the same result as equation 4.

Any analysis of samples of a drop size distribution is restricted by the number of samples taken. Gwyn *et at* recognize that there are always drops not encountered in the samples whose sizes are larger than the largest size observed in the samples. By not allowing for the presence of these larger drops, the calculation of the drop volume and surface area will always be low.

Taking the data again and applying the corrections of Gwyn *et al*, yields the following data.

1) Number of particles $= 503 + 1 = 504$
2) Total Surface area $= 6595\ \mu^2$
3) Total Volume $= 46{,}900\ \mu^3$

Calculating

$$\langle D_p \rangle^2_{20} = \frac{6595}{504} = 13.06\ \mu^2$$

$$\langle D_p \rangle^3_{30} = \frac{46{,}900}{504} = 93.0\ \mu^3$$

and

$$\langle D_p \rangle_{32} = \frac{93.0}{13.06} = \underline{7.12\ \mu}$$

Assuming the applicability of the Gwyn *et al* method, it may be concluded that all past literature not allowing for sampling size limitations will consistently under estimate $\langle D_p \rangle_{32}$.

A5·d Measure of Dispersion

The above sections have been concerned with the definition of a mean diameter to characterize a distribution. By itself, a mean diameter tells nothing about the range of drop sizes. Specifying that the distribution is log-normal still leaves an infinite number of possible log-normal distributions. This is shown by Herdan (H-1) who gives the following expression for $\langle D_p \rangle_{32}$:

$$\ln \langle D_p \rangle_{32} = \exp \left(\ln \langle D_p \rangle_g + 2.5 \ (\ln \sigma_g)^2 \right)$$

Therefore if $\langle D_p \rangle_{32}$ is fixed, an infinite number of combinations of $\langle D_p \rangle_g$ and σ_g will still exist. A way to completely specify a log-normal drop size distribution is to give two of $\langle D_p \rangle_{32}$, $\langle D_p \rangle_g$, and σ_g, with the last two usually being given for a log-normal distribution.

A5·e Drop Size Measurement

Two important questions must be answered when an attempt is made to measure drop sizes. First, are the drops spherical? Using the Zeiss analyzer, the diameter of a circle of the same area as the projected view of the droplet is the estimate of the drop size. If the drops measured are not spherical, shape factors must be taken into account in calculating $\langle D_p \rangle_{32}$. By observation of all photographs, the drops appeared as circles. This is expected from a calculation of the Laplace radius which is defined as

$$\beta = \left(\frac{\sigma_{1-2}}{\Delta \rho \ g} \right)^{\frac{1}{2}}$$

For the oil/water system used

$$\sigma_{1-2} = 38.5 \text{ dynes/cm.}$$

$$\Delta \rho = 0.583 \text{ gm/cc.}$$

$$g = 981 \text{ cm./sec.}^2$$

Then

$$\beta = 0.265 \text{ cm.}$$

$$= 2650\ \mu$$

The maximum observed drop size was about 500 μ, and so all drops are expected to be spherical, since the Laplace radius is much greater the largest drop size in the dispersion.

The second question concerns whether or not the drops are breaking up in the feed line because of shear forces. Sleicher (S-5) calculates the maximum stable drop size in turbulent flow from the following equation for the maximum stable drop size, $(D_p)_{max.}$:

$$\frac{(D_p)_{max.}\,\rho_c\,V^2}{\sigma}\sqrt{\frac{\mu_c\,V}{\sigma}} = 38\left[1 + 0.7\left(\frac{\mu_d\,V}{\sigma}\right)^{0.7}\right]$$

Using the following data for this work

$$\rho_c = 1.00 \text{ gm/cc.}$$

$$V_1 = 254 \text{ cm./sec.}$$

$$\sigma = 38.5 \text{ dynes/cm.}$$

$$\mu_c = .00894 \text{ gm/cm.-sec.}$$

$$\mu_d = .00915 \text{ gm/cm.-sec.}$$

$$D_1 = 0.475 \text{ inches}$$

$$\text{Reynolds Number} = \frac{D_1\,V\,\rho_c}{\mu_c} = 35{,}000$$

and $\qquad (D_p)_{max.} = 940\ \mu$

Therefore, the drops observed were probably not breaking up under shear force in the feed line. Since the problem of drop-drop coalescence was considered in Chapter 4, the drop size distributions photographed were probably not changing with distance along the feed line.

While the above questions are answered, the problem of drop size measurement is not yet free from error. Two other factors may introduce error in the drop size distributions photographed. If one drop happens to come between the photographed drop in the focal plane and the camera, the photographed drop's image size may be increased or decreased, depending on the difference in refractive index. This is shown in Figure A5-1. No quantitative estimate of this effect can be made, since the change in image size is also dependent on the diameter of the intervening drop.

The problem of emulsion and paper shrinkage raises a valid objection to the photographic technique. Emulsion shrinkage on celluloid flim is negligible. The shrinkage of photographic paper is very small (1 mm. in 300 mm.), but measureable. It was neglected in this work.

The photographic technique has objections, but they do not seem serious enough to restrict the applicability of the method to this work.

A5·f <u>Necessary Number of Drops to Represent a Drop Size Distribution</u>

The larger the number of drops measured the better the sample population will represent the actual population, especially in the

FIGURE A5-1 EFFECT OF INTERVENING DROP ON DROP SIZE IMAGE

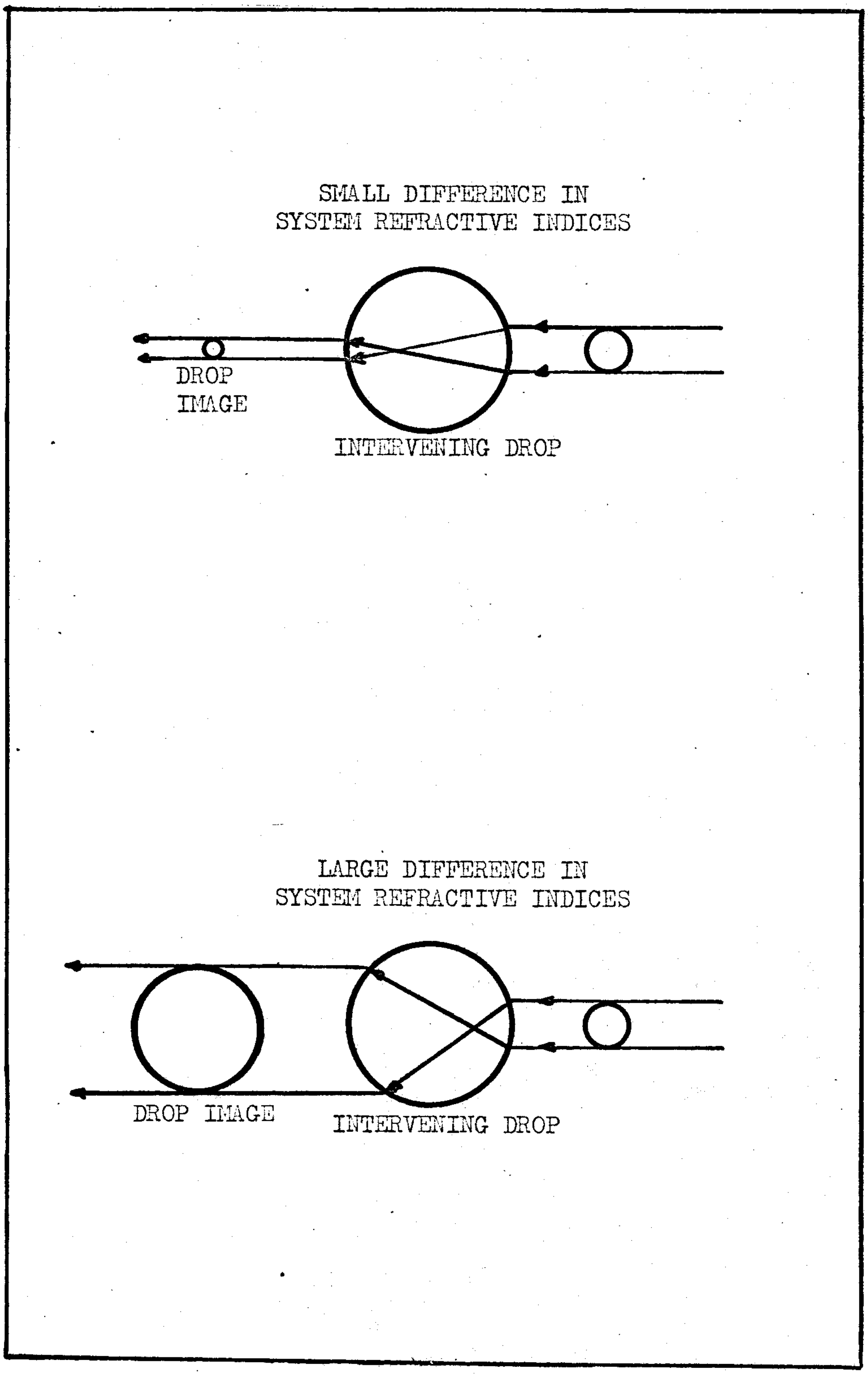

small drop frequency regions (commonly referred to as the tails).

In this work, the same drop size distribution was sampled 4 times. When all the drops are represented by a summation curve, and all five distributions are plotted on log-probability paper, the data in Table A5-1 result.

This table shows that $\langle D_p \rangle_g$ and σ_g for the summation curve and for Run 7 are about the same. Therefore, counting 500 drops gives the same distribution as when 4500 drops are counted. In all other runs, at least 1000 drops were counted, so that the sample population is expected to closely represent the actual population.

TABLE A5-1 GEOMETRIC MEAN DIAMETER AND GEOMETRIC STANDARD DEVIATION AS A FUNCTION OF THE NUMBER OF DROPS MEASURED

RUN	NUMBER OF DROPS COUNTED	$\langle D_p \rangle_g$	σ_g
1	2000	94	1.92
2	1000	79	1.95
8	1000	80	1.82
7	500	84	1.88
Summation Curve	4500	87	1.87